Roma Tre

BIOLOGIA MOLECOLARE CELLULARE E AMBIENTALE

XXXVIII CICLO

BEETLE-DERIVED CANTHARIDIN AND ITS DERIVATIVES AS POTENTIAL THERAPEUTIC AGENTS FOR THE TREATMENT OF SOLID TUMOURS: DESIGN AND DEVELOPMENT OF ANTIBODY-DRUG CONJUGATES

PhD Student

Riccardo Proietti

Supervisor

Prof. Marco Colasanti

Co-Supervisor

Prof.ssa Tiziana Persichini

Coordinator

Prof. Antonio Antoccia

INDEX

INDEX 2

ABSTRACT 6

SINTESI 11

INTRODUCTION 17

1. Cantharidin and its analogue Norcantharidin: origin, chemical properties, and pharmacological context 17

1.1 Cantharidin history, from beetles to bench 18

1.2 Norcantharidin 22

1.3 CTD and NCTD effects on cellular pathways 23

1.3.1 Induction of apoptosis in different cell lines 24

1.3.2 Elevation of cytosolic calcium levels 25

1.3.3 Oxidative Stress and ROS Generation 26

1.4 Development of drug delivery systems to overcome CTD and NCTD side effects. 28

1.4.1 Targeted Delivery: The Antibody drug conjugate as the “magic bullet” 29

1.4.2 Possible ADC Targets: EGFR Family, System Xc-, and CD44 Variants 32

2. Target solid tumors: Gliomas, Melanomas and Squamous cell carcinoma 35

2.1. Gliomas: overview and focus on Glioblastoma multiforme (GBM) 35

2.1.1. Glioblastoma multiforme and glioblastoma stem cells 36

2.2 Skin Cancer: Melanoma tumor and Squamous cell cancer 39

2.2.1 Melanomas 39

2.2.2 Squamous cell carcinoma 43

AIM OF THE WORK 45

MATERIALS AND METHODS 46

Materials 46

ADC Conjugation 47

Cell cultures 47

Treatment conditions 49

MTT assay 50

Parallel Artificial Membrane Permeability Assay (PAMPA) 50

Nuclear Extract Preparation 51

Total Extracts Preparation 52

Western Blotting 52

Quantitative Real-Time Reverse Transcription–Polymerase Chain Reaction 53

Flow Cytometry Analysis 54

Immunofluorescence and Confocal Analysis 55

Measurement of calcium influx 55

Measurement of ROS production 55

Statistical Analysis 56

RESULTS 57

1. Screening of cantharidin and norcantharidin effects on the viability of glioma and skin cancer cells 57

1.1 Cantharidin exerts a dose dependent reduction in the viability of both astrocytes and glioma cells 57

1.2 The comparison of Cantharidin effects on cellular viability of human astrocytes and glioma cells 60

1.3 The cytotoxic effect of CTD increases in longer exposure 61

1.4 Cantharidin reduces cell viability of melanoma cells and shows milder effects on melanocytes 62

1.5 Norcantharidin displays a reduced cytotoxicity compared to CTD and shows low side effects on melanocytes 66

2. Dissecting the cytotoxic mechanisms of cantharidin and norcantharidin: from membrane permeability to the impairment of Nrf2 signaling 69

2.1 CTD and NCTD are able to diffuse through the plasma membrane: assessment by means of PAMPA Assay 69

2.2 Both NCTD and CTD induce enhanced reactive oxygen species production 70

2.3 Cantharidin induces distinct effects on the ARE-dependent antioxidant response in U373 cells 74

2.4 NRF2 transcription factor is inhibited by the presence of CTD and NCTD 76

2.5 The ROS scavenger N-acetylcysteine reduces reactive oxygen species levels but does not restore cell viability 81

2.6 NCTD and CTD both increase cytosolic Ca^{2+} levels 84

3. Evaluation of potential tumour targets for the design of antibody-drug conjugates 89

3.1 System X_c^- expression in astrocytes and glioma cells 89

3.2 CD44 expression in cells from brain and skin cancers 90

3.3 Analysis of the expression of different CD44 isoforms in glioma cells. 91

3.4 The expression of the EGFR family of proteins in glioma and melanoma cells shows promise as a tumour marker. 93

4. Development of the antibody-drug conjugate and analysis of its effects on melanoma cells ... 97

4.1 The antibody chosen for the ADC internalize efficiently before and after the conjugation 98

4.2 The validation assays for ADC demonstrate its effectiveness in reducing tumour vitality without causing side effects. 100

DISCUSSION 104

CONCLUSIONS 113

ABBREVIATIONS 115

ACKNOWLEDGMENTS 117

REFERENCES 118

ABSTRACT

Historically, natural products have served as a cornerstone of therapeutic innovation, with around half of all current clinical drugs originating from natural sources. One such example is cantharidin (CTD), a terpenoid toxin produced by blister beetles of the Meloidae family. It demonstrates how ancient remedies can inspire modern cancer therapy. Used in traditional Chinese medicine for over two millennia to treat various ailments, CTD has only recently gained scientific attention for its potent anti-cancer properties. However, the clinical application of CTD has been severely hindered by dose-limiting toxicities, particularly nephrotoxicity, gastrointestinal distress and systemic adverse effects, which occur even at therapeutic doses. To address these limitations, norcantharidin (NCTD), the demethylated synthetic analogue of CTD, was developed and has been used in China since 1984 to treat cancer. While NCTD retains the anticancer efficacy of its parent compound, it exhibits significantly reduced nephrotoxicity and systemic toxicity, making it a more clinically viable candidate. Both molecules primarily act by inhibiting protein phosphatases PP1 and PP2A, which are critical enzymes that regulate cell cycle progression, apoptosis, and DNA repair mechanisms. PP2A is a key enzyme involved in regulating essential cellular processes, such as the cell cycle, apoptosis and cell-fate determination. Alteration of this enzyme impacts multiple downstream signaling pathways involved in cell cycle regulation, stress responses, and the initiation of apoptotic mechanisms. Despite these promising characteristics, the precise molecular mechanisms underlying the cytotoxic actions of both compounds, their differential effects on tumour versus normal cells, and optimal strategies to enhance their therapeutic selectivity, still need to be fully understood, forming the basis of this comprehensive investigation.

The primary objectives of this research were multifaceted and are as follows:

1) to systematically characterize the cytotoxic effects of CTD and NCTD across multiple solid tumour types, including gliomas, melanomas and squamous cell carcinomas, alongside their normal cellular counterparts.

2) to elucidate the molecular mechanisms driving their anti-cancer activity with particular emphasis on oxidative stress pathways, calcium homeostasis and antioxidant defense systems.

3) to identify and validate tumour-selective surface markers suitable for targeted drug delivery

4) to design and develop an antibody-drug conjugate capable of achieving tumour-selective delivery of one of the two molecules while minimizing off-target toxicity.

The preliminary screening for cytotoxicity revealed complex and cell-type-specific responses to both compounds. CTD showed dose-dependent cytotoxicity across all tested cell lines. In glioma cells, the half-maximal inhibitory concentration (IC_{50}) was approximately 10 μM after 24 hours of treatment, while in normal human astrocytes the IC_{50} value was 5 μM. Long-term exposure studies extending up to 192 hours demonstrated that the cytotoxic effects persist over time, increasing in a dose- and time-dependent manner. In melanoma cell lines, significant toxicity was observed at a concentration as low as 5 μM CTD, whereas normal human melanocytes (NHM) exhibited notably milder responses, requiring substantially higher concentrations to achieve a comparable rate of cell death. This differential toxicity profile suggests a potential therapeutic window for the treatment of melanoma. Squamous cell carcinoma cells proved remarkably resistant, with IC_{50} values ranging from 25 to 50 μM, indicating that sensitivity varies significantly across different cancer types. Findings relating to NCTD provide important insights into the assessment of a therapeutic window for melanomas, which exhibit a significant response to concentrations ranging from 12,5 to 25 μM. In contrast, normal cells show minimal toxicity even at 100 μM. This remarkable differential toxicity profile of NCTD immediately positioned it as a more promising candidate for clinical development, particularly for melanoma therapy.

To understand how these molecules access their intracellular targets, membrane permeability studies were conducted utilizing the Parallel Artificial Membrane Permeability Assay (PAMPA). Both CTD and NCTD exhibited robust passive membrane permeability. It should be noted that NCTD permeability was particularly high, being comparable to that of caffeine, a well-known high-permeability compound. Following internalization within the cells, both compounds triggered a cascade of molecular events that were systematically dissected. Flow cytometric analysis revealed a rapid production of reactive oxygen species (ROS) following treatment of glioma cells (U373) with CTD, reaching a peak at 6 hours, followed by gradual decline. Conversely, melanoma cells showed a distinct pattern: ROS levels increased after 6 hours and remained persistently elevated for up to 24 hours, reaching levels 4- to 6-fold higher than the control group. Importantly, normal melanocytes exhibited only a transient ROS peak, fully recovering to baseline levels within 24 hours. The same effects were obtained following NCTD treatment. Notably, NHM showed that even at elevated NCTD concentrations, ROS levels were restored after 24 hours.

Upon examining the activation of the antioxidant response, a notable characteristic of CTD and NCTD was revealed: a potent inhibition of Nrf2, the primary transcriptional regulator of the cellular antioxidant response. Western blot analysis revealed dramatic reductions in nuclear Nrf2 levels following treatment, with a 50% reduction observed at 2 hours progressing to 60-65% by 24 hours. Note that Nrf2 mRNA levels remained unchanged with CTD treatment, suggesting that the inhibition occurs at the post-translational level, affecting protein localization rather than synthesis. Most remarkably, CTD prevented Nrf2 nuclear accumulation even in the presence of dimethyl fumarate, a potent Nrf2 activator which works by releasing Nrf2 from its negative regulator, KEAP1. This finding indicates that CTD may block a step downstream of Nrf2 stabilization, potentially by interfering with the nuclear import machinery or promoting the rapid export of Nrf2 from the nucleus. By disarming the master regulator of antioxidant defenses prior to inducing oxidative stress, these compounds effectively render the cell impervious to incoming damage.

The consequences of Nrf2 inhibition were evident in our analysis of antioxidant gene expression. Rather than a coordinated response, marked heterogeneity was observed: catalase mRNA decreased steadily whereas the expression of the cystine transporter xCT and the heme oxygenase-1 (HO-1) increased substantially. At the protein level, xCT increased modestly while HO-1 showed a substantial increase. However, there was a significant decrease in glutathione peroxidase 4 (GPX4) levels. Treating cells with N-acetylcysteine (NAC), a potent ROS scavenger, xCT and HO-1 levels were fully restored to baseline values, thus suggesting that their induction was a direct response to the increase in ROS rather than being Nrf2-mediated transcription.

Given the elevated level of ROS production, it was hypothesized that oxidative stress might be the primary mechanism of cell death. To test this, NAC was used, resulting in complete restoration of ROS levels to baseline at all analysed time points. However, this complete neutralization only resulted in a modest 10% improvement in cell viability, thereby demonstrating that although ROS production was caused by the treatment, oxidative stress was not the main executor of cell death. This unanticipated outcome prompted further investigation into alternative mechanisms.

Real-time calcium imaging revealed an additional critical mechanism: both compounds induced a progressive increase in cytosolic calcium concentration, which began approximately 170 minutes after treatment and persisted throughout all examined time windows. This fundamental observation was derived from experiments conducted with extracellular calcium chelators and channel blockers, which were unsuccessful in preventing calcium accumulation. This suggests that calcium originates from intracellular stores, most likely the endoplasmic reticulum, rather than from extracellular space.

After studying the cytotoxicity properties of NCTD and identifying a potential upper therapeutic window in melanomas, the focus shifted to developing a targeted delivery strategy to further increase tumour selectivity. A systematic evaluation of potential tumour markers was conducted, encompassing System X_c^-, CD44 and its variant isoforms, and members of the epidermal growth factor receptor (EGFR) family, such as HER1, HER2, HER3. Expression profiles revealed significant

differences between tumour types: glioma cells predominantly expressed HER1, with lower levels of HER2 and HER3; meanwhile melanoma cells exhibit minimal HER1 expression, alongside high levels of HER2 and HER3. Initially, it was hypothesized that there would be potential toxicity issues because normal melanocytes express high levels of HER3. However, normal keratinocytes, which surround melanocytes in the skin, exhibit minimal HER3 expression, with only 4.5% of cells being positive for the marker. This suggests that an antibody conjugate directed against HER3 could be more selective for melanoma, while sparing the surrounding normal tissue, due to the inherent resistance of melanocytes to NCTD.

Thus, an antibody conjugated with NCTD (ADC) targeting HER3 in a DAR4 configuration (i.e., with four drug molecules linked to each antibody) was developed. The NCTD was conjugated via a linker designed to release the payload into the lysosomal environment following receptor-mediated endocytosis. Internalization studies confirmed that both the unconjugated antibody and the ADC are efficiently internalized by melanoma cells. This validates the uptake mechanism required for drug delivery. Preliminary cytotoxicity studies provided proof-of-concept for selective tumour elimination. At an ADC concentration of 60 μM, melanoma cells exhibited a 24% reduction in viability after 72 hours, while HER3-negative keratinocytes showed no change.

CTD and NCTD have been observed to induce cell death in both tumour types. It is important to note that these agents impede Nrf2 nuclear translocation, resulting in the deactivation of antioxidant defenses and interference with various cellular processes. Cytotoxicity may result from calcium homeostasis and endoplasmic reticulum impairment, and Nrf2 deactivation, with ROS production acting as a secondary inducer of death.

In conclusion, NCTD is the most promising candidate for the development of an ADC directed against HER3. It is selectively toxic to melanoma cells while sparing keratinocytes, providing a solid basis for precision anti-tumour strategies.

SINTESI

I prodotti naturali hanno storicamente rappresentato un pilastro dell'innovazione terapeutica, con circa la metà dei farmaci attualmente in uso clinico derivati da fonti naturali. Tra questi, la cantaridina (CTD), una tossina terpenoide prodotta dai coleotteri vescicanti della famiglia Meloidae, rappresenta un esempio affascinante di come rimedi antichi possano ispirare la moderna terapia antitumorale. Utilizzata per oltre due millenni nella medicina tradizionale cinese per il trattamento di diverse patologie, la cantaridina ha acquisito solo recentemente attenzione scientifica per le sue potenti proprietà antitumorali. Tuttavia, l'applicazione clinica della cantaridina è stata fortemente limitata da tossicità dose-limitanti, in particolare nefrotossicità, disturbi gastrointestinali ed effetti avversi sistemici che si manifestano anche a dosi terapeutiche. Per superare tali limitazioni è stata sviluppata la norcantaridina (NCTD), analogo sintetico demetilato della cantaridina, utilizzata in Cina dal 1984 per il trattamento dei tumori. Sebbene la norcantaridina mantenga l'efficacia antitumorale del composto parentale, essa mostra una nefrotossicità e una tossicità sistemica significativamente ridotte, rendendola un candidato clinicamente più praticabile. Queste molecole agiscono principalmente inibendo le fosfatasi proteiche PP1 e PP2A, enzimi critici che regolano la progressione del ciclo cellulare, l'apoptosi e i meccanismi di riparazione del DNA. PP2A è un enzima chiave nel controllo di processi cellulari fondamentali quali il ciclo cellulare, l'apoptosi e la determinazione del destino cellulare. Questa alterazione influenza molteplici vie di segnalazione a valle coinvolte nella regolazione del ciclo cellulare, nelle risposte allo stress e nell'attivazione dei meccanismi apoptotici. Nonostante queste caratteristiche promettenti, i meccanismi molecolari precisi alla base dell'azione citotossica di entrambi i composti, i loro effetti differenziali su cellule tumorali rispetto a cellule normali e le strategie ottimali per aumentarne la selettività terapeutica sono rimasti non completamente chiariti e costituiscono il razionale di questo progetto di ricerca.

Gli obiettivi principali di questa ricerca sono stati molteplici e sono elencati di seguito:

1) caratterizzare sistematicamente gli effetti citotossici della cantaridina e della norcantaridina in diversi tipi di tumori solidi, inclusi gliomi, melanomi e carcinomi squamosi, insieme alle rispettive controparti cellulari normali;

2) chiarire i meccanismi molecolari responsabili della loro attività antitumorale, con particolare attenzione allo stress ossidativo, all'omeostasi del calcio e ai sistemi di difesa antiossidante;

3) identificare e validare marcatori di superficie tumorali il più possibile selettivi e idonei al drug delivery;

4) progettare e sviluppare un anticorpo coniugato (antibody–drug conjugate, ADC) per un futuro approccio terapeutico che renda la somministrazione della cantaridina/norcantaridina più selettiva verso il tumore minimizzando la tossicità off-target.

Lo screening iniziale di citotossicità ha rivelato risposte, ad entrambi i composti, complesse e specifiche per tipo cellulare. La cantaridina ha mostrato una citotossicità dose-dipendente in tutte le linee cellulari testate, con concentrazioni inibitorie (IC_{50}) di circa 10 μM nelle cellule di glioma dopo 24 ore di trattamento e di 5 μM negli astrociti umani normali. Studi di esposizione a lungo termine, fino a 192 ore, hanno dimostrato che gli effetti citotossici persistono nel tempo, con un aumento della tossicità sia dose- che tempo-dipendente. Nelle linee cellulari di melanoma, una tossicità significativa è stata osservata a partire da 5 μM di cantaridina, mentre i melanociti normali hanno mostrato effetti nettamente più lievi, essendo necessarie concentrazioni sostanzialmente più elevate per ottenere una percentuale di morte cellulare comparabile. Questo profilo di tossicità differenziale suggeriva l'esistenza di una finestra terapeutica sfruttabile per il trattamento del melanoma. Le cellule di carcinoma squamoso si sono dimostrate particolarmente resistenti, con valori di IC_{50} compresi tra 25 e 50 μM, indicando una sensibilità eterogenea tra i diversi tipi di tumore. La norcantaridina ha fornito uno dei primi risultati chiave nell'identificazione di una finestra terapeutica per il trattamento dei melanomi. Infatti, nei melanociti normali è stata osservata una tossicità minima anche a dosi molto

elevate come 100 μM, mentre le cellule di melanoma hanno mostrato elevata mortalità alle dosi più basse nell'intervallo 2,5–25 μM. Questa marcata tossicità differenziale ha immediatamente posizionato la norcantaridina come il candidato più promettente per lo sviluppo clinico, in particolare in prospettiva per la terapia del melanoma.

Per comprendere come queste molecole raggiungano i loro bersagli intracellulari, sono stati condotti studi di permeabilità di membrana mediante il Parallel Artificial Membrane Permeability Assay (PAMPA). Sia la cantaridina sia la norcantaridina hanno mostrato una robusta permeabilità passiva di membrana, con la norcantaridina che ha evidenziato una permeabilità particolarmente elevata, paragonabile a quella della caffeina, un composto noto per l'elevata permeabilità. Una volta all'interno delle cellule, entrambi i composti hanno innescato una cascata di eventi molecolari che è stata analizzata in modo sistematico. L'analisi mediante citofluorimetria ha rivelato una rapida produzione di specie reattive dell'ossigeno (ROS) in seguito al trattamento con la cantaridina. In particolare, nelle cellule di glioma è stato osservato un picco di ROS dopo 6 ore di trattamento, seguito da un graduale declino. Nelle cellule di melanoma è stato osservato un andamento diverso in cui livelli di ROS, in aumento dopo 6 ore e persistentemente elevati fino a 24 ore, hanno raggiunto valori 4–6 volte superiori al controllo. Al contrario, i melanociti normali hanno mostrato solo un picco transitorio di ROS, con un completo ritorno ai livelli basali entro 24 ore. Effetti analoghi sono stati osservati anche dopo trattamento con NCTD. In particolare, i melanociti umani normali hanno dimostrato che, anche se esposti a concentrazioni molto più elevate di NCTD, i livelli di ROS venivano ripristinati dopo 24 ore.

Analizzando l'attivazione della risposta antiossidante, è stata individuata una delle caratteristiche più sorprendenti dell'azione di cantaridina e norcantaridina, ovvero, una potente inibizione di Nrf2, il principale regolatore trascrizionale della risposta antiossidante cellulare. L'analisi mediante western blot ha rivelato una drastica riduzione dei livelli nucleari di Nrf2 dopo il trattamento, con una diminuzione del 50% a 2 ore che progrediva fino al 60–65% a 24 ore. È importante sottolineare che

i livelli di mRNA di NRF2 rimanevano invariati dopo trattamento con CTD, indicando che l'inibizione avviene a livello post-traduzionale, influenzando la localizzazione proteica piuttosto che la sintesi. In modo particolarmente rilevante, la cantaridina ha impedito l'accumulo nucleare di Nrf2 anche in presenza di dimetil fumarato, un potente attivatore di Nrf2 che agisce liberando Nrf2 dal suo regolatore negativo KEAP1. Questo risultato indica che la cantaridina blocca una fase a valle della stabilizzazione di Nrf2, probabilmente interferendo con i meccanismi di importazione nucleare o promuovendo una rapida esportazione nucleare. Disattivando il principale regolatore delle difese antiossidanti, questi composti impediscono alla cellula di contrastare lo stress ossidativo rendendola di fatto "cieca" al danno imminente.

Le conseguenze dell'inibizione di Nrf2 sono risultate evidenti nell'analisi dell'espressione dei geni antiossidanti. Invece di una risposta coordinata, è stata osservata una marcata eterogeneità: l'mRNA della catalasi diminuiva costantemente, mentre il trasportatore della cistina xCT e l'eme ossigenasi-1 (HO-1) mostravano una forte induzione. A livello proteico, xCT aumentava in modo modesto, mentre HO-1 mostrava un incremento sostanziale. Tuttavia, i livelli di glutatione perossidasi 4 (GPX4) diminuivano in modo significativo. Il trattamento delle cellule con N-acetilcisteina, in grado di neutralizzare l'aumento di ROS, ha riportato i livelli di xCT e HO-1 ai valori basali, indicando che la loro induzione era una risposta diretta innescata dall'aumento di ROS piuttosto che una trascrizione mediata da Nrf2.

Dato l'elevato livello di produzione di ROS, abbiamo ipotizzato che lo stress ossidativo potesse rappresentare il principale meccanismo di morte cellulare. Per verificarlo, abbiamo utilizzato la N-acetilcisteina, un potente *scavenger* dei ROS, che ha completamente ripristinato i livelli di ROS ai valori basali in tutti i tempi analizzati. Sorprendentemente, questa completa neutralizzazione ha determinato solo un modesto miglioramento del 10% della vitalità cellulare, dimostrando in modo conclusivo che, sebbene la produzione di ROS sia causata dal trattamento, lo stress ossidativo non è

il principale esecutore della morte cellulare. Questo risultato inatteso ci ha spinto a indagare meccanismi alternativi.

L'imaging del calcio in tempo reale ha rivelato un altro meccanismo critico: entrambi i composti hanno indotto un aumento progressivo della concentrazione di calcio citosolico che iniziava circa 170 minuti dopo il trattamento e persisteva in tutte le finestre temporali esaminate. L'osservazione chiave è emersa dagli esperimenti con chelanti del calcio extracellulare e bloccanti dei canali, che non sono riusciti a prevenire l'accumulo di calcio. Ciò suggerisce che il calcio provenga da riserve intracellulari, molto probabilmente dal reticolo endoplasmatico, piuttosto che da un influsso dallo spazio extracellulare.

Dopo aver studiato la citotossicità e identificato una possibile finestra terapeutica superiore della norcantaridina nei melanociti, ci siamo concentrati sullo sviluppo di una strategia di delivery mirato per aumentare ulteriormente la selettività tumorale. Sono stati valutati sistematicamente potenziali marcatori tumorali, tra cui il sistema X_c^-, CD44 e le sue differenti isoforme, e i membri della famiglia EGFR (HER1, HER2, HER3). I profili di espressione hanno rivelato differenze marcate tra i tipi tumorali: le cellule di glioma esprimono prevalentemente HER1 (EGFR) con livelli più bassi di HER2 e HER3, mentre le cellule di melanoma mostrano un'espressione quasi assente di HER1 ma livelli elevati di HER2 e HER3. Anche i melanociti normali esprimono alti livelli di HER3, sollevando inizialmente preoccupazioni circa una potenziale tossicità. Tuttavia, i cheratinociti normali, che circondano i melanociti nella pelle, mostrano un'espressione minima di HER3, con solo il 4,5% delle cellule positive per il marcatore. Questo pattern di espressione, combinato con la resistenza intrinseca dei melanociti alla norcantaridina, ha suggerito che un anticorpo coniugato diretto contro HER3 potesse fornire una selettività maggiore per il melanoma risparmiando il tessuto normale circostante.

È stato sviluppato un ADC coniugato con norcantaridina mirato a HER3 in configurazione DAR4, ovvero con quattro molecole di norcantaridina legate a ciascun anticorpo. La NCTD è stata coniugata tramite un linker progettato per rilasciare il carico nel compartimento lisosomiale a seguito di

endocitosi mediata dal recettore. Studi di internalizzazione hanno confermato che sia l'anticorpo non coniugato sia l'ADC sono efficientemente internalizzati nelle cellule di melanoma, validando il meccanismo di uptake necessario per la somministrazione del farmaco. Gli studi di citotossicità hanno fornito una prova preliminare per l'eliminazione selettiva del tumore. Alla concentrazione di ADC corrispondente a 60 μM, le cellule di melanoma hanno mostrato una riduzione del 24% della vitalità dopo 72 ore, mentre i cheratinociti HER3-negativi hanno mantenuto invariata la vitalità.

È stato dimostrato come la cantaridina e la norcantaridina siano in grado di indurre la morte cellulare in entrambi i tipi tumorali. È importante sottolineare che questi agenti bloccano la traslocazione nucleare di Nrf2, disattivando le difese antiossidanti e interferendo con diversi processi cellulari. La citotossicità potrebbe derivare dalla compromissione dell'omeostasi del calcio e del reticolo endoplasmatico e dalla disattivazione di Nrf2, mentre la produzione di ROS potrebbe agire come induttore secondario della morte cellulare. Complessivamente, i risultati di questa ricerca evidenziano come la norcantaridina sia la molecola più idonea per lo sviluppo di un ADC diretto contro HER3 mostrando una citotossicità selettiva verso le cellule di melanoma e risparmiando i cheratinociti, e pongono così le basi per strategie antitumorali di precisione.

INTRODUCTION

1. Cantharidin and its analogue Norcantharidin: origin, chemical properties, and pharmacological context

A contemporary investigation reveals that almost 50% of the therapeutics currently used in clinical settings originate from natural sources, highlighting their indispensable importance. This development stems from the recognition of these natural substances as reservoirs of innovation rather than merely as target entities (Puerto Galvis CE et al., 2013).

Plants, bacteria and fungi have long been studied as sources of small molecules (SMs) that act as important bioprobes, shedding light on cellular processes. Among the animal kingdom, the group of invertebrate species, particularly insects such as beetles, has not received similar attention. Nevertheless, the therapeutic properties of certain beetles, particularly those in the Meloidae family, have recently attracted significant scientific interest. Within this taxonomic group, compounds such as cantharidin and its derivatives show great potential as candidates for novel, effective and selective anti-cancer treatments (Puerto Galvis CE et al., 2013).

1.1 Cantharidin history, from beetles to bench

Cantharidin (CTD) is a highly toxic terpene produced by beetles of the Meloidae family, or "blister beetles," a widespread family of Coleoptera Tenebrionoidea that includes nearly 3,000 species, all characterized by their ability to produce and store cantharidin (Fig. 1) (Bologna MA. et al., 2008).

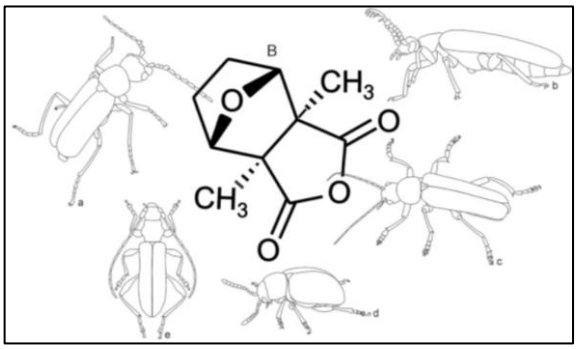

Fig. 1 Cantharidin molecule and some cantharid insects (Safenraiter ME, et al., 2024).

CTD is present in the haemolymph of both male and female blister beetles, but interestingly, it is only produced by the males, who utilize it as a pheromone to attract mates. This substance plays a significant role like an aphrodisiac in these insects during mating. CTD is passed on to female beetles to safeguard their eggs, aiming to shield and sustain the larvae as they begin their development. Nevertheless, egg protection is not the sole function of CTD in the beetles' life cycle; clearly, these insects use this chemical to protect themselves, if beetles feel threatened by predators CTD is released in small amounts (Fig. 2) (Puerto Galvis CE et al., 2013).

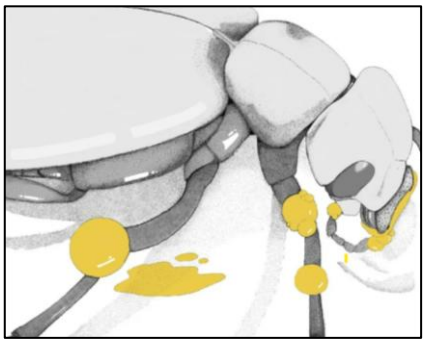

Fig. 2 Release of cantharidin from the joints of legs and antennae (Safenraiter ME, et al., 2024).

The scientific history of cantharidin chemical proprieties' discovery is well-documented, dating back to its first isolation in 1810 by the French chemist Pierre Robiquet from the blister beetle *Lytta vesicatoria*. While the chemical formula was subsequently described by Piccard in 1877, the molecule's structural elucidation remained a challenge for over a century due to its deceptively simple yet rigid framework reaching the final result in 1953 with Stork's works (Safenraiter ME et al., 2024).

Nevertheless, this compound has been used in traditional medicine for over two millennia to treat various ailments (Puerto Galvis CE et al., 2013). Historically, extracts from these beetles, known as "Spanish fly", were used in traditional Chinese medicine to treat various skin diseases, but were always categorized as high toxic drug (Wang G et al., 2018). The ancient Greeks and Romans used cantharidin, derived from blister beetles' bodies, as a diuretic, abortifacient, and legendary aphrodisiac, with Hippocrates prescribing it for conditions like dropsy for over 2000 years (Fig. 3).

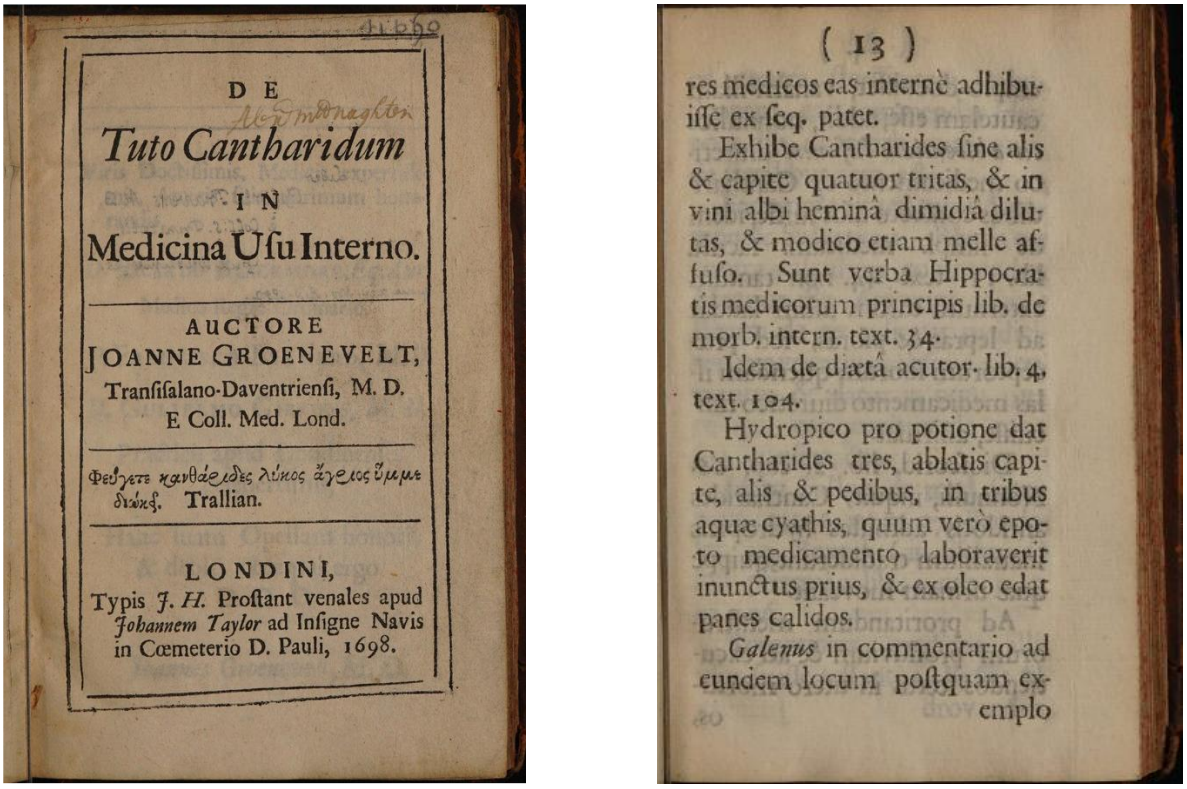
DE

Tuto Cantharidum

IN

Medicina Uſu Interno.

AUCTORE

JOANNE GROENEVELT,

Tranſiſalano-Daventrienſi, M. D.

E Coll. Med. Lond.

Φεύγετε κανθάρίδες λύκος ἄγριος ὕμμε διώκῃ. Trallian.

LONDINI,

Typis *J. H.* Proſtant venales apud *Johannem Taylor* ad Inſigne Navis in Cœmeterio D. Pauli, 1698.

(13)

res medicos eas internè adhibuiſſe ex ſeq. patet.

Exhibe Cantharides ſine alis & capite quatuor tritas, & in vini albi heminâ dimidiâ dilutas, & modico etiam melle affuſo. Sunt verba Hippocratis medicorum principis lib. de morb. intern. text. 34.

Idem de diætâ acutor. lib. 4. text. 104.

Hydropico pro potione dat Cantharides tres, ablatis capite, alis & pedibus, in tribus aquæ cyathis, quum verò epoto medicamento laboraverit inunctus prius, & ex oleo edat panes calidos.

Galenus in commentario ad eundem locum poſtquam exemplo

Fig. 3 Frontispiece of the historical treatise "De Tuto Cantharidum in Medicina Usu Interno" by Joannes Groenevelt (1698). Published in London, this work marks an early pharmacological attempt to define a safe therapeutic window for the internal use of Cantharides (the biological source of cantharidin). The text argues for the medicinal value of the toxin when administered with specific vehicles, such as wine and honey, as noted in the translated excerpts referring to Hippocratic practices." Credit: De tuto cantharidum in medicina usu interno / [Joannes Groeneveld]. Source: Wellcome Collection.

It was also widely used until the nineteenth century to treat fevers, rabies, and to relieve pain in conditions like pleurisy, often considered the most powerful drug available (Safenraiter ME et al., 2024).

In addition to all these historical applications, a lot of papers have demonstrated that cantharidin's most important activity is its anti-tumor effect. CTD is a potent cytotoxic compound with extensive anti-tumour potential across a diverse array of human cancer cell lines. It operates by causing DNA damage, including single- and double-strand breaks, in carcinoma cells (Naz F et al., 2020).

CTD effectively halts the advancement and multiplication of various human malignancies, such as Non-Small Cell Lung Cancer (NSCLC), colorectal, hepatocellular, gastric, oral, ovarian, and bladder cancers. Some of its anti-tumor effects include repression of cancerous cell growth and proliferation, induction of cancerous cell apoptosis, DNA damaging and repair associated proteins, inhibition of cancer cell metastasis, and cell cycle arrest (Fig. 4) (Naz F et al., 2020).

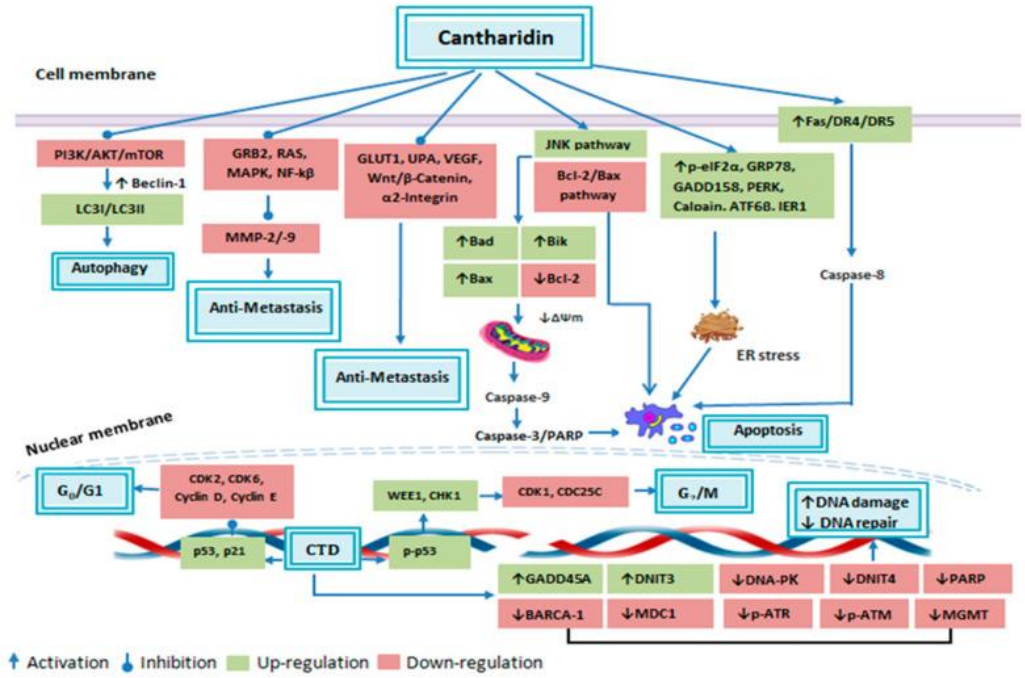

Fig. 4 Anti-tumor effects of CTD on different cell lines (Naz F et al., 2020).

The anti-cancer effect of this toxin was discovered by Chen and colleagues in 1980 (Chen RT et al., 1980). Subsequently, additional investigation was performed to clarify its cytotoxic effects, ultimately uncovering that its activity is due to the inhibition of protein phosphatase 1 (PP1) and protein phosphatase type 2A (PP2A). These phosphatases play a key role in regulating essential cellular processes, including cell cycle progression, apoptosis, and DNA repair. The inhibition of these enzymes modifies the balance between protein phosphorylation and dephosphorylation, resulting in cellular alterations that trigger cell cycle arrest and apoptosis (Kim JA et al., 2013).

However, as medicine advanced, strong evidence emerged showing that the compound is extremely toxic when ingested, with a low lethal dose. Citing Wilbur W. Oaks et al. in their 1960 paper "Cantharidin Poisoning", the therapy of cantharidin poisoning is discussed, particularly regarding the management of renal toxicity and diminished renal function. In conclusion the authors stressed that cantharidin is a highly toxic substance and it must be made inaccessible.

Infact, upon contact with the epidermis, cantharidin leads to the formation of blisters and it is therefore classified as a vesicant substance. If ingested, it can cause severe side effects in the gastrointestinal, genitourinary, cardiac, haematological, and pulmonary tracts (Bischoff K, 2023). It follows that, given this evidence on the effects associated with the use of CTD, researchers endeavour to discover methods to mitigate toxicity. However, some CTD derivatives exhibit comparable functions with fewer side effects. For example, both cantharidin and norcantharidin have anti-metastatic properties because they inhibit the expression of MMP-9 via Sp1 pathways. Norcantharidin also reduces toxicity in hepatocytes (Wang G et al., 2018).

In light of this evidence, it is crucial to analyse not only cantharidin, but also its derivatives, to determine the efficacy of these potential drugs.

1.2 Norcantharidin

Norcantharidin (NCTD - $C_8H_8O_4$), or Hexahydro-4,7-epoxyisobenzofuran-1,3-dione, is the demethylated chemical analog of CTD (Fig. 5). It has been utilized in China since 1984 for the treatment of malignant tumors (Wang G et al., 2018).

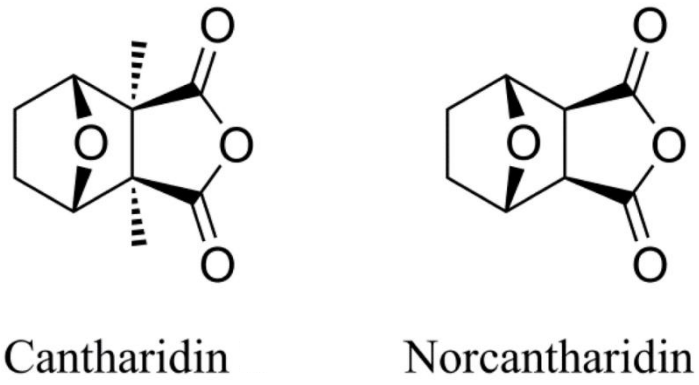

Fig. 5 Chemical structure of Cantharidin and Norcantharidin (*Sun W. et al.,* 2013).

Like CTD, norcantharidin also exhibits potential anticancer properties, however, the nephrotoxicity associated with cantharidin treatment is absent. NCTD is effective *in vitro* against several tumour cell lines, including those of the cervix, liver, ovaries, larynx, colon, bone, and leukaemia. Nevertheless, some published papers have demonstrated that norcantharidin is approximately ten times less cytotoxic than cantharidin in many of these cell lines (Tarleton M et al., 2012).

Given its important function, many studies have been conducted to understand its effects on apoptosis activation pathways in cancer cells. In vitro treatment with NCTD inhibits DNA synthesis and the cell cycle during the G2/M phases, or during the formation of postmitotic daughter cells. These inhibitory mechanisms may be due to the inhibition of PP2A activity (Liu XH et al., 1995).

In particular, the effects on leukemia, gallbladder carcinoma and colorectal cancer cells have been studied in vitro. Additionally, an increase in reactive oxygen species (ROS) generation due to

mitochondrial dysfunction has been reported in the literature (Shen B et al., 2013). Despite many encouraging studies, there are still significant side effects on non-tumour cells.

1.3 CTD and NCTD effects on cellular pathways

It has been demonstrated that both CTD and NCTD possess the capacity to act as anti-tumour molecules. The primary therapeutic effect of these agents is thought to be the induction of apoptosis (Naz F et al., 2020) (Tarleton M et al., 2012). CTD is recognized as a potent and selective inhibitor of Protein Phosphatase 2A, an important enzyme that regulates critical cellular processes such as cell cycle control, apoptosis, and cell-fate determination (Li W et al., 2010). The inhibition of this enzyme induces a significant shift in the cellular phosphorylation balance. This alteration impacts multiple downstream signaling pathways involved in cell cycle regulation, stress responses, and the initiation of apoptotic mechanisms (Naz F et al., 2020). It is known that also the NCTD possesses the same capacity to inhibit PP2A (Liu XH et al., 1995). This shared biochemical activity suggests a common effect on cellular pathways, resulting in significant cytotoxic effects against tumour cells, as demonstrated extensively in the literature (Liu XH et al., 1995) (Li W. et al. 2010) (Hong C.Y. et al., 2000).

CTD has also been reported to induce DNA damage and simultaneously hinder principal DNA repair mechanisms, while also causing cell cycle arrest at critical checkpoints (e.g., G0/G1 or G2/M). Moreover, its capability to impede metastasis is demonstrated through the suppression of cell migration and the decrease of enzymatic activity of Matrix Metalloproteinases (MMP-2 and MMP-9) (Naz F et al., 2020).

Importantly, while both compounds share these mechanisms, NCTD provides a notable clinical benefit: it largely preserves the antineoplastic effectiveness of CTD but lacks the related severe nephrotoxicity (Tarleton M et al., 2012).

1.3.1 Induction of apoptosis in different cell lines

Cancer cells use a variety of molecular mechanisms to escape apoptosis, which not only facilitates their abnormal growth and proliferation, but also makes them resistant to anticancer therapies (Pistritto G et al., 2016). Therefore, identifying therapeutic agents that accelerate apoptosis represents a significant strategy for treating cancer.

Several studies have documented that CTD can trigger apoptosis in a variety of cancer cell lines by activating both the extrinsic and intrinsic pathways (Naz F et al., 2020).

The extrinsic pathway of apoptosis begins when an external ligand binds to a specific receptor on the cell surface that activates a series of intracellular signals that lead to the formation of a complex known as the Death-Inducing Signaling Complex (DISC). DISC causes the activation of procaspase-8, which in turn activates effector caspases 3, 6, and 7 (Kim JA et al., 2013).

The intrinsic pathway, on the other hand, is activated in response to internal stress signals, such as DNA damage, oxidative stress, or growth factor deprivation (Naz F et al., 2020).

Studies on the effects of cantharidin on different tumour cell lines have shown that it increases the levels of molecules involved in inducing intrinsic apoptosis, such as TNF-α, TRAIL-1, and TRAIL-2. In a human skin cancer cell line, it was found that stimulation with CTD increases the expression of death-associated receptors, including DR4, DR5, and TRAIL, and the activity of caspases-8, 9, and 3 (Pistritto G. et al., 2016) (Wang G et al., 2018) (Naz F et al., 2020) (Liu YP et al., 2018). Norcantharidin also can induce apoptosis in AGS human gastric cancer cells by promoting cell cycle arrest at the Go/G1 phase, increasing ROS production, reducing mitochondrial membrane potential, and activating both mitochondria- and caspase-dependent pathways, along with modulating the expression of various apoptosis-related proteins and death receptors (Zheng LC et al., 2016).

1.3.2 Elevation of cytosolic calcium levels

Calcium ions (Ca^{2+}) are second messengers whose cytosolic concentration is finely regulated to maintain cellular homeostasis, signal transduction, and cell survival (Koss DJ et al., 2007). Under physiological conditions, the concentration of free cytosolic Ca^{2+} is maintained at a certain concentration by the action of plasma membrane Ca^{2+}-ATPases, sodium-calcium exchangers, and intracellular sequestration by the endoplasmic reticulum (ER) and mitochondria (Koss DJ et al., 2007).

This regulation allows calcium to act as signaling messenger, with transient elevations triggering different cellular responses such as enzyme activation, gene transcription, and cell survival pathways (Koss DJ et al., 2007). The alteration of calcium homeostasis can lead to sustained increases in cytosolic Ca^{2+} causing some possible pathological outcomes such as oxidative stress, mitochondrial dysfunction, and apoptosis (Koss DJ et al., 2007).

Recent literature demonstrates that treatment with cantharidin significantly alters intracellular calcium handling in various cell types. Studies on bladder carcinoma cells show that cantharidin induces an increase in cytosolic Ca^{2+} and by certain markers of ER stress (Su CC et al., 2015).

Similar calcium dysregulation has been documented in melanoma, lung and skin cancer cell lines, as well as in erythrocytes and cardiomyocytes. In these cells, cantharidin first increases Ca^{2+}, then promotes the generation of ROS, reduces the mitochondrial membrane potential, and finally activates apoptotic pathways (Hsiao YP et al., 2014).

NCTD also increases the intracellular Ca^{2+} concentration in various tumor cell lines, promoting apoptosis associated with mitochondrial depolarization and caspase activation (Zheng LC et al., 2016).

The mechanisms underlying calcium dysregulation induced by cantharidin and norcantharidin appear to be multifactorial, involving altered phosphorylation of calcium channels and regulatory proteins,

mobilization of ER calcium stores, reduced calcium reuptake, and mitochondrial calcium overload (Naz F. et al., 2020) (Zheng LC et al., 2016).

1.3.3 Oxidative Stress and ROS Generation

The increase of reactive oxygen species that lead to oxidative stress can strongly affect cellular functions. ROS act both as second messengers for survival pathways and as triggers of oxidative damage when overproduced (Sies H & Jones DP, 2020).

Under physiological conditions, ROS are mainly generated by mitochondria and neutralized by enzymatic (superoxide dismutase, catalase, glutathione peroxidase) and non-enzymatic (glutathione, vitamin E, vitamin C) antioxidant systems. The main factor regulating the activation of the antioxidant response is the nuclear factor erythroid 2-related factor 2 (Nrf2) transcription factor (Sies H & Jones DP, 2020). When ROS levels increase, this transcription factor dissociates from its inhibitor KEAP1, allowing the translocation into the nucleus, where Nrf2 heterodimerizes with small sMaf proteins. This complex recognizes and binds to the ARE (Antioxidant Responsive Element) gene promoter. This activates the transcription of genes that encode for detoxifying and antioxidant proteins such as catalase (CAT), γ-glutamylcysteine ligase (GCL), superoxide dismutase (SOD), heme oxygenase-1 (HO-1), glutathione peroxidase (GPX), and the xCT subunit of System X_c^- (D'Ezio et al., 2021). When ROS production exceeds cellular antioxidant capacity, oxidative stress occurs, damaging lipids, proteins, and DNA, compromising cellular structural and functional integrity (Rauh R. et al., 2020) (Zhou et al., 2018).

Some papers show that cantharidin can induce marked ROS generation in several cellular models. In A375.S2 melanoma cells, CTD increases both ROS levels and intracellular Ca^{2+} concentration, followed by reduction in mitochondrial membrane potential and the activation of caspases leading to the release of pro-apoptotic factors (Hsiao YP et al., 2014). The oxidative stress induction profile of norcantharidin is comparable to that of CTD. Studies on AGS gastric carcinoma cells demonstrate

that NCTD induces apoptosis through ROS production, mitochondrial depolarization, and caspase activation (Zheng LC et al., 2016).

The mechanisms through which cantharidin and norcantharidin induce oxidative stress are multiple and interconnected. The inhibition of PP2A by cantharidin also alters redox-sensitive signaling pathways such as NF-κB and MAPK, amplifying the response to oxidative stress (Zhou H et al., 2018).

The close relationship between calcium dysregulation and oxidative stress creates a vicious cycle: an increase in cytosolic Ca^{2+} promotes the generation of mitochondrial ROS, meanwhile, ROS damage calcium channels and pumps, further exacerbating calcium dysregulation (Fig. 6) (Hsiao YP et al., 2014) (Zheng LC et al., 2016).

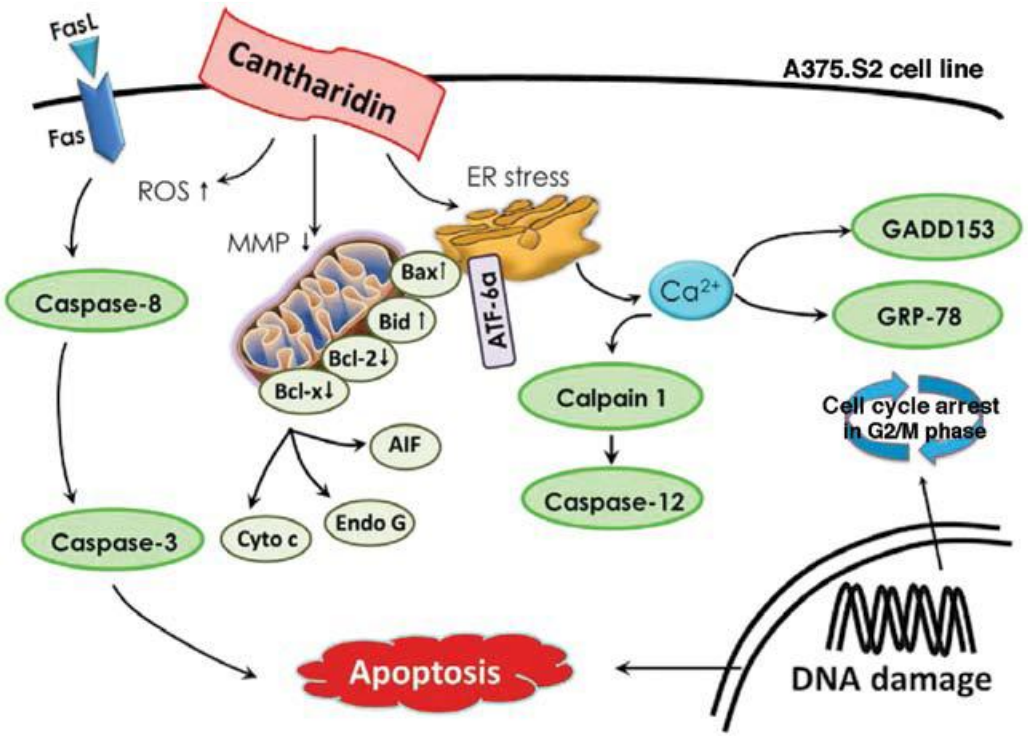

Fig. 6 – The effect of CTD on cA375.S2 cell line proposed by Hsiao YP et al., 2014.

1.4 Development of drug delivery systems to overcome CTD and NCTD side effects.

Despite CTD and NCTD anti-tumor properties, their clinical utility is severely compromised by dose-limiting toxicities. The most prominent adverse effect of CTD is nephrotoxicity, manifesting as acute kidney injury, proteinuria, and hematuria even at therapeutic doses (Tarleton M. et al., 2012). As already said in chapter 1.1, if ingested, CTD can cause severe side effects in the gastrointestinal, genitourinary, cardiac, haematological, and pulmonary tracts (Bischoff K, 2023).

While NCTD demonstrates improved safety compared to CTD, significant adverse effects persist (Tarleton M. et al., 2012). The systemic distribution of both CTD and NCTD leads to off-target effects on normal tissues, limiting the maximum tolerable dose and consequently restricting therapeutic efficacy.

To overcome this issue, various approaches are constantly evolving to improve drug effectiveness. These include the use of nanoparticles, such as liposomes and polymeric nanoparticle systems, as well as antibody-drug conjugates (ADCs). These can deliver drugs directly to specific tumour targets, making treatment much more efficient and free of side effects (Jain KK, 2020).

Exosomes can also be used as natural drug carriers and, since they are extracellular vesicles secreted by cells, they are less likely to trigger an immune response (Zeng W. et al., 2023).

For targeted drug delivery, therefore, selective recognition of target cells is crucial.

1.4.1 Targeted Delivery: The Antibody drug conjugate as the “magic bullet”

Antibody-drug conjugates represent a revolutionary approach to cancer therapy that addresses the fundamental limitation of conventional cytotoxic agents: lack of tumor selectivity. ADCs bind the specificity of an antibody with the cytotoxicity of the chosen drug through a linker that is able to release its payload in preset conditions (Fig. 7A). The first concept of ADC was first proposed by Paul Ehrlich in 1910 with the concept of the “magic bullet”, a drug that could directly access to some desired targets in cell to cure diseases. Theoretically, these compounds should be effective in killing cancer cells, but harmless to normal cells (Fu Z et al., 2022).

The mechanism of action of an ADC involves multiple coordinated steps: tumor antigen recognition and binding by the antibody component; receptor-mediated endocytosis; intracellular trafficking to lysosomes; linker cleavage by lysosomal enzymes or at an acidic pH; and, finally, payload release to exert cytotoxic effects (Fig. 7B) (Fu Z et al., 2022).

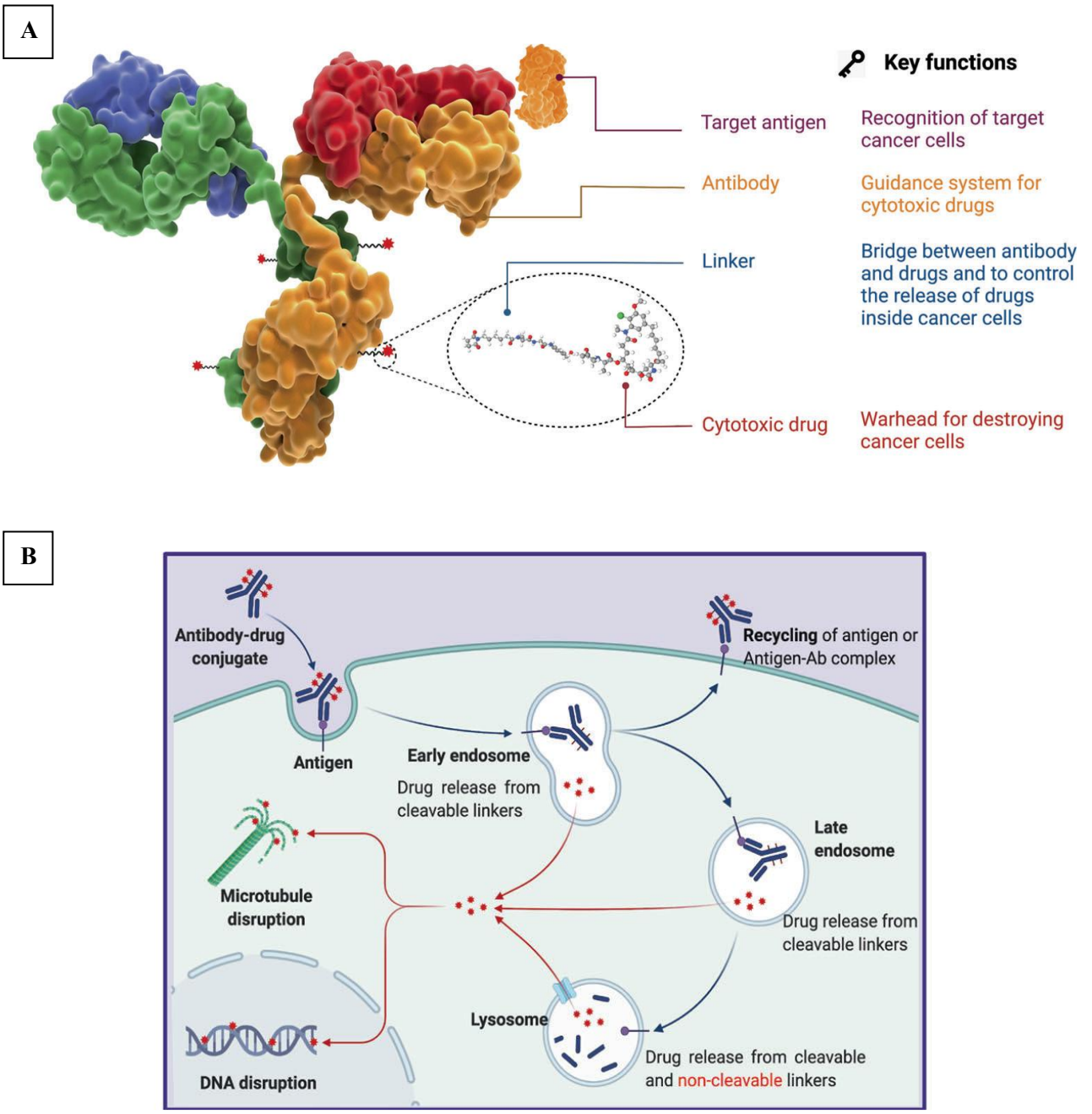

Fig. 7 Schematic representation of the structure of an Antibody-drug conjugate (**A**) and its mechanism of action (**B**) (Fu Z et al., 2022).

The critical innovation of ADCs lies in their self-immolative linker technology, which enables controlled, tumor-specific drug release. The linkers present in ADC structure remain stable in systemic circulation but undergo to rapid cleavage in the acidic tumor microenvironment or upon exposure to tumor-specific enzymes such as cathepsins. This dual-level selectivity—antibody-

mediated targeting followed by environment-responsive drug released dramatically reduces systemic exposure to cytotoxic agents and minimizes off-target toxicity (Edupuganti VVSR et al., 2021).

Recent advances in ADC technology have demonstrated remarkable success in reducing chemotherapy-related adverse effects. Nanostructured lipid carriers and non-ionic surfactant vesicles loaded with CTD have shown the ability to enhance anti-tumour activity while simultaneously reducing systemic toxicity in preclinical models (Han W et al., 2013). There is no strong evidence in the literature for the incorporation of CTD and NCTD into ADC. However, in the context of drug delivery, (Han W et al., 2013) has demonstrated that it reduces CTD side effects and increases its anti-tumour activity. These findings support the feasibility of ADC-based strategies for CTD/NCTD delivery

1.4.2 Possible ADC Targets: EGFR Family, System Xc-, and CD44 Variants

The success of ADC therapy depends on selecting appropriate tumor-associated antigens that are preferentially or exclusively expressed on cancer cells. Also, this target must be internalized in order to reach the specific condition for payload release (Fu Z et al., 2022). This research project has analyzed the epidermal growth factor (EGFR) family of receptor tyrosine kinases, the System X_c^- cystine-glutamate antiporter, and CD44, along with its variant isoforms, as potential tumor target.

The EGFR family comprises four members EGFR (HER1 or ERBB1), HER2 (ERBB2), HER3 (ERBB3), and HER4 (ERBB4) (Fig 8). These proteins regulate cell proliferation, survival, differentiation, and migration through complex homo- and heterodimerization patterns (Yu J et al., 2024). HER2 is a key member of the EGFR family and is overexpressed in various tumors, most notably in breast cancer. It represents one of the most clinically validated ADC targets, evidenced by the FDA approval of two HER2-directed agents: trastuzumab emtansine and trastuzumab deruxtecan (Yu J et al., 2024). Beyond HER2, EGFR-directed ADCs and HER3-directed ADCs are currently under clinical investigation (Yu J et al., 2022).

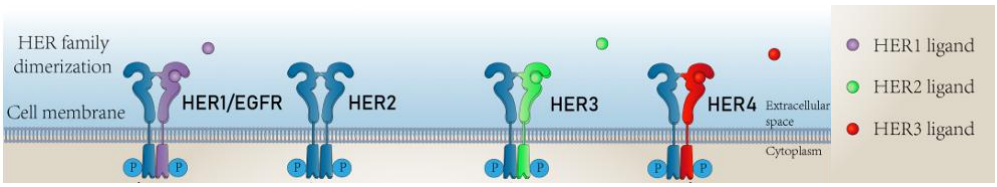

Fig. 8 HER family dimerization (*Yu J et al., 2024*).

System X_c^-, composed of the SLC7A11 (xCT) light chain and SLC3A2 heavy chain, functions as a cystine-glutamate antiporter. This transport system is crucial for glutathione synthesis, thereby playing a significant role in cellular protection against oxidative stress (Jyotsana N et al., 2022). System X_c^- is overexpressed in numerous malignancies including ovarian, lung, and colorectal cancers, where it promotes chemoresistance by suppressing ferroptosis (Guo Y et al., 2025).

Recent studies indicate that SLC7A11 overexpression can also enhance tumor growth and contribute to drug resistance, highlighting its significance as a therapeutic target in cancer treatment (Jyotsana N et al., 2022).

The targeting System X_c^- may offer a dual therapeutic advantage by limiting side effects, targeting a prognostic biomarker in cancer cells, and affecting drug-resistant cells to improve the efficacy of chemotherapy. While dedicated ADCs targeting this protein remain in early development, the biological rationale is compelling. ADC-mediated delivery of CTD or NCTD to System X_c^--expressing tumors could combine the antiproliferative effects of cantharidin derivatives with ferroptosis induction, creating a synergistic lethal effect while avoiding systemic toxicity.

CD44, a transmembrane glycoprotein and hyaluronic acid receptor, exists in multiple variant isoforms generated through alternative splicing (Misra S et al., 2015) (Fig. 9).

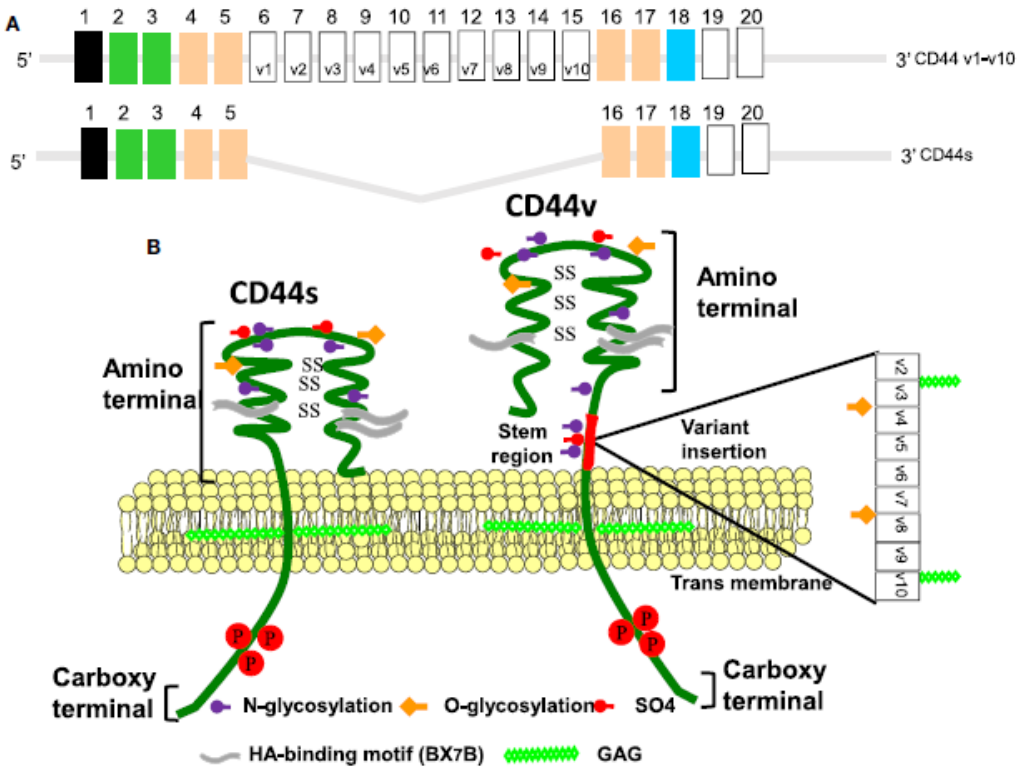

Fig. 9 Mouse CD44 gene/protein structures in mice. Model structure of alternative splicing in CD44. CD44 pre-mRNA is encoded by 20 exons in mouse and 19 exons in human being. The common standard CD44s (hematopoietic) form contains no extra exons, and the protein has a serine motif encoded in exon 5 that can initiate synthesis of a chondroitin sulfate or dermatan sulfate chain (**A**). Model structure of alternatively spliced CD44 proteins (**B**) (*Misra S. et al., 2015*).

CD44 is demonstrated to be a cancer stem cell (CSC) marker associated with tumor initiation, progression and metastasis, as well as therapeutic resistance, and disease recurrence (Li F et al., 2024). CD44 variants orchestrate tumor progression through distinct roles: while the standard form accelerates epithelial-mesenchymal transition, variant isoforms promote metastatic colonization, apoptosis resistance, and chemoresistance (Fig. 10).

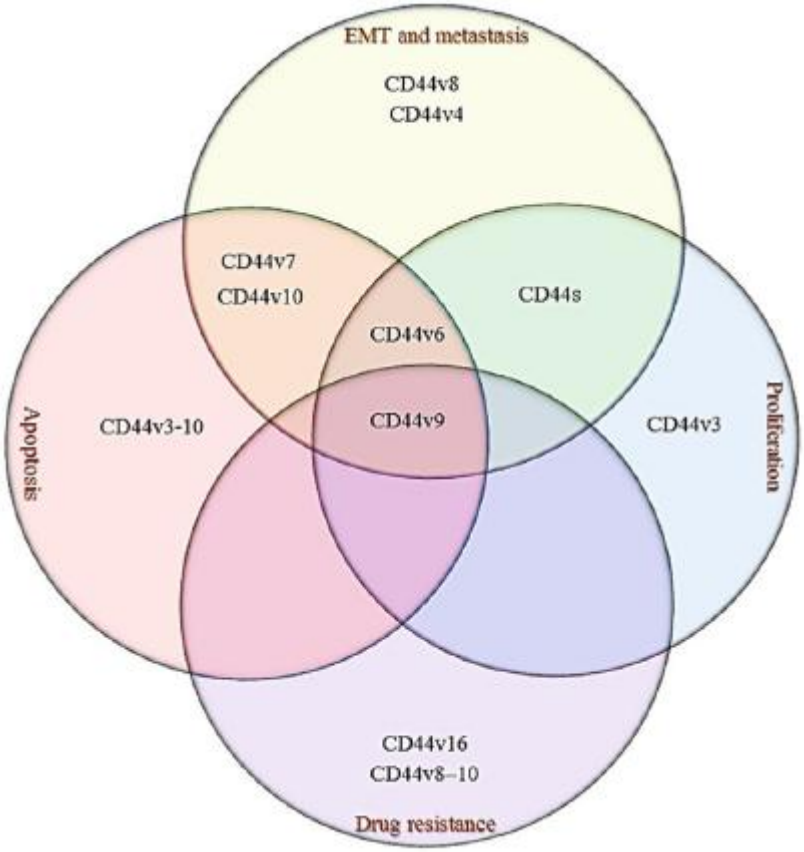

Fig. 10 The function of various CD44 forms in the physio-pathological traits of tumors in Venn diagram layout (*Gomari MM et al., 2021*).

CD44-expressing CSCs represent a critical therapeutic target because they drive tumor heterogeneity and are responsible for post-treatment relapses. Preclinical studies have demonstrated that CD44-targeted drug delivery systems, including acetylated human serum albumin nanoparticles conjugated to cytotoxic agents, achieve preferential endocytosis by CD44-expressing CSCs (Xiong G et al., 2025). CD44-targeted ADCs carrying CTD or NCTD payloads could specifically eradicate the CSC population responsible for cancer recurrence while sparing normal stem cells that express lower levels of CD44.

2. Target solid tumors: Gliomas, Melanomas and Squamous cell carcinoma

Gliomas, melanomas, and carcinomas are biologically disparate neoplasms whose differences in cell of origin, key oncogenic drivers, and microenvironmental context determine clinical behavior and response to therapies. Parallel studies of these tumor classes elucidate the rationale behind a single cytotoxic compound exerting heterogeneous effects and the manner in which mechanistic vulnerabilities can be exploited in a tumor-selective manner.

This chapter provides detailed descriptions of the biological and molecular characteristics of gliomas, melanomas, and carcinomas. The primary focus of this study is to explore the potential of CTD, NCTD and ADC to generate novel therapeutic interventions for the management of these serious cancer diseases.

2.1. Gliomas: overview and focus on Glioblastoma multiforme (GBM)

Gliomas account for approximately 40% of all primary tumors of the central nervous system in adults (Louis DN et al., 2021). The distinction between these two categories is primarily determined by the type of glial cell from which the tumor cells originate and the extent of their differentiation. This signifies the degree to which the tumor cells maintain the characteristics of their original cells, in contrast to their potential for de-differentiation (Gritsch S. et al., 2022). The glioma group includes astrocytomas, oligodendrogliomas, ependymomas, and glioblastoma multiforme (Louis DN et al., 2021).

Astrocytomas are among the least aggressive types of gliomas and are derived from astrocytes. These tumors can be categorized as low grade, designated as grade I and II, and are therefore characterized by relatively advanced differentiation, reduced invasiveness, and a less aggressive nature. Anaplastic

astrocytomas (grade III) are regarded as more malignancy-prone, representing an intermediate stage between low-grade astrocytomas and glioblastomas (Gritsch S. et al., 2022).

The most malignant and invasive subtype of glioma is GBM, classified by the World Health Organization (WHO) as grade IV. It is characterized by poorly differentiated cells, with rapid proliferation and high invasiveness of the surrounding brain tissue, which makes treatment difficult (Louis DN et al., 2016).

2.1.1. Glioblastoma multiforme and glioblastoma stem cells

Historically, the classification of brain tumors, including glioblastomas, was based on histopathological characteristics. Since 2016, molecular characteristics have also been incorporated into the WHO classification (Louis DN et al., 2016). Subsequently, in 2021, the classification was further refined to include genetic mutations that influence prognosis and response to treatment, with particular importance given to the isocitrate dehydrogenase (IDH) gene (Louis DN et al., 2021) (Kayabolen A. et al., 2021).

The mutational status of the IDH gene serves as a discriminator between the wildtype form, which manifests in 90% of cases, and the mutated variant. The wildtype form is characterized by the production of the oncometabolite 2-hydroxyglutarate, which leads to a much more severe phenotype in the wildtype form. Furthermore, additional markers, including TERT mutation and 1p/19q deletion, contribute to definitive classification of the tumor.

At the molecular level, the presence of EGFR amplification and oncogenic EGFR variants is a recurring feature in IDH-wildtype gliomas. These alterations contribute to proliferative signaling and therapeutic resistance. The most prevalent EGFR variant, designated as EGFRvIII, is the result of an in-frame deletion of exons 2-7, leading to the production of a constitutively active receptor that signals independently of ligand binding (Noorani I et al., 2020).

The genetic heterogeneity of GBM, in conjunction with the blood-brain barrier (BBB) and an immunosuppressive microenvironment, results in the current treatments' limited effectiveness (Louis DN et al., 2021). The highly infiltrative nature of GBM makes complete resection at the cellular level nearly impossible, exposing the body to high risks of recurrence.

Intratumoral heterogeneity and therapeutic resistance, hallmarks of glioblastomas, are believed to be promoted by the presence of glioblastoma stem cells (GSCs). These cells constitute a subpopulation that exhibits self-renewal properties, the capacity to differentiate into diverse tumor cell types, and elevated invasiveness, rendering them pivotal in the progression and recurrence of GBM (Prager BC et al., 2020).

This phenomenon contributes to the tumor's ability to adapt to various stresses, including therapeutic interventions. For instance, stem cells in a state of quiescence exhibit reduced susceptibility to therapies that target rapidly dividing cells (Prager BC et al., 2020).

A critical factor in the maintenance and resistance of GSCs is the tumor microenvironment (TME). The latter consists of immune cells, including tumor-associated macrophages (TAMs), which are frequently polarized towards the M2 phenotype. This phenotype is pro-tumor and immunosuppressive (Fig. 2). These macrophages secrete growth factors, including vascular endothelial growth factor (VEGF), transforming growth factor beta (TGF-β), and chemokines, which promote the survival and invasiveness of GSCs (Prager BC et al., 2020).

The TME contains soluble factors, including growth factors, cytokines, and certain enzymes such as matrix metalloproteinases (MMPs). These enzymes facilitate the degradation of the extracellular matrix, thereby promoting tumor invasion (Prager BC et al., 2020).

The tumor microenvironment of glioblastoma is therefore a complex ecosystem that interacts closely with GSCs to promote tumor growth, invasiveness, and resistance to therapies. A comprehensive

understanding of the intricate interplay between GSCs and the TME is imperative for the development of novel therapeutic interventions that target the stemness of these cells.

In this regard, for the development of therapies directed against GSCs, it would be appropriate to identify a series of biomarkers that are mainly or exclusively expressed by these cells. Some of these biomarkers are already known, such as CD133, CD44, and CD24 (Tang X et al, 2021). CD44 antagonism has been shown to reduce tumor growth in preclinical glioblastoma models, thereby identifying this surface marker as a potential target to reduce stemness and enhance chemosensitivity (Xu Y et al., 2010).

Consequently, therapies that target GSCs are considered to be among the most promising strategies for enhancing the treatment of glioblastoma. However, further investigation is necessary to fully understand their biological complexity and the manner in which they interact with the tumor microenvironment (Tang X et al, 2021).

2.2 Skin Cancer: Melanoma tumor and Squamous cell cancer

Skin cancers derived from keratinocytes (non-melanoma skin cancer; NMSC) and melanocytes (melanoma) are among the most common malignant tumors worldwide, affecting approximately 3 million people. NMSC is known for its aggressive local behavior and its rarity in metastasizing (5% of cases), with a mortality rate that is comparable to the 2% mortality rate observed in melanoma cases. According to the AIRTUM and AIOM 2023 report, the incidence of NMSC in Italy is 8%, with 20,000 new cases of squamous cell carcinoma and 64,000 cases of basal cell carcinoma diagnosed (AA.VV., 2023). Melanoma is characterized by its rapid spread tendency to metastasize, leading to its intrinsic resistance to most conventional chemotherapeutic agents. In Italy, the incidence of this cancer was 14,900 new cases in 2020, making it the second most common cancer in men and the third most common in women under 50. A global forecast indicates that 510,000 new cases will occur in 2040, resulting in 96,000 deaths (AA.VV., 2023).

2.2.1 Melanomas

Melanomas are derived from neural-crest-derived melanocytes, which are the pigment-producing cells located primarily in the basal layer of the epidermis, but also in the uveal tract of the eye, mucosal surfaces, and other sites (Slominski RM et al., 2024). Melanoma is classified into different subtypes, including cutaneous melanoma (the most common form), uveal melanoma, mucosal melanoma, and acral melanoma. Each of these subtypes exhibits distinct epidemiology, molecular characteristics, and metastatic proclivities. Cutaneous melanoma incidence has increased significantly in recent decades, particularly among individuals with fair skin who are exposed to ultraviolet radiation (UV-A and UV-B). While early-stage disease is often curable with surgical excision, metastatic melanoma has historically been associated with poor prognosis (Slominski RM et al., 2024).

The malignant transformation of melanocytes into metastatic melanoma is the result of a complex interaction between exogenous stimuli, endogenous factors, and dynamics intrinsic to the tumor and

the immune system. Given the low frequency of melanocyte division, a constant increase in the proliferative index is evident, marking the initial phase in the evolution of melanocytic neoplasms. This is followed by a progressive accumulation of point mutations and alterations in the number of genomic copies (Schadendorf D et al., 2018). While it is presumed that numerous pathogenetically significant alterations in melanoma derive from a direct mutagenic impact of ultraviolet radiation, indirect influences such as the generation of free radicals resulting from the biochemical interaction of ultraviolet A with melanin, also induce mutations and genetic anomalies (Schadendorf D et al., 2018).

Melanin pigments play a complex and paradoxical role in melanoma genesis, often described as a 'Yin and Yang' relationship. While eumelanin serves as a critical physical shield against ultraviolet radiation (UVR) by dissipating energy and scavenging reactive oxygen species (ROS), it can also act as a facultative pro-oxidant and mutagen. Furthermore, the synthesis of pheomelanin contributes to an inherently pro-oxidative and pro-inflammatory microenvironment, which facilitates tumor initiation and increases therapeutic resistance, marking a definitive shift of melanin from a photoprotective agent to a biological risk factor (Slominski RM et al., 2024).

The process of tumorigenesis occurs in stages. The BRAF V600 mutation is a hallmark of the formation of benign nevi, while additional mutations, such as those affecting the TERT promoter, are necessary for progression to intermediate and in situ lesions. The acquisition of invasive potential is associated with mutations in genes that regulate the cell cycle, such as CDKN2A, or in protein involved in chromatin remodeling, such as the ARID family. These genetic alterations ultimately lead to the metastatic phase, marked by the emergence of mutations in PTEN or TP53 (Schadendorf D et al., 2018).

Members of the EGFR family have been observed to engage in crosstalk with MAPK and PI3K pathways under specific conditions. This interaction has been implicated in the development of adaptive resistance to targeted therapeutic agents and in the process of tumor plasticity. Although

classical EGFR signaling is less central than MAPK pathway activation in melanoma pathogenesis, expression or modulation of members of the ERBB family (*e.g.*, ERBB2/HER2) has been observed in preclinical treatment studies with norcantharidin combinations. This suggests a context-dependent contribution of the EGFR-family to melanoma biology (Fig. 11) (Lara-Vega I et al., 2025).

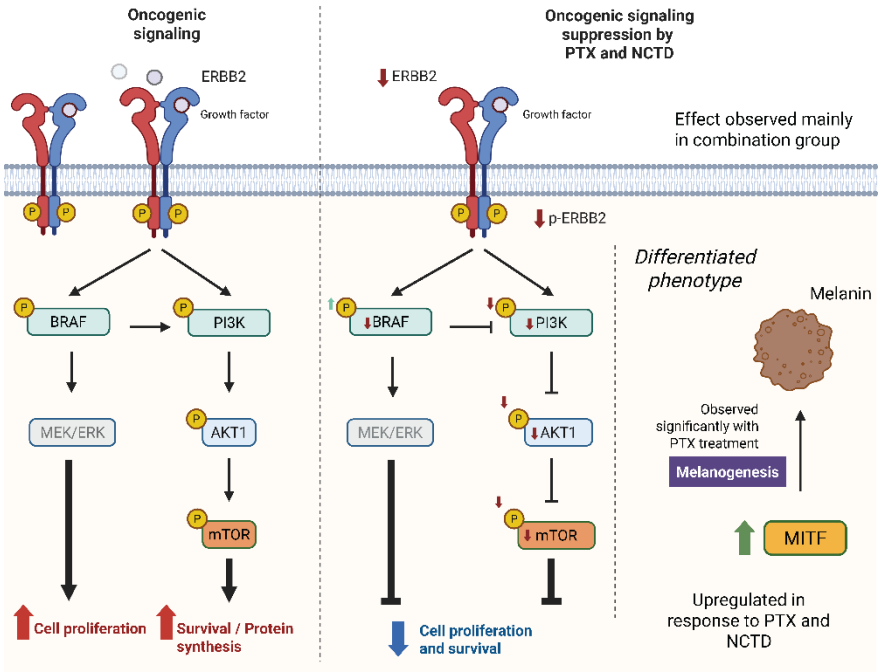

Fig. 11 Schematic summary of the main signaling pathways modulated by pentoxifylline (PTX), norcantharidin (NCTD), and their combination in B16-F1 melanoma tumors (Lara-Vega I et al., 2025).

The role of System X_c^- in modulating redox balance influences melanoma biology by sustaining glutathione pools and modulating extracellular glutamate signaling. Perturbation of the xCT function has been demonstrated to alter tumor-immune interactions and can paradoxically impair the efficacy of anti-PD-1/PD-L1 therapy through effects on exosomal PD-L1 and macrophage polarization (Liu N et al., 2021). Specifically, pharmacologic inhibition of xCT has been demonstrated to modify melanoma responses to immune checkpoint blockade via modulation of immunosuppressive exosome secretion by tumor cells, which promotes M2 polarization of tumor-associated macrophages (Liu N et al., 2021). This finding indicates that xCT plays a significant role in therapy resistance and immune

crosstalk within the melanoma tumor microenvironment, highlighting the complex interplay between tumor redox metabolism and immunotherapy response. Consequently, the targeting of xCT requires careful consideration regarding its potential immune implications and might prove most efficacious when integrated with immunomodulatory strategies.

The TME is a critical factor in oncogenic progression, facilitating immune evasion in melanoma by upregulating the PD-1/PD-L1 axis. This is an adaptive resistance mechanism that inhibits the cytotoxic activity of T lymphocytes. A notable correlation has been observed between disease progression and elevated plasma glutamate levels, which are associated with SLC7A11 activity. While this protein is essential for maintaining tumor redox homeostasis, its pharmacological inhibition initially suppresses neoplastic growth but then triggers a resistance mechanism. The resultant oxidative stress from xCT blockade induces the activation of transcription factors that promote the overexpression of PD-L1 as a compensatory response. This increase is not limited to the cell surface but also involves the secretion of PD-L1-rich exosomes. After their release into the microenvironment, these exosomes act as paracrine mediators, inducing the polarization of macrophages towards the immunosuppressive M2 phenotype. Consequently, this results in the weakening of anti-PD-1/PD-L1 immunotherapies, leading to the development of a sophisticated metabolic-immune resistance mechanism that limits the effectiveness of targeted treatments (Liu N et al., 2021).

In this context, System X_c^- becomes a valid tumor target in all mechanisms of tumor progression.

2.2.2 Squamous cell carcinoma

Squamous cell carcinoma (SCC) is a malignant neoplasm originating from keratinocytes of the epidermal spinous layer, representing the second most common cutaneous malignancy (Cozma EC et al., 2023). Histologically, SCC is characterized by the presence of atypical squamous epithelial cells that extend from the epidermis into the dermis. These cells are distinguished by their eosinophilic cytoplasm, vesicular nuclei, and variable keratinization, which can manifest as keratin pearl formation (Cozma EC et al., 2023). The hallmark pathological features of this condition include nuclear atypia, cellular pleomorphism, frequent mitoses, and dyskeratosis. SCC manifests in over 15 histologic subtypes, with the World Health Organization recognizing six primary forms: verrucous, acantholytic, lymphoepithelial, clear cell, spindle cell, and sarcomatoid variants (Cozma EC et al., 2023).

The pathogenesis of SCC is characterized by a high mutational burden induced by UV radiation. TP53 gene mutations serve as critical early events that lead to genomic instability and the accumulation of additional oncogenic mutations (Piipponen M et al., 2021). SCC typically progresses from precursor lesions, particularly actinic keratosis, through squamous cell carcinoma in situ to invasive carcinoma (Cozma EC et al., 2023). The major risk factors associated with this condition include exposure to UV radiation, immunosuppression, chronic inflammation, and high-risk viral infections (Cozma EC et al., 2023). Current treatment approaches include surgical excision with immunotherapy, which has demonstrated approximately 45% durable response rates in advanced disease (Trinconi Cunha M et al., 2025).

Cancer cells undergo a metabolic reprogramming process that enables them to support rapid proliferation and survival under stress conditions. Upregulation of System X_c^-/xCT (SLC7A11) is a common feature across epithelial cancers and serves to maintain redox homeostasis and resist ferroptotic cell death (Fantone S et al., 2024). Elevated SLC7A11/xCT expression has been implicated in various hallmarks of epithelial cancers, including proliferation, invasion, chemoresistance, and suppression of ferroptosis. In ovarian carcinoma, SLC7A11 overexpression is

associated with poor prognosis and resistance to platinum-based chemotherapy (Fantone S et al., 2024). CD44 isoform switching, particularly the expression of variant exon-containing isoforms such as CD44v3, has been demonstrated to correlate with invasive and metastatic competence in carcinoma models (Giraud J et al., 2022). CD44v3 has been identified as a marker of invasive cancer stem cells driving metastasis in gastric carcinoma, where its expression identifies subpopulations with enhanced metastatic potential (Giraud J et al., 2022).

AIM OF THE WORK

The aim of this thesis is to use cantharidin and norcantharidin, natural compounds with potent antitumour activity but significant systemic toxicity, in precision therapeutic agents through the development of targeted delivery strategies.

In particular, the main objectives are to clarify the complex molecular mechanisms through which these compounds induce cell death; to identify validated tumour biomarkers for targeted therapy; and finally to construct a molecule that has the ability to exploit the cytotoxic properties of CTD and NCTD but limited to tumour cells such as the ADCs. Its efficiency and delivery to tumour cells alone will then need to be tested, with a particular focus on malignant melanoma and glioma cells.

This work is an example of how translational research can bridge the gap between laboratory discoveries and clinical applications, potentially transforming an ancient traditional medicine remedy into modern precision oncology medicine.

MATERIALS AND METHODS

Materials

For Melanocytes Cascade Biologics Medium 254, Gibco Opti-MEM I Reduced Serum Medium, Human Melanocyte Growth Supplement (HMGS); for Keratinocyte cells and Human Carcinoma cells Cascade Biologics Medium 154 and Human Keratinocyte Growth Supplement (HKGS) were purchased from Thermofisher Scientific (Waltham, MA, USA).

Dulbecco's modified Eagle's medium (DMEM), fetal bovine serum (FBS), 0.25% Trypsin–EDTA solution, gentamicin solution 50 mg/ml and Thiazolyl blue tetrazolium bromide (MTT) were obtained from Sigma–Aldrich (Milan, Italy). Bradford reagent was obtained from Bio-Rad Italia (Milan, Italy).

Human Astrocytes were cultured in Astrocytes Medium kit Astrocyte Medium Kit a complete medium designed for optimal growth of normal primary astrocytes in vitro. Each Astrocyte Medium Kit consists of the next components: Astrocyte basal medium, fetal bovine serum, Astrocyte Growth supplement, penicillin/streptomycin solution. Confluent monolayers of HA cells were subcultured by usage of Primary Cells Detach Kit from Innoprot contains the following reagents for primary cells detach and subculture: DPBS (Dulbecco's Phosphate-Buffered Saline), T/E Solution (Trysin / EDTA solution) and TNS (Trysin Neutralization Solution).

PUREzol RNA Isolation Reagent was from Bio-Rad Italia, (Milan, Italy). The kit Go Taq 2-Step RT-qPCR System was obtained from Promega (Promega Italia Srl, Milan, Italy). The reagent for Bradford assay was from Bio-Rad Italia (Milan, Italy).

For Western Blot analysis and immunofluorescence, the following primary antibodies were used: anti-Actin 1:1000 (Sigma), anti-Vinculin 1:1000 (Sigma), anti-System X_c^- 1:1000 (Abcam), anti-Tubulin 1:1000 (Abcam), anti-CD44 1:1000 (Cell Signaling), anti-HO-1 (Cell signaling), anti-Nrf2

1:1000 (ab137550, Abcam; Milan, Italy), and anti-GPx4 (59735, cell signaling; Milan, Italy) and anti-HER1, anti-HER2 and anti-HER3 have been obtained from Takis Biotec. For Western blot, secondary peroxidase-labeled anti-rabbit IgG antibodies were from Bio-Rad Italia (Milan, Italy). For immunofluorescence, secondary anti-Rabbit IgG Alexa Fluor 488 (A32731) was obtained from Invitrogen. For the detection of ROS production, 2',7'-Dichlorofluorescein diacetate (DCFH-DA) (35845) was obtained from Sigma-Aldrich, (St. Louis, USA). For the evaluation of calcium influx, Fluo-4 direct Calcium Assay Kit Starter Pack (F10471) was purchased from Thermofisher Scientific (Waltham, MA, USA).

Cantharidin C7632 was purchased from SIGMA-ALDRICH. Norcantharidin sc 280719 was purchased from Chemcruz (Santa Cruz), SKF96365 (S7809, Sigma-Aldrich), Caffeine CO750-1008, EGTA, Molecular Biology Grade 324626 (Millipore), Dimethyl fumarate 242926 (Sigma Alderich), Anticorpo II antihuman (Thermofisher), anti-mouse (Biorad), N-acetyl-L-cystein (Sigma Alderich)

All chemicals were of analytical or reagent grade and were used without further purification.

ADC Conjugation

ADC was conjugated by ProteoGenix SAS (Espace Europèen de l'Entreprise; 19 rue de la Haye 67300 Schiltigheim, France).

Cell cultures

Human Astrocytes (HA) were purchased from Innoprot. Cells were cultured in Astrocytes Medium kit Astrocyte Medium Kit a complete medium designed for optimal growth of normal primary astrocytes in vitro. Each Astrocyte Medium Kit consists of the next components: Astrocyte basal medium, fetal bovine serum, Astrocyte Growth supplement, penicillin/streptomycin solution. Confluent monolayers of HA cells were subcultured by usage of Primary Cells Detach Kit from Innoprot contains the following reagents for primary cells detach and subculture: DPBS (Dulbecco's Phosphate-Buffered Saline), T/E Solution (Trypsin / EDTA solution) and TNS (Trysin Neutralization

Solution). For the experiments, 3×10^4 and 2.5×10^5 cells were seeded in 24 multi well plate and 35-mm tissue culture dishes respectively and grown up to 80% confluence for 18–24 h before treatments.

For melanoma cell lines we would like to thank the "Laboratorio di Fisiopatologia Cutanea dell'Istituto San Gallicano" (Dr Barbara Bellei and Dr Daniela Kovacs) for providing the Mel16-AR-P, Mel16-AR-Ldx, Mel66-CL, Mel77-DM, NHMS32, NHMA29, NHKD30 and SCC1300-UC cell lines (Kovacs D. et al., 2016) (Bellei B. et al., 2021). The melanoma cell lines were maintained in OPTIMEM medium supplemented with 10% Fetal Bovine Serum (FBS), L-glutamine, and penicillin/streptomycin. These lines were subcultured 2–3 times per week at splitting ratios between 1:2 and 1:3; detachment was achieved using 3 mL of trypsin, subsequently neutralized with 3 mL of complete medium, yielding approximately 4 x 10^6 cells per T75 flask after 48 hours. Carcinoma lines (SCC1300-UC) and primary keratinocytes (NHKD30, used until passage 4) were cultured in Cascade 154 medium supplemented with penicillin/streptomycin, specific growth factors (500 µL per 50 mL), and 0.07mM Ca^{2+}. NHKD30 cells were split weekly at ratios of 1:5 to 1:6 following three PBS washes and a 5-minute incubation with 2 mL of trypsin, neutralized with 2 mL of complete DMEM. Normal Human Melanocytes (NHM, used until passage 12–13) were maintained in Cascade 254 medium with growth factors, with media changes every other day due to their slow growth rate. NHM cells were split weekly at ratios of 1:3 to 1:4 using 2 mL of trypsin neutralized with complete DMEM. Centrifugation for melanoma lines was performed at 1200 RPM for 7 minutes, while NHKD30 and NHM lines were centrifuged at 800 RPM for 5 minutes, all at 24°C. Experimental seeding densities were defined as follows: 50,000 cells/well for 24-well plates (70,000 for flow cytometry), 7,000 cells/well for 96-well plates, and 25,000 cells for round coverslips.

U373-MG human astrocytoma cells, U251-MG human glioblastoma cells and U87MG human glioblastoma cells were purchased from ATCC (Manassas, VA, USA). Glioma cells were cultured in DMEM supplemented with 10% FBS, 2 mM L-glutamine, and 40 µg/ml gentamicin at 37 °C in a humidified 5% CO_2 incubator. Confluent monolayers of U373 cells were subcultured by conventional

trypsinization (EuroClone). For the experiments, 3×10^4 and 2.5×10^5 cells were seeded in 24 multi well plate and 35-mm tissue culture dishes respectively and grown up to 80% confluence for 18–24 h before treatments.

Cell density was:

10 cm Plate: 1,000,000 cells.

6 cm Plate: 400,000 cells.

3.5 cm Plate: 250,000 cells.

24-well Plate: 30,000 cells.

96-well Plate: 5,000 cells.

Tissue culture dishes respectively and grown up to 80% confluence for 18–24 h before treatments. To expand the culture, all cells were detached from the substrate by its corresponding detach procedure and seeded in other 25- or 75-cm2 flasks. Each procedure was performed under laminar flow hood (Biohazard) to ensure sterile conditions.

Treatment conditions

Cells were maintained in culture for 24 h in medium. At the end of 24 h, medium was removed from each plate, and fresh medium supplemented with specific treatment was added to perform the stimulation. Treatments were performed in:

- 10 mL in case of using 10-cm Plate.

- 2.5 mL in case of using 6-cm Plate.

- 1 mL in case of using the 3.5-cm diameter plates.

- 0.5 mL in case of using the 1.5-cm diameter plates

- 50-100 µL in case of using 96-well Plate.

Cells were treated with Cantharidin and Norantharidin at different concentrations and with different combinations of the different stimuli as indicated in the results.

Cantharidin was dissolved in dimethyl sulfoxide (DMSO) to obtain a solution of known concentration of 50 µM. Norcantharidin was dissolved in dimethyl sulfoxide (DMSO) to obtain a solution of known concentration of 100 µM.

MTT assay

MTT assay was performed as indicated by manufacturer's instructions on HA, SH-SY5Y cells and U373 cells at the end of each incubation period. Briefly, MTT solution (stock solution of 0.5 mg/ml) was added to the cell culture at the final concentration of 10%. After incubation at 37 °C for 4 hours, formazan crystals were dissolved in lysis buffer (4 mM HCl, 0.1% NP40 (v/v) in isopropanol) and the optical density (O.D.) of each sample was measured using a microplate reader at 570 nm using Tecan Spark10M reader (Tecan, Mannedorf, Switzerland).

Parallel Artificial Membrane Permeability Assay (PAMPA)

Passive permeability was evaluated using the Corning® BioCoat™ Pre-coated PAMPA Plate System (Discovery Labware, Inc., Bedford, MA; Catalog Number 353015). The plate system was equilibrated to room temperature for at least 30 minutes. Compound solutions (100–200 µM) were prepared by diluting stock solutions into Phosphate Buffered Saline (PBS). The assay was performed by adding 300 µL of the compound solution to each well of the receiver plate (donor plate) and 200 µL of PBS to each well of the filter plate (acceptor plate). The filter plate was then lowered onto the receiver plate and the assembly was incubated at room temperature for 5 hours. Following incubation, the plates were separated, and compound concentrations in both donor (C_D) and acceptor (C_A) wells were determined using UV-VIS spectroscopy. The effective permeability coefficient (P_e), expressed in cm/s, was calculated using the following formula:

$$P_e = \left(-ln\left(1 - (C_A(t)/C_e q)\right)\right)/(A * (1/V_D + 1/V_A) * t)$$

Where:

A = filter area (0.3 cm^2)

V_D = donor well volume (0.3 mL)

V_A = acceptor well volume (0.2 mL)

t = incubation time (18 000 s)

$$C_eq = (C_D(t) * V_D + C_A(t) * V_A) / (V_D + V_A)$$

Nuclear Extract Preparation

To evaluate protein translocation, cytosolic and nuclear fractions were isolated using a differential lysis protocol. Cells were washed with room-temperature PBS, harvested in cold PBS using a cell scraper, and collected on ice to preserve protein integrity. Following centrifugation at 5000 RPM (4°C, 5 min), cell pellets were resuspended in 4–5 volumes of hypotonic Buffer A (Cytoplasmic Lysis: 10 mM HEPES (pH 7.9), 10 mM KCl, 1.5 mM $MgCl_2$, and 0.5 mM DTT) supplemented with a 1:100 protease inhibitor cocktail and incubated on ice for 10 minutes. Cytosolic membranes were selectively lysed by adding 0.1% NP40, followed by 10 seconds of vortexing and centrifugation at 12,000 RPM (4°C, 10 min); the resulting supernatant containing cytosolic proteins was collected. The remaining nuclear pellet was resuspended in 4–5 volumes of hypertonic Buffer C (Nuclear Lysis: 20 mM HEPES (pH 7.9), 420 mM NaCl, 1.5 mM $MgCl_2$, 25% (v/v) glycerol, 0.2 mM EDTA, and 0.5 mM DTT) (1:50 protease inhibitors) and subjected to mechanical agitation via vortexing and periodic flicking every 2–3 minutes for a total of 15 minutes. Final nuclear lysis was achieved by adding 0.05% NP40, followed by another 15-minute period of agitation and a final centrifugation at 14,000 RPM (4°C, 15 min). The supernatant, containing the nuclear fraction, was recovered for downstream Western Blot analysis.

Total Extracts Preparation

After treatments at the indicated time points, the cells were mechanically detached with a scraper in cold PBS. Thereafter, the cells were centrifuged at 5000 rpm, 4°C for 5 min. Total extracts were prepared by adding buffer TEEN (10 Mm Tris HCl pH 7.4, 1 mM EGTA, 1 mM EDTA, 150 mM NaCl, 1% Triton X-100, protease inhibitor cocktail) to the cell pellets. The samples were kept at 4°C for 30 min, shaking every minute. Next, the samples were centrifuged at 14000 rpm, 4°C for 15 minutes. At the end of centrifugation, the supernatant containing the cell proteins was taken out and stored in aliquots at -80°C. The total protein content was determined according to the Bradford method.

Western Blotting

Proteins were separated by SDS-PAGE and electroblotted onto nitrocellulose (TRANS-BLOT Turbo Transfer System, Bio-Rad Italia, Milan, Italy). Following transfer, each membrane was incubated in blocking solution (EveryBlot Blocking Buffer, Bio-Rad Italia, Milan, Italy) for 5 minutes at room temperature. The membrane was incubated overnight at 4 °C with primary antibody dissolved in TBS-T (Tris Buffer Saline: 20 mM Tris-HCl pH 7.4; 137 mM NaCl; 0.1% Tween 20) containing 5% non-fat dried milk powder (Blotting-Grade Blocker, PanReac AppliChem, ITW reagents, Monza, Italy). The following primary antibodies were employed: anti-Vinculin 1:1000 (Sigma), anti-System Xc- 1:1000 (Abcam), anti-Tubulin 1:1000 (Abcam), anti-CD44 1:1000 (Cell Signaling), anti-HO-1 (Cell signaling), anti-Nrf2 1:1000 (ab137550, Abcam; Milan, Italy), and anti-GPx4 (59735, cell signaling; Milan, Italy) anti-α-Actin 1:1000 (A2066, Sigma-Aldrich; Milan, Italy, anti-GPx4 (59735, cell signaling; Milan, Italy). The membrane was incubated overnight at 4 °C with primary antibody dissolved in TBS-T containing 5% Bovin Serum Albumin (BSA). The membrane was then incubated with the appropriate HRP-conjugated secondary antibody (Biorad, Milan, Italy) (1:3000) in TBS-T containing 2.5% milk or 2.5% BSA for 1 h at room temperature. The reagent used for detection was Clarity Western ECL substrate (170-5061, Biorad, Milan, Italy). Differences between samples with

respect to the presence of the proteins of interest were normalized using α-actin or Vinculin or α-Tubulin protein as reference.

Quantitative Real-Time Reverse Transcription–Polymerase Chain Reaction

Total RNA was purified by using PUREzol Reagent and reverse transcribed with GoTaq 2-step RT-qPCR system. cDNA was then amplified for the following genes: NF-E2-like basic leucine zipper transcriptional activator (NRF2; S74017.1), System X_c^- (xCT subunit; NM_014331.4), superoxide dismutase (SOD1; NM_000454.5), catalase (CAT; NM_001752), heme-oxygenase-1 (HO-1; NM_002133.3). mRNA for Glyceraldehyde 3-phosphate dehydrogenase (GAPDH; NM_002046.7) was examined as the reference cellular transcript. The sequences of primers used for RT-qPCR were reported in table 1. The SYBR-Green method was applied to calculate PCR product quantification. Reactions were performed in an Agilent Aria Mx machine (Agilent technologies) using the following program: 45 cycles of 95 °C for 15 s, 60° C for 60 s, 72 °C for 20 s. GAPDH mRNA amplification products were present at equivalent levels in all cell lysates. Values were calculated relative to the internal housekeeping gene according to the second derivative test (delta–delta Ct ($2^{-\Delta\Delta CT}$) method).

NRF2	Forward 5'- AAC TAC TCC CAG GTT GCC C- 3'
	Reverse 5' - CGA AGA AAC CTC ATT GTC ATC - 3'
xCT	Forward 5'- GGT GGT GTG TTT GCT GCT- 3'
	Reverse 5' – GCT GGT AGA GGA GTG TGC - 3'
SOD1	Forward 5'- AGT AAT GGA CGA GTG AAG - 3'
	Reverse 5' – GGA TAG AGG ATT AAA GTG AGG A - 3'
CAT	Forward 5'- TCA GGT TTC TTT CTT GTT CAG- 3'
	Reverse 5' – CTG GTC AGT CTT ATA ATG GAA TT - 3'
GAPDH	Forward 5'- TTG TTG CCA TCA ATG ACC C- 3'
	Reverse 5' – CTT CCC GTT CTC AGC CTT G- 3'
HO-1	Forward 5'- AAG CTG GTG ATG GCC TCC- 3'
	Reverse 5' – GGG ATG ACC TCC TGC CAG - 3'
CD44s	Forward 5'- GCG GCT CCT CCA GTG AAA G- 3'
	Reverse 5' – CTT GGT CTC TGG TAG CAG GG - 3'
CD44A	Forward 5'- CAC CCC AAA TTC CAG AAT GGC - 3'

Reverse 5’ – CTT CTG CCC ACA CCT TCT TC - 3’

CD44v2 Forward 5’- CCAAGAGGCAAGAAACCTG - 3’

Reverse 5’ – GTG TTG TTG TGT GAA GAT GAT TC - 3’

CD44v3 Forward 5’- GCA GGC TGG GAG CCA AAT G - 3’

Reverse 5’ – CTG ATC CAG AAA AAC TGA GGT G - 3’

CD44v4 Forward 5’- CAC ACA AAA CAG AAC CAG GAC - 3’

Reverse 5’ – CCT TGT GGT TGT CTG AAG TAG - 3’

CD44v5 Forward 5’- GGC ACC ACT GCT TAT GAA GG - 3’

Reverse 5’ – GCT CAT GGT GAA TGA GGG G - 3’

CD44v6 Forward 5’- GTA CAA CGG AAG AAA CAG CTA C - 3’

Reverse 5’ – GTC CCT GTT GTC GAA TGG G - 3’

CD44v7 Forward 5’- GCC TCA GCT CAT ACC AGC C - 3’

Reverse 5’ – CTT GAT GAC CTC GTC CCA TG - 3’

CD44v8 Forward 5’- CTC CAG TCA TAG TAT AAC GCT TC - 3’

Reverse 5’ – GGT CCT GTC CTG TCC AAA TC - 3’

CD44v9 Forward 5’- CTA CAT CAC ATG AAG GCT TGG - 3’

Reverse 5’ – GAT GTC AGA GTA GAA GTT GTT GG - 3’

CD44v10 Forward 5’- GCT CAA CTA CTT TAC TGG AAG G - 3’

Reverse 5’ – CCA GTC TTA GCT GAG GTC AC - 3’

Flow Cytometry Analysis

For flow cytometric analysis, cells were detached 24 hours after seeding, centrifuged at 1200 rpm for 5 minutes, and washed with Phosphate Buffered Saline (PBS). For the assessment of surface expression and internalization, cell pellets were resuspended in a staining buffer consisting of PBS supplemented with 0.5% Bovine Serum Albumin (BSA) and incubated for 30 minutes with primary antibodies against Her1 (40 µg/mL), Her2, Her3, or CD44 (1:100). To evaluate receptor internalization, samples were split: one half was incubated at 37°C to allow endocytosis, while the other half remained at 4°C to serve as the surface-expression control. After three washes in PBS, cells were incubated with secondary anti-mouse or anti-human antibodies (5 µg/mL) for 30 minutes at 4°C in the dark, followed by final washes. For Reactive Oxygen Species (ROS) detection in NAC-treated experiments, cells were detached following the treatment period and resuspended in a 1 µM solution

of 2',7'-dichlorofluorescin diacetate (DCFH-DA) for 30 minutes at 37°C. Following three washes in PBS, at least 10,000 events per sample were acquired and analyzed using a flow cytometer. Analysis and graphs of the data were performed using CytExpert software.

Immunofluorescence and Confocal Analysis

Cells were grown on coverslips and fixed with 4% PFA in PBS, followed by permeabilization with 0.1% Triton X-100 in PBS. Nrf2 primary antibody (1:100) were incubated overnight at 4°C with the fluorophore-conjugated secondary antibodies (Alexa Fluor™488, Invitrogen, Carlsbad, CA, USA) and DAPI for nuclei visualization, were mounted in antifade (SlowFade Diamond, antifade mountant with DAPI, Invitrogen, Carlsbad, CA, USA), and examined under a confocal microscope (Nikon A1HD25) equipped with CFI Plan Apochromat Lambda D 40X.

Measurement of calcium influx

For the detection of calcium influx, Fluo-4 direct Calcium Assay Kit Starter Pack (Thermofisher Scientific, Waltham, MA, USA) was used. Cells were seeded in 96-well plate and, at the end of the treatment, a 2X Fluo-4 Direct calcium reagent loading solution was added directly into the wells. The plates were incubated for 45 minutes at 37°C with the reagent. At the end of the incubation period, the fluorescence was measured with excitation at 494 nm and emission at 516 nm at ImageXpress Pico with a result in positive cell average intensities (Molecular Devices San Jose, California USA).

Measurement of ROS production

ROS production was measured using 2',7'-Dichlorofluorescein diacetate (DCFH-DA) (Sigma-Aldrich, St. Louis, USA). DCFH-DA is a non-fluorescent probe capable of permeating cells, which can be hydrolyzed by intracellular esterase to yield DCFH, which forms fluorescent DCF upon oxidation by intracellular ROS. Cells were mechanically detached with T/E solution and centrifuge

at 2500 rpm for 5 min. DCFH-DA 1 μM is added to the cell pellets and is kept in incubation for 30 min at 37°C. At the end of the incubation period, the cells were washed two times in PBS and centrifuge at 2500 rpm for 5 min. The samples were resuspended with 400 μL of PBS and read with FITC filter at CytoFlex (Excitation 488 nm – Emission 525/40 BP) (Beckman Coulter, Brea, California USA).

Statistical Analysis

All data are expressed as mean ± standard error of the mean (SEM) of *n* observations. Statistical analysis of the data was performed using Graph Pad PRISM software (San Diego, CA, USA). Statistical significance was assessed with the one-way ANOVA test or *t*-test, followed by the Tukey post-test or two-way ANOVA followed by Sidak post-test. Differences are considered statistically significant at $p \leq 0.05$.

RESULTS

1. Screening of cantharidin and norcantharidin effects on the viability of glioma and skin cancer cells

In order to determine the most efficacious molecule for the treatment of solid tumours, a screening was performed of the cytotoxic effects on glioma and skin tumour cells of CTD and NCTD. It has been established that these molecules are potent cytotoxic agents (Naz F. et al., 2020) (Tarleton M. et al., 2012), yet despite their presentation as antitumour agents, there is a paucity of data in the literature regarding their effects on normal cells. The objective of these preliminary experiments is to evaluate lethal concentrations in tumours and their non-tumour counterparts, in order to accurately determine the side effects of a potential treatment.

1.1 Cantharidin exerts a dose dependent reduction in the viability of both astrocytes and glioma cells

Initially, a dose-response curve was performed on several human glioma lines (U251, U87 and U373) and on human astrocyte cells (HA) using the MTT assay.

For this purpose, growing concentrations of CTD were used, ranging from a minimum of 0.1 µM to a maximum of 50 µM. The treatment was administered for 24 hours (Fig. 12 A, C and E) and 48 hours (Fig. 12 B, D and F).

Results show that the effect of CTD on cell viability is dose-dependent. Indeed, higher concentrations lead to greater reduction in cell viability in comparison to the control. In the U87 cell line, CTD induces a significant reduction in viability starting at a concentration of 10 µM (Fig. 12 A), while in the U373 and U251 cells this result is obtained at half the concentration (5 µM).

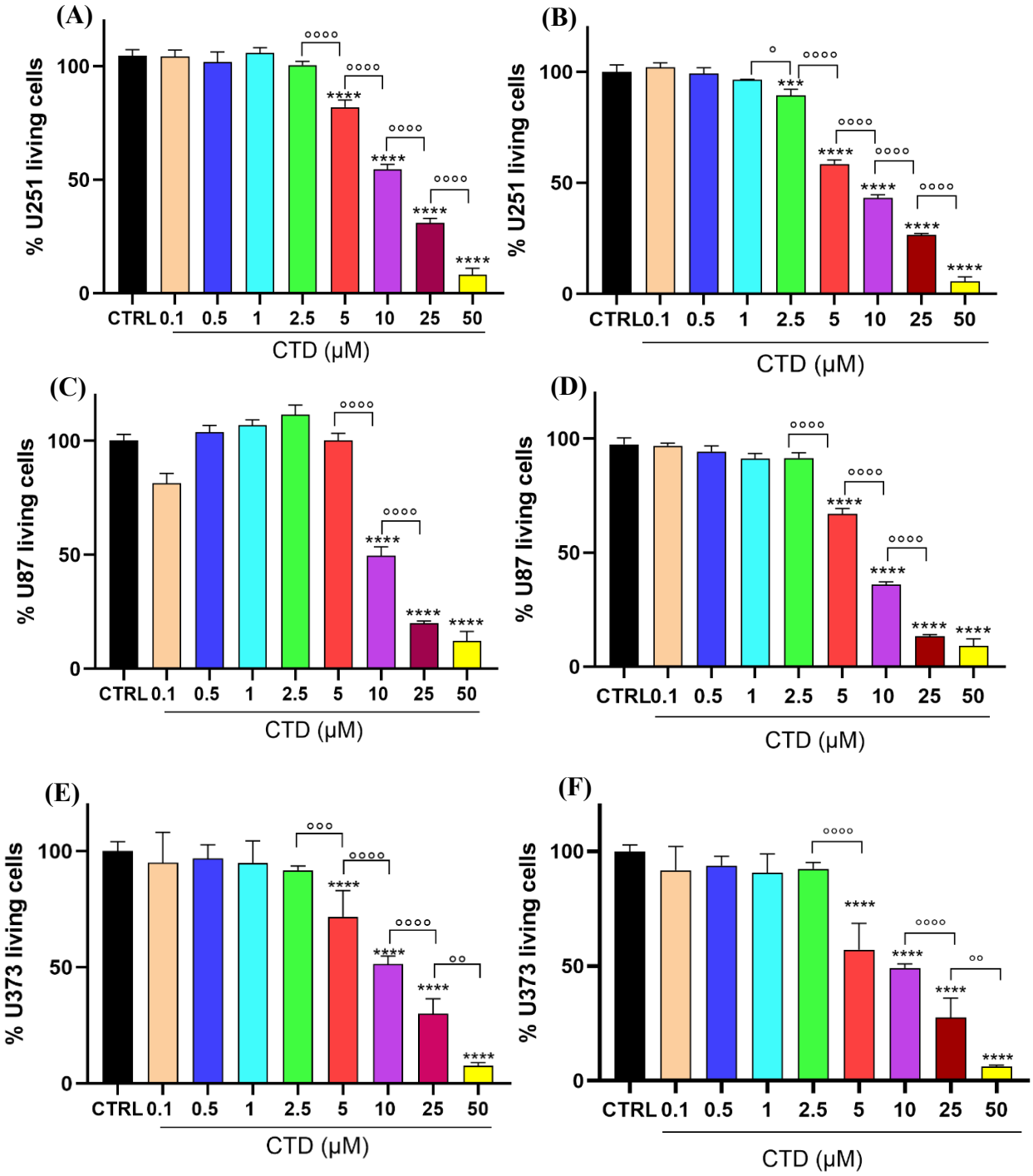

Fig. 12. Impact of growing concentrations of CTD on U251 (**A** and **B**), U87 (**C** and **D**) and U373 (**E** and **F**) for 24h (**A**, **C** and **E**) and 48h (**B**, **D** and **F**) of exposure. Cell viability was assessed by MTT performed as specified in materials and methods. Data are expressed as a percentage of viable cells relative to the untreated control (CTRL). Bars represent the mean ± standard deviation (SD) of n=3 independent experiments for panels A-D and n=9 for panels E-F. Statistical significance was determined by One-way ANOVA followed by Tukey's post-hoc test. Significance levels: **** $p < 0.0001$ vs. CTRL; °°°° $p < 0.0001$, °°° $p < 0.001$, °° $p < 0.01$ and ° $p < 0.05$.

It is noteworthy that the administration of the same doses results in a substantial decline in viability

48 hours after the commencement of treatment. The findings of the experiment suggest that the inhibitory concentration of cantharidin, defined as the dose that results in a reduction in viability of approximately 50% (IC_{50}) compared to the control group, corresponds to 10 µM. This concentration will be used in the analysis of cell pathway activation.

In order to assess the effects of CTD on non-tumour cells, the viability of normal HA was analysed using the MTT assay in a dose-response experiment. Treatment with CTD for 24 hours resulted in a reduction in viability, even at lower concentrations than those previously found in tumour cell lines, and again in a dose-dependent manner. Indeed, the inhibitory concentration at which cell viability is reduced by 50% corresponds to 5 µM (Fig. 13).

Cantharidin has been demonstrated to exert a substantial cytotoxic effect on diverse cell lines, particularly on non-tumour astrocytes.

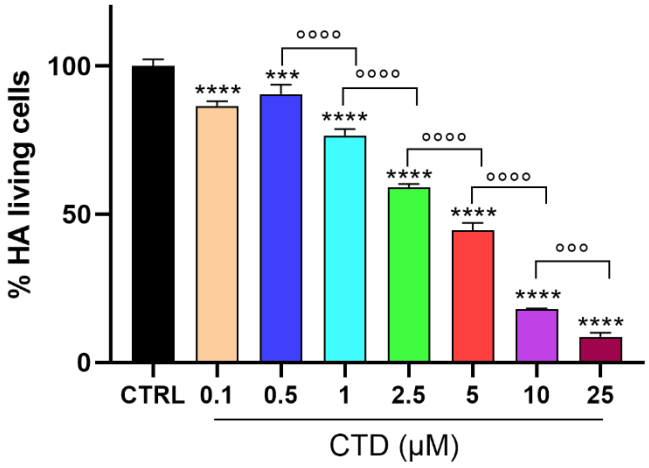

Fig. 13 Dose-dependent effect of a 24-hour treatment with CTD on the viability of HA cells. Cell viability was assessed by MTT that was performed as specified in materials and methods. Data are expressed as a percentage of viable cells relative to the untreated control (CTRL). Bars represent the mean ± standard deviation (SD) of n=3 independent experiments. Statistical significance was determined by One-way ANOVA followed by Tukey's post-hoc test. Significance levels: **** $p < 0.0001$ and *** $p < 0.001$ vs. CTRL; °°°° $p < 0.0001$ and °°° $p < 0.001$

1.2 The comparison of Cantharidin effects on cellular viability of human astrocytes and glioma cells

The comparative impact of the molecule on tumour cells and healthy cells (HA) was initially to be greater on the former. However, the data may have been distorted by the significant disparity in the basal proliferation rates exhibited by the two lines. In order to distinguish the net cytotoxic effect and ascertain whether the molecule acts with different mechanisms or efficacy between the two cell models, the data were reprocessed by normalising growth over 24 hours of treatment. The elimination of the kinetic bias of proliferation was achieved by the subtraction of the physiological cell increase from both the control and treated samples. This methodological approach permitted the evaluation of the intrinsic lethal efficacy of the molecule, thereby determining whether the greater susceptibility observed in HA was an artefact of their slower growth or reflected a real divergence in biochemical sensitivity to treatment.

The result of this analysis performed on HA and U373 (Fig. 14) indicates that the net effect of CTD is comparable between the two cell lines. This finding suggests that CTD may induce cell death in an analogous manner to that observed in normal and tumour cells.

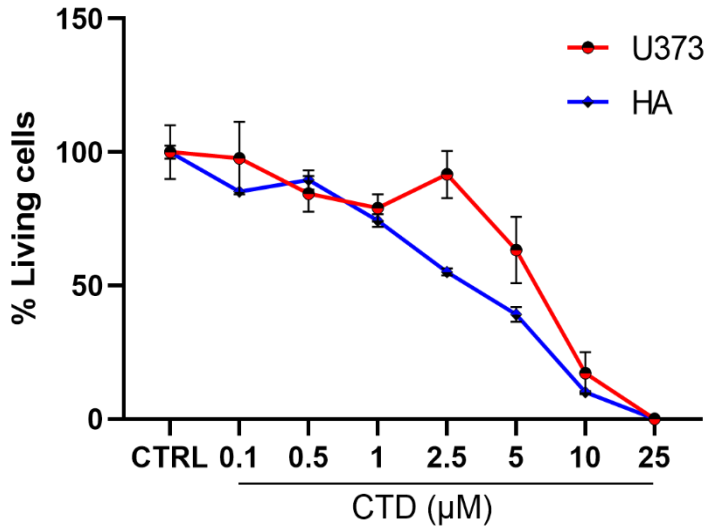

Fig. 14 Analysis of previous experiments normalized by subtraction of the physiological cell increase from both the control and treated samples in U373 and HA cells after 24 h of treatment.

1.3 The cytotoxic effect of CTD increases in longer exposure

To evaluate the persistence of the cytotoxic effect of cantharidin, the MTT assay was performed on U373 cells over longer periods of time.

The treatment was performed with a single administration on day one (Fig. 15), in this way, it was possible to verify if CTD effect could persist in longer exposure.

Cell viability was tested at the initial time point (T=0), i.e. when treatments began, and subsequently on a daily basis for the following days.

The objective of this procedure is to simulate the effectiveness of treatment with a cytotoxic drug in reducing tumour cells despite their high proliferative capacity. The vitality analysis demonstrated that CTD preserves its toxic effect over time, persisting for up to 192 hours following treatment, thereby suggesting that the molecule exhibits notable stability.

Moreover, these experiments demonstrate that lower concentrations of CTD result in elevated toxicity levels over time. This experiment revealed that a reduction in viability was observed even at low concentrations of cantharidin, starting at CTD 2.5 µM seven days after treatment. Moreover, the toxic

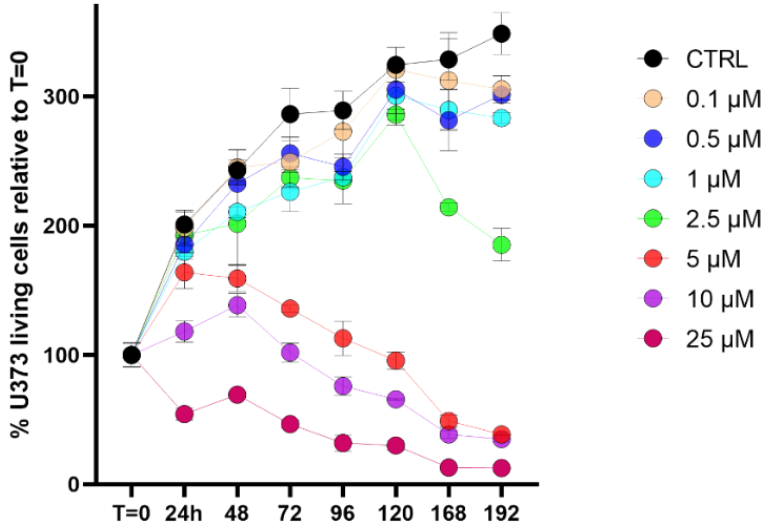

Fig. 15. Long-term growth kinetics and viability of U373 cells under chronic CTD exposure over time. The x-axis represents the incubation time expressed in hours (h). Data represent the mean ± standard deviation (SD) of n=3 independent experiments.

effect is sustained over time, persisting in its reduction of cell viability. Furthermore, it was shown that the toxicity of CTD increases with time, indicating that, in addition to dose dependence, there may also be time dependence.

1.4 Cantharidin reduces cell viability of melanoma cells and shows milder effects on melanocytes

Subsequently, a screening was conducted for melanoma and carcinoma cells with the objective of determining the level of cell toxicity of CTD and its antitumour properties. As with gliomas, a dose-response curve was then performed on three *ex vivo* human melanoma cell lines (MEL77-DM, MEL66-CL and MEL16-AR-P), one *ex vivo* human carcinoma cell line (SCC1300-UC) and normal human melanocyte cells (NHMS32) using the MTT assay.

As in the preceding experiment, growing concentrations of CTD were used, starting from a minimum of 0.1 µM but decreasing the maximum point, which in this experiment reached 25 µM (Fig. 16). The duration of treatment was limited to a maximum of 24 hours.

The graph shows that the effect of CTD on cell viability is not dose-dependent, as previously observed in gliomas. However, significant levels of toxicity are detected starting from the concentration of 5 µM, indicating a slight increase but not a substantial progression (Fig. 16).

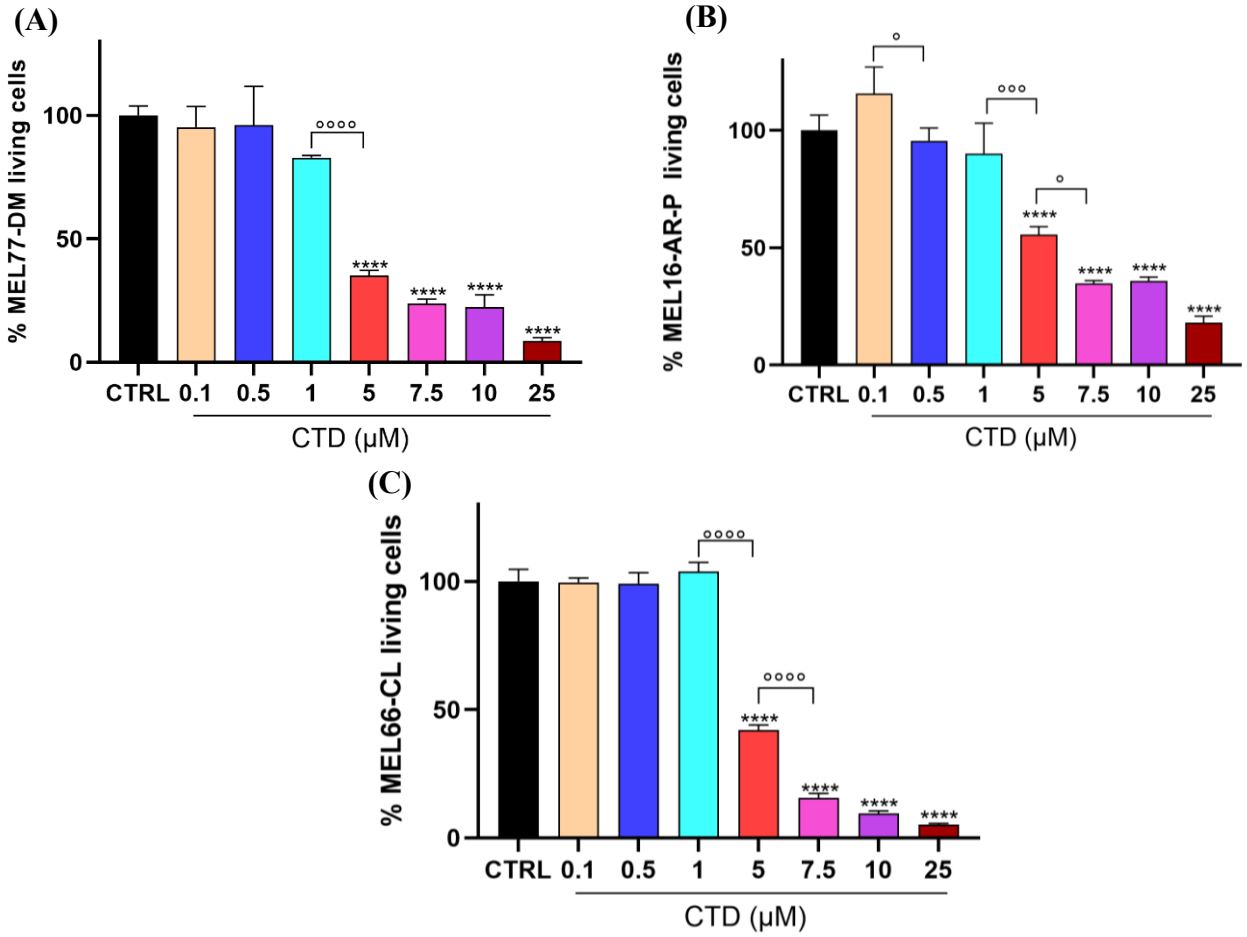

Fig. 16. Impact of growing concentrations of CTD on MEL77-DM (**A**), MEL16-AR-P (**B**) and MEL66-CL (**C**) for 24h of exposure.

Cell viability was assessed by MTT performed as specified in materials and methods. Data are expressed as a percentage of viable cells relative to the untreated control (CTRL). Bars represent the mean ± standard deviation (SD) of *n*=3. Statistical significance was determined by One-way ANOVA followed by Tukey's post-hoc test. Significance levels: **** $p < 0.0001$ vs. CTRL; °°°° $p < 0.0001$, °°° $p < 0.001$ and ° $p < 0.05$.

In contrast to the concentration that was utilised for gliomas, the concentration that has been selected for subsequent experiments analysing the cellular pathways activated by cantharidin is 5 or 7.5 µM, depending on the type and duration selected for the experiment.

In the viability analysis experiment performed on carcinoma/keratonocytes cells (SCC1300-UC, NHKD30) and normal melanocytes (NHMS32), the same concentrations chosen for gliomas were used for SCC1300-UC, while for NHMS32 those of their tumour counterpart were used and only four concentrations were used to treat NHKD30 (0.1, 1, 10, 25 µM).

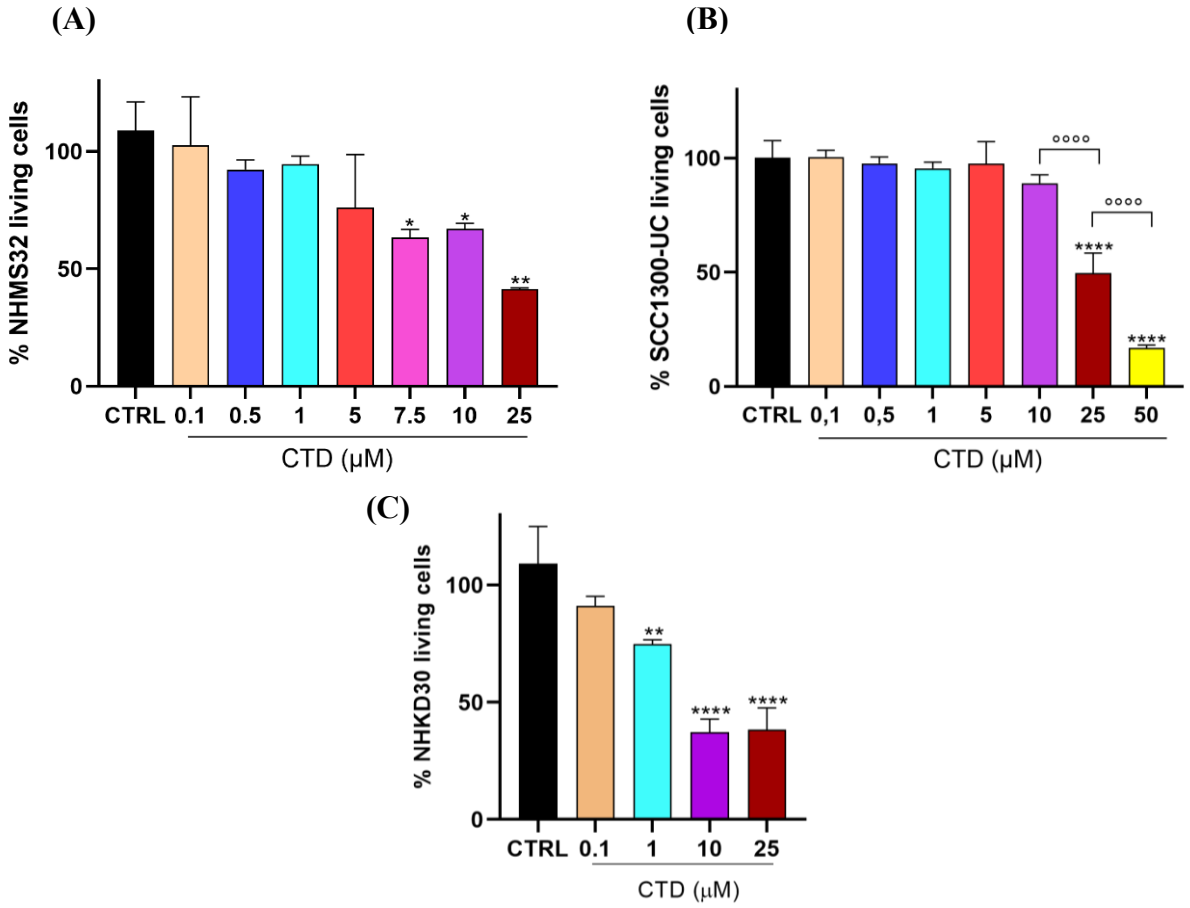

Fig. 17. Impact of growing concentrations of CTD on NHMS32 (**A**), SCC1300-UC (**B**) and NHKD30 (**C**) for 24h of exposure. Cell viability was assessed by MTT performed as specified in materials and methods. Data are expressed as a percentage of viable cells relative to the untreated control (CTRL). Bars represent the mean ± standard deviation (SD) of *n*=3 independent experiments for panel A and C and *n=6* for panel B. Statistical significance was determined by One-way ANOVA followed by Tukey's post-hoc test. Significance levels: **** $p < 0.0001$, ** $p < 0.01$ and * $p < 0.05$vs. CTRL; °°°° $p < 0.0001$.

The results obtained on these two cell lines differ significantly from all previous viability experiments. Indeed, a milder effect of CTD on NHMS32 was detected, with the same toxicity being detected at higher doses in comparison to previous data (Fig. 17 A). The findings indicate that melanomas exhibit heightened response, with the potential to mitigate adverse on healthy cells.

In a similar manner, the results obtained on SCC1300-UC demonstrate that the CTD cytotoxic effects begin at a concentration of 25 µM, reaching 50% of viability levels (Fig 17 B). This is a highly significant difference when compared to other tumour lines, thus indicating the high level of resistance of these cells to this particular molecule. On the contrary NHKD30 shown more sensitivity to CTD cytotoxicity, with a significant reduction in cell viability starting from 1 µM concentration but reaching a comparable level of vital cells at 25 µM to melanocytes.

In summary, the results demonstrate that CTD has exhibited pronounced cytotoxic effects on the majority of the cell lines examined, with this effect being exacerbated by increasing concentrations and exposure times. This result is encouraging in the context of the development of an anti-cancer drug, particularly in melanoma lines where the cytotoxic effect on normal cells is milder. This property lends itself more to a therapy with a more limited number of side effects.

1.5 Norcantharidin displays a reduced cytotoxicity compared to CTD and shows low side effects on melanocytes

In order to evaluate the effects of NCTD and assess a possible reduction in side effects as reported in the literature, a dose-response curve with this molecule was also performed.

Previous data obtained in our laboratory demonstrated that NCTD induced mortality comparable to that of CTD at concentrations approximately 10 times higher. However, considerable variability was observed between the cell types analysed (Fig. 18 A).

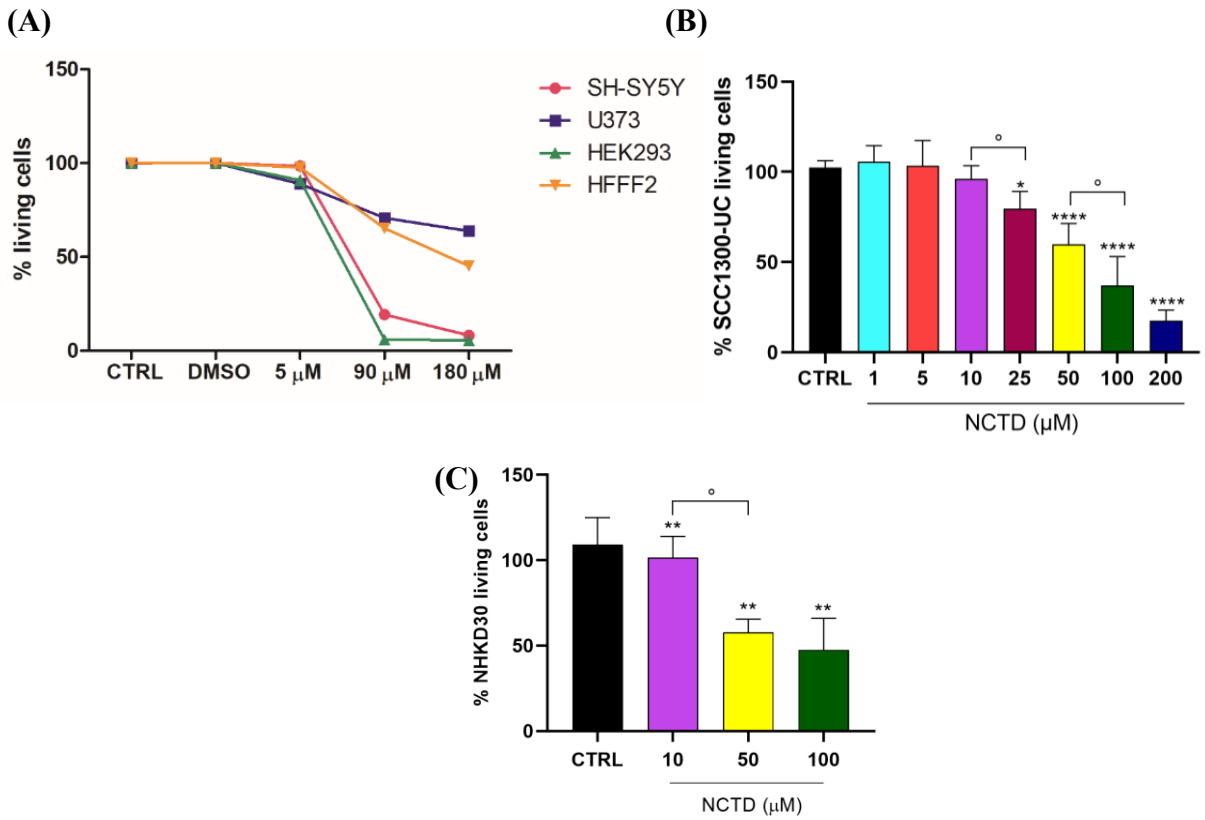

Fig. 18. Impact of growing concentrations of NCTD on different cell lines (**A**), SCC1300-UC (**B**) and NHKD30 (**C**) for 24h of exposure. Data in panel A consist of previously generated laboratory findings, provided for comparative purposes. Cell viability was assessed by MTT performed as specified in materials and methods. Data are expressed as a percentage of viable cells relative to the untreated control (CTRL). Bars represent the mean ± standard deviation (SD) of *n=6* for panel B and *n=3* for panel C. Statistical significance was determined by One-way ANOVA followed by Tukey's post-hoc test. Significance levels: **** $p < 0.0001$ and * $p < 0.05$ vs. CTRL; ° $p < 0.05$.

Among these, U373 glioma cells showed that even at very high concentrations of NCTD (180 μM), cell viability did not fall below 50%. This observation underscores the notion that NCTD exerts a comparatively milder effect on this cell type than that observed in Human Foreskin Fibroblast-2 (HFF2) and human neuroblastoma cells (SHSY5Y). In human carcinoma cells, however, the cytotoxicity of NCTD is comparable to that of CTD, exhibiting significant mortality starting at a concentration of 25 μM and reaching IC_{50} at a concentration of 50 μM (Fig. 18 B). Unlike CTD, the toxicity of NCTD appears to be very similar in carcinomas and their normal counterparts (Fig. 18 B and C), indicating a lesser side effect of the second molecule.

With regard to human melanoma and human melanocyte lines, the results suggest a highly encouraging therapeutic potential. In tumour cells, despite lower sensitivity than that observed with CTD treatment, where the IC_{50} value is obtained with a concentration 2.5 times higher on MEL66-CL and MEL16-AR-P cells (Fig. 19 A and B) but reaches the same toxicity levels at the same concentration as CTD (Fig. 19 C).

Finally, the effect on cell viability observed in normal melanocyte cells is much less pronounced, occurring only at concentrations 10 times higher than those observed in tumour cells (Fig. 19 D).

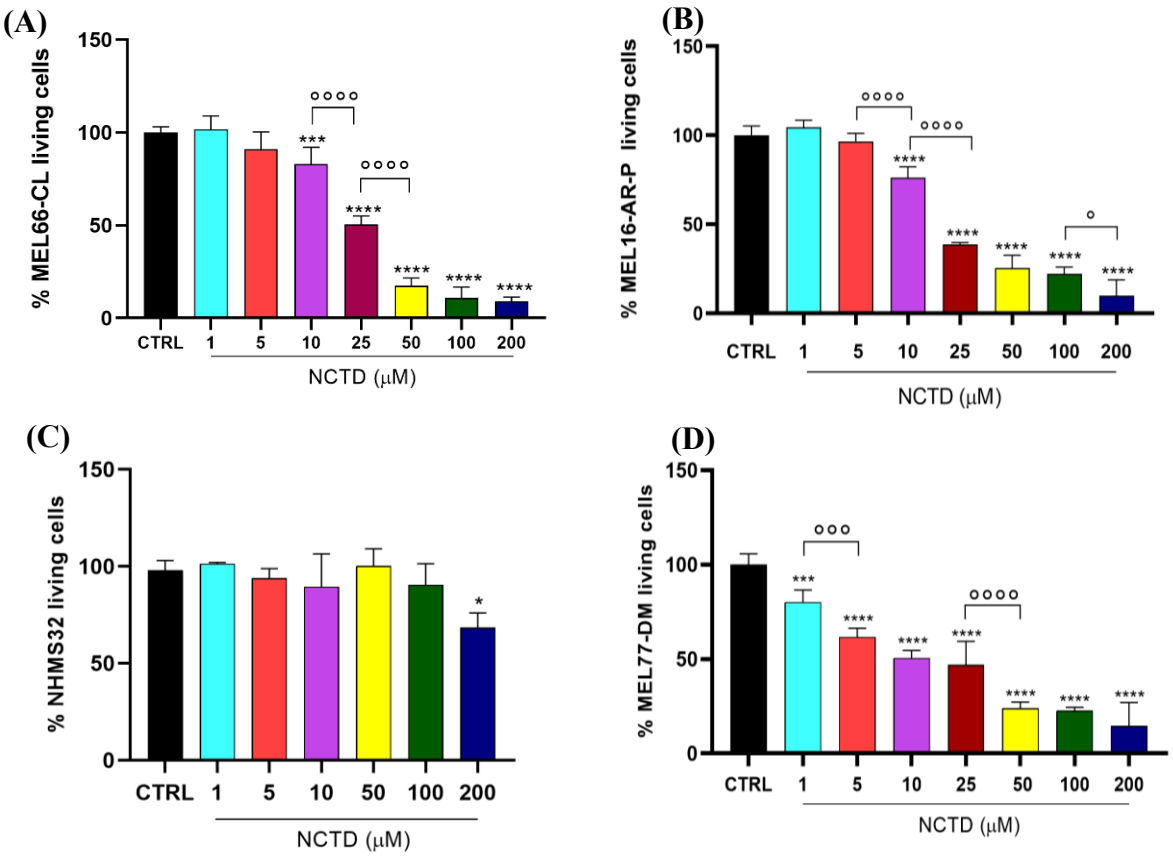

Fig. 19. Impact of growing concentrations of NCTD on MEL66-CL (**A**), MEL16-AR-P (**B**), NHMS32 (**C**) and MEL77-DM (**D**) for 24h of exposure. Cell viability was assessed by MTT performed as specified in materials and methods. Data are expressed as a percentage of viable cells relative to the untreated control (CTRL).

Bars represent the mean ± standard deviation (SD) of *n=6*. Statistical significance was determined by One-way ANOVA followed by Tukey's post-hoc test. Significance levels: **** $p < 0.0001$, *** $p < 0.001$, and * $p < 0.05$ vs. CTRL; °°°° $p < 0.0001$ and °°° $p < 0.001$.

2. Dissecting the cytotoxic mechanisms of cantharidin and norcantharidin: from membrane permeability to the impairment of Nrf2 signaling

2.1 CTD and NCTD are able to diffuse through the plasma membrane: assessment by means of PAMPA Assay

To study the mechanisms underlying the effects were of CTD and NCTD on cell viability, it is important to understand how these two molecules initially interact with the cell. Given some intrinsic characteristics of CTD and NCTD such as their small dimensions (MW: 196.20 g/mol and 168.15 g/mol respectively), and their lipophilic properties we hypothesised that they could cross biological membranes independently of protein transporters. To test this hypothesis a PAMPA assay was performed. The PAMPA (Parallel Artificial Membrane Permeability Assay) test is one of the most established high-throughput screening tools for evaluating the passive transcellular permeability of xenobiotics and potential drugs. Initially developed by Kansy et al. in 1998, this non-cellular *in vitro* model allows the quantification of a molecule's ability to cross a biological barrier by pure diffusion, eliminating complex variables related to cellular metabolism or active transport.

To evaluate the passive transport of CTD and NCTD, we assessed the concentration of CTD and NCTD across the membrane model after 5 hours of incubation at room temperature. The permeability of two control molecules was also analysed: trypan blue as a low permeability control and caffeine as a high permeability control. In order to determine the passive permeability coefficients (P_e) the "Corning® BioCoat™ PAMPA Plate System" was utilized. The obtained results indicated that NCTD exhibited a P_e of 11.10 x 10^{-6} cm/s, which was comparable to the high-permeability control, Caffeine P_e 12.10 x 10^{-6} cm/s. Meanwhile, CTD exhibited a permeability of 7.38 x 10^{-6} cm/s, which was slightly lower but still robust (Fig. 20). Both compounds significantly exceeded the P_e of the low-

permeability marker Trypan Blue, thus confirming their ability to readily access the intracellular compartment via passive diffusion.

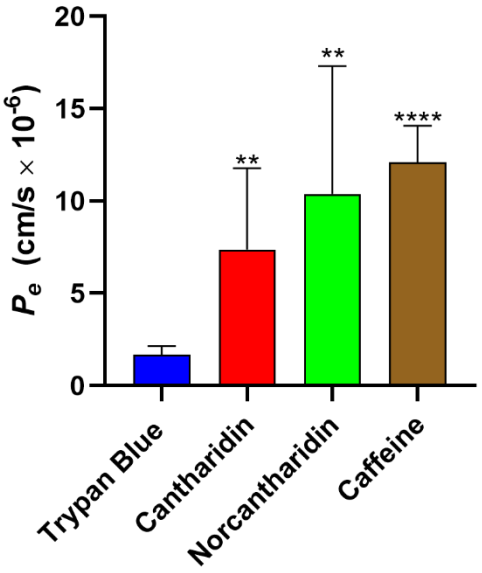

Fig. 20 Passive permeability assessment using the PAMPA assay. The graph illustrates the effective permeability coefficient (P_e), expressed in cm/s × 10^{-6}, for Trypan Blue (low-permeability negative control), Cantharidin, Norcantharidin, and Caffeine (high-permeability positive control). Bars represent the mean ± standard deviation (SD) of *n=6*. Statistical significance was determined by One-way ANOVA followed by Tukey's post-hoc test. Significance levels: **** $p < 0.0001$ and ** $p < 0.01$ vs Trypan Blue

2.2 Both NCTD and CTD induce enhanced reactive oxygen species production

To assess the possible involvement of oxidative stress in the cytotoxic action exerted by cantharidin, ROS production was first measured in U373 cells treated with 10µM CTD for 2h, 6h and 16h. At the end of the treatment, the probe dichlorofluorescein diacetate (DCFH-DA) was added, which oxidises and emits fluorescence in the presence of ROS.

The intensity of the fluorescence emitted by each cell was measured using a flow cytometer, thereby obtaining quantitative data on the presence of ROS.

As demonstrated in Figure 21, the mean fluorescence intensity exhibited an increase two hours after treatment, reaching a peak at 6 hours and then decreasing after 16 hours. However, it remained higher than the control and returned to baseline levels after 24 hours.

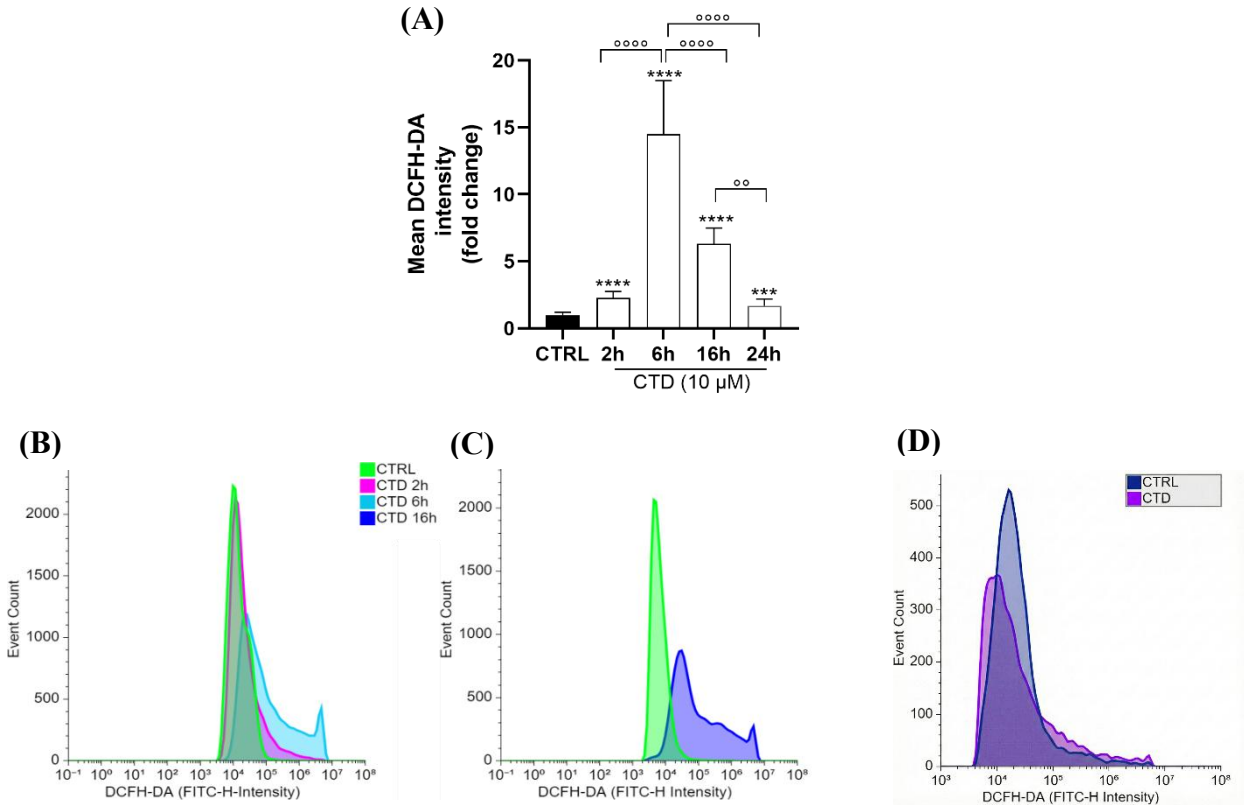

Fig. 21 Flow cytometric analysis of intracellular ROS production. (**A**) Mean fluorescence intensity (MFI) of DCFH-DA at 2h (2.27), 6h (14.5), 16h (6.3), and 24h (1.7) following treatment with 10 µM Cantharidin (CTD) on U373 cells. (**B**) Representative flow cytometry histograms showing fluorescence intensity at 2h and 6h compared to control. (**C**) Histogram showing fluorescence intensity at 16h. (**D**) Histogram showing fluorescence intensity at 24h. Bars represent the mean ± standard deviation (SD) of *n=3*. Statistical significance was determined by One-way ANOVA followed by Tukey's post-hoc test. Significance levels: **** $p < 0.0001$ and *** $p < 0.001$ vs. CTRL; °°°° $p < 0.0001$ and °° $p < 0.01$

To further investigate whether the temporal trend of ROS production observed in U373 cells was a consistent feature of cantharidin-induced cytotoxicity, the study was extended to melanoma cells (MEL66-CL and MEL77-DM) and normal human melanocytes (NHMS32) (see Fig. 22).

CTD treatment (10 µM) revealed a striking kinetic difference between the cell lines. While healthy melanocytes exhibited a transient response similar to that of U373 cells, characterized by a moderate ROS peak (2.7-fold vs. control) at 6 hours followed by a full recovery to baseline levels within 24

hours (Fig. 22 C), melanoma cells showed persistent oxidative stress (Fig. 22 A, B). In the latter, ROS levels began to rise after 6 hours and remained elevated up to 24 hours, reaching levels 4 to 6 times higher than the control without showing any signs of resolution.

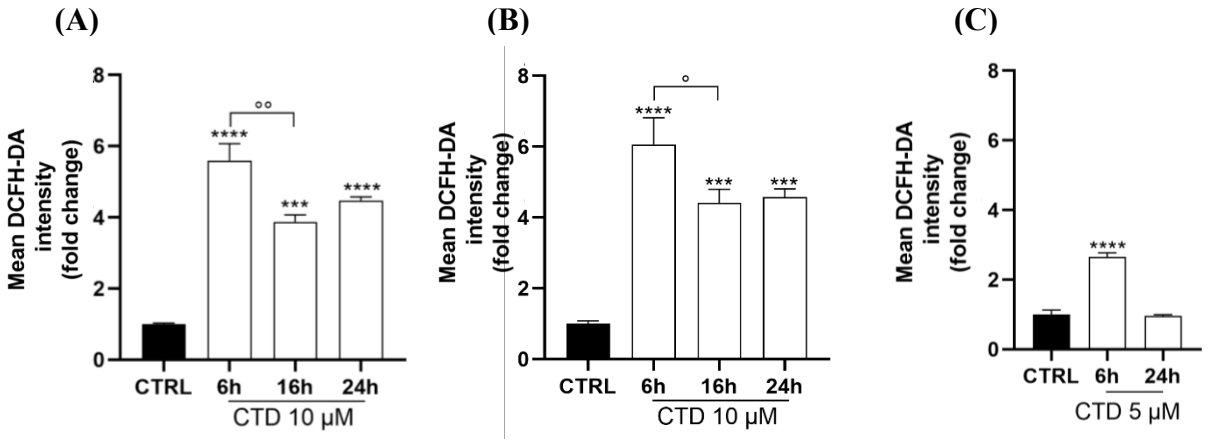

Fig. 22 Flow cytometric analysis of intracellular ROS production following treatment with 10 µM Cantharidin (CTD). Representative histograms showing the mean fluorescence intensity (MFI) of DCFH-DA after 6h, 16h, and 24h. Panels (**A**) and (**B**) show the results for the two melanoma cell lines, MEL77-DM and MEL66-CL. Panel (**C**) shows the results for melanocytes (NHMS32). Bars represent the mean ± standard deviation (SD) of *n=3*. Statistical significance was determined by One-way ANOVA followed by Tukey's post-hoc test. Significance levels: **** $p < 0.0001$ and *** $p < 0.001$ vs. CTRL; °° $p < 0.01$ and ° $p < 0.05$.

In parallel, the effects of norcantharidin were assessed in MEL66-CL and MEL77-DM cells (Fig. 23 A and B), were at a concentration of NCTD 25 µM induced a progressive increase in ROS levels, peaking at 24 hours. Conversely, in NHMS32 (Fig. 23C), even when exposed to significantly higher concentrations (100 µM), ROS production remained transient, showing a peak at 6 hours (3.2-fold vs. control) and returning to baseline by 24 hours.

These findings suggest that, in comparison to their healthy counterparts, melanoma cells are unable to effectively manage the oxidative stress induced by these compounds even when the former have been challenged with much higher pharmacological doses.

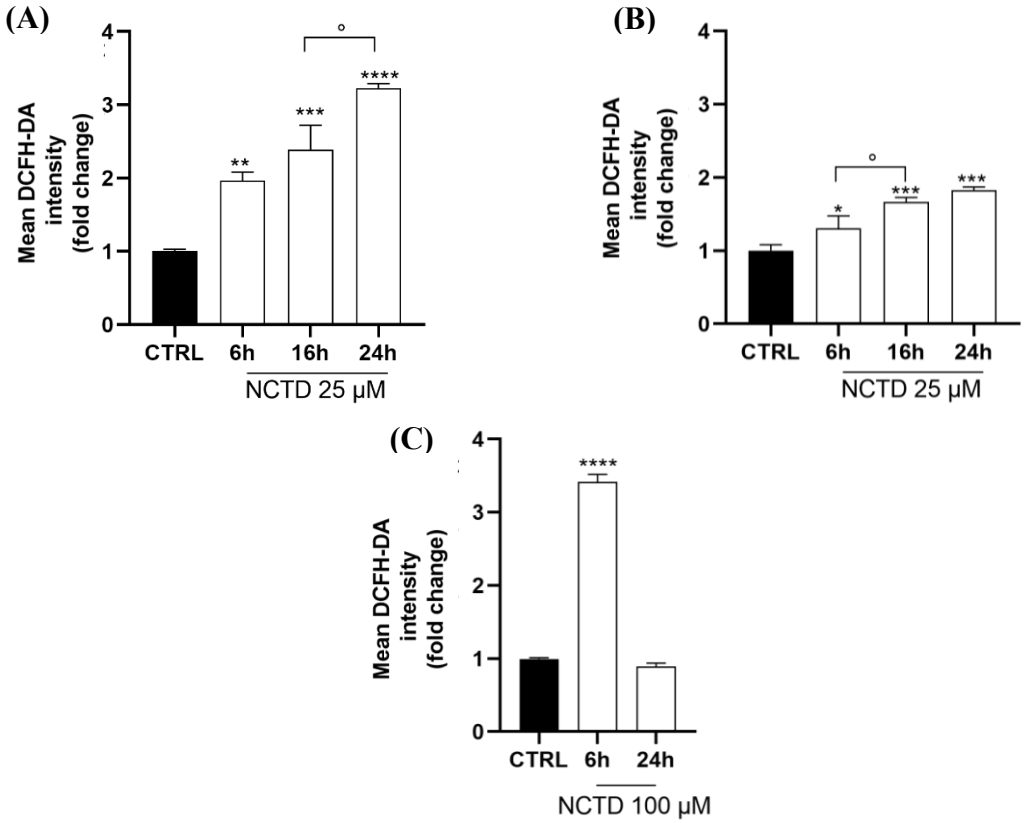

Fig. 23 Flow cytometric analysis of intracellular ROS production following treatment with Norcantharidin (NCTD) with two different concentrations 25 µM (Melanomas) and 100 µM (Melanocytes). Representative histograms showing the mean fluorescence intensity (MFI) of DCFH-DA after 6h, 16h, and 24h. In panels are displayed two melanomas cell lines MEL77-DM (**A**) and MEL66-CL (**B**), and in panel (**C**) the melanocytes (NHMS32). Bars represent the mean ± standard deviation (SD) of *n=3*. Statistical significance was determined by One-way ANOVA followed by Tukey's post-hoc test. Significance levels: **** $p < 0.0001$, *** $p < 0.001$ and * $p < 0.05$ vs. CTRL; ° $p < 0.05$.

2.3 Cantharidin induces distinct effects on the ARE-dependent antioxidant response in U373 cells

As a result of the previously observed decrease in ROS dynamics, it was imperative to explore the underlying molecular defense mechanisms. This investigation focused on the regulation of a specific set of genes containing the ARE, aiming to determine whether the cell mounts a coordinated defensive strategy.

However, RT-qPCR data collected on U373 at 4-, 8-, and 24-hours following treatment with 10 µM CTD revealed a deeply heterogeneous transcriptional response (Fig. 24). While Catalase mRNA

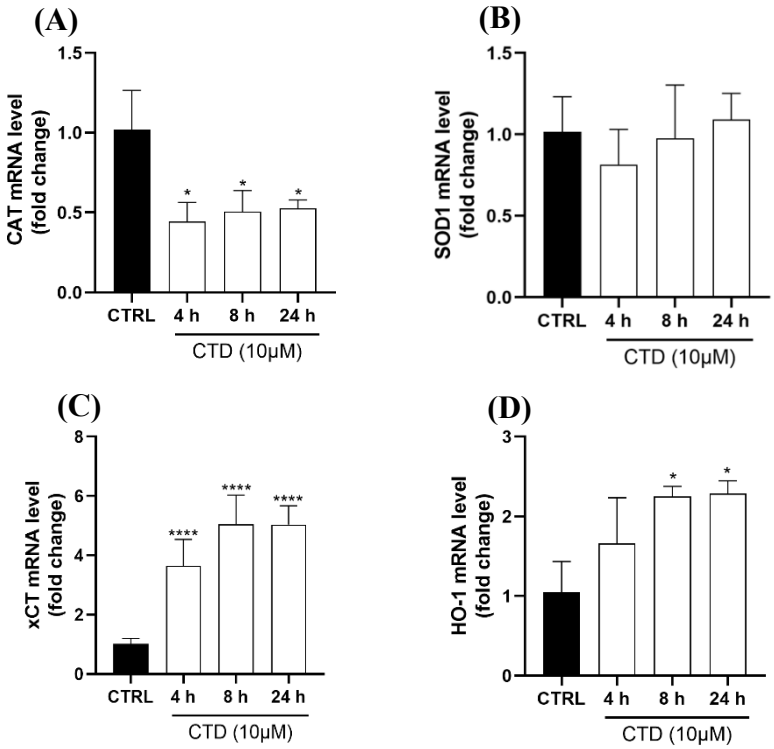

Fig. 24 Effect of CTD on the mRNA expression of antioxidant and stress-response genes. Relative mRNA fold change of (A) Catalase (CAT), (B) Superoxide Dismutase 1 (SOD1), (C) System X_c^- (xCT), and (D) Heme Oxygenase-1 (HO-1) following treatment with 10 µM CTD for 4h, 8h, and 24h on U373 cells. Data are presented as mean ± SD with varying sample sizes: $n = 3$ (A, D), $n = 6$ (B), and $n = 9$ (C). Statistical significance was determined by One-way ANOVA followed by Tukey's post-hoc test. Significance levels: **** $p < 0.0001$ and * $p < 0.05$ vs. CTRL

levels significantly and consistently decreased across all time points, SOD1 expression remained largely stable, suggesting a lack of coordination between these two pivotal peroxide-scavenging enzymes (Fig 24 A and B). In stark contrast, System X_c- and Heme Oxygenase-1 showed strong induction: the cystine transporter xCT increased 3.8-fold as early as 4 hours, eventually peaking at 5-fold, while HO-1 exhibited a significant 2.2-fold increase from 8 hours onwards (Fig. 24 C, D). This fragmented response was further corroborated at the protein level via Western Blot analysis. The translation of transcriptional signals into protein effectors displayed distinct nuances: although xCT expression significantly increased after 24 hours (Fig. 25A), the 1.5-fold rise was notably less pronounced than the massive induction seen at the mRNA level. Conversely, HO-1 protein showed a much more substantial increase, reaching levels 3.9-fold higher than the control at 24 hours (Fig. 25

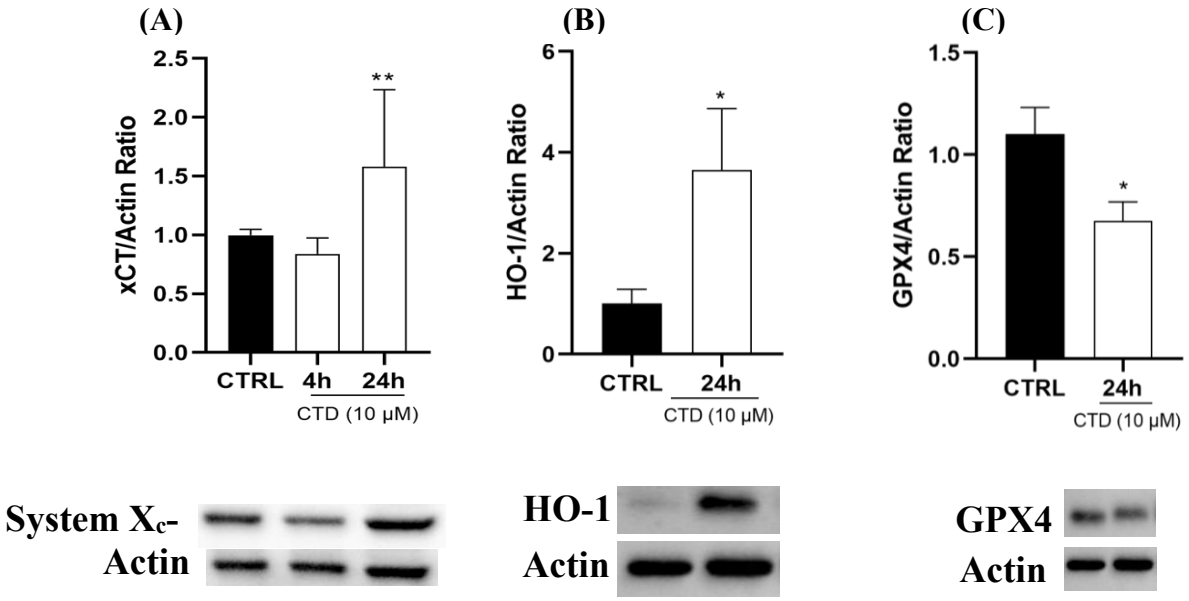

Fig. 25 Effect of CTD on the protein expression of antioxidant and stress-response genes. Western Blot analysis. Relative ratio protein/housekeeping (Actin) of (**A**) System X_c- (xCT), (**B**) Heme Oxygenase-1 (HO-1), (**C**) Glutathione Peroxidase 4 (GPX4) following treatment with 10 µM CTD for 24h on U373 cells. Data are presented as mean ± SD with varying sample sizes: $n = 3$ (4 h panel A and panel B), $n = 6$ (C), and $n = 12$ (24 h panel A). Statistical significance was determined by One-way ANOVA followed by Tukey's post-hoc test (A) and Student's t-test for pairwise comparisons between the treated groups and the control (CTRL). Significance levels: ** $p < 0.01$ and * $p < 0.05$ vs. CTRL

B). Within this scenario of partial activation, the data regarding Glutathione Peroxidase 4 introduced further complexity, as protein levels dropped to 0.65 relative to the control (Fig. 25 C).

Taken together, these findings delineate a state of profound enzymatic disequilibrium, where the activation of certain pathways (xCT, HO-1) is not accompanied by the maintenance of other essential defenders (Catalase, GPX4).

Such evidence suggests a major disruption within the redox control network. The subsequent chapter will therefore investigate the involvement of Nrf2, the master transcription factor that regulates ARE-genes, in this dysfunctional response or whether its activity is compromised by CTD treatment.

2.4 NRF2 transcription factor is inhibited by the presence of CTD and NCTD

To examine the activation of the Nrf2 transcription factor, protein extraction was performed by separating nuclear proteins from cytosolic proteins in U373 cells treated with CTD for 2h, 4h, 16h and 24h. Western blotting was used to evaluate nuclear Nrf2 levels, with the results indicating a decrease of 50% in treated cells at 2 hours and 40% at 4 hours in comparison to the control. At 16 and 24 hours the decline was recorded as 0.45 and 0.37-fold respectively (Fig. 26).

To confirm the Nrf2 inhibition, U373 cells were treated with 10µM CTD in the presence or absence of its activator dimethyl fumarate (DMF 30µM). Furthermore, nuclear levels of Nrf2 were analysed after a 4-hour exposure period (Figure 27). As expected, cantharidin has been shown to result in a substantial decrease in nuclear Nrf2 levels compared to the control. Conversely, treatment with DMF has been observed to cause a 60% increase in Nrf2 nuclear translocation. It is noteworthy that in samples treated with DMF in the presence of CTD, Nrf2 levels are equivalent to those of the control. These results suggest that cantharidin has the ability to prevent the activation of Nrf2, even in the presence of its activator.

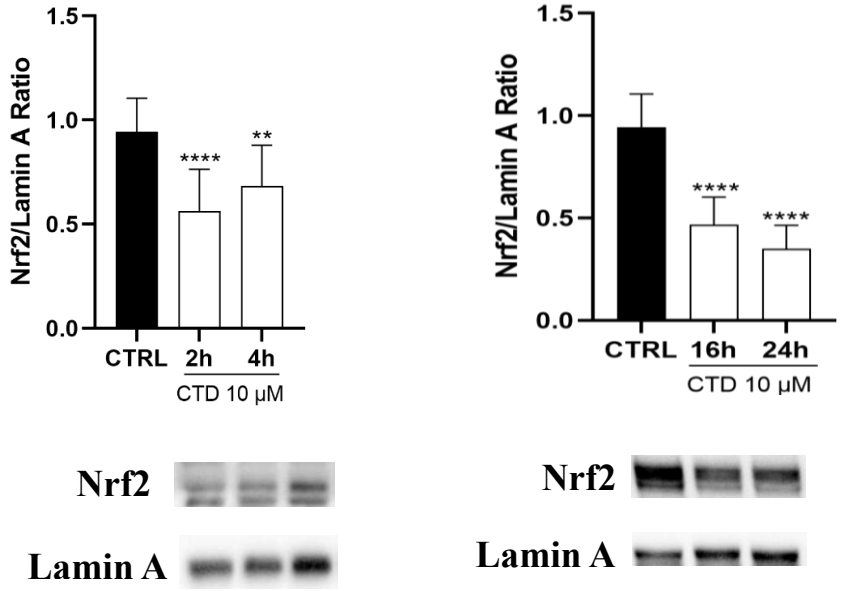

Fig. 26 Western blot analysis of nuclear Nrf2 levels in U373 cells. The graphs and representative blots show the nuclear protein levels of Nrf2 relative to Lamin A (loading control) following treatment with 10 µM Cantharidin (CTD) at 2h and 4h (left) and 16h and 24h (right). Data are expressed as the Nrf2/Lamin A ratio (mean ± SD). Sample sizes: $n = 9$ for 2h, $n = 18$ for 4h, and $n = 6$ for 16h and 24h. Statistical significance: ** $p < 0.01$, **** $p < 0.0001$ vs. CTRL.

To rule out the possibility that reduced nuclear NRF2 levels were caused by a decrease in transcriptional synthesis, mRNA expression was evaluated in U373 cells treated with 10 µM CTD for 4, 8, and 24 hours. RT-qPCR results demonstrated that NRF2 transcript levels remained unchanged across all time points (Fig. 28), thus confirming that cantharidin's inhibitory effect does not occur

upstream at the gene transcription level. Instead, it acts directly at the post-translational level, affecting the protein itself or its compartmentalization dynamics.

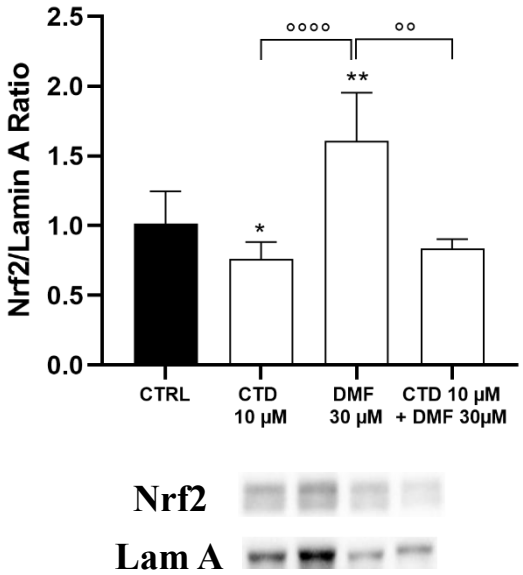

Fig. 27 Western blot analysis of nuclear Nrf2 levels in U373 cells. The graphs and representative blots show the nuclear protein levels of Nrf2 relative to Lamin A (loading control) following treatment with 10 µM Cantharidin (CTD) in presence or absence of Nrf2 activator DMF at 4h. Data are expressed as the Nrf2/Lamin A ratio (mean ± SD) of $n = 6$. Statistical significance was determined by One-way ANOVA followed by Tukey's post-hoc test. Significance levels: ** $p < 0.01$ and * $p < 0.05$ vs. CTRL; °°°° $p < 0.0001$ and °° $p < 0.01$.

This finding is particularly significant when considered alongside the results obtained using Dimethyl Fumarate. DMF is a well-known NRF2 activator that works by covalently binding to cysteine residues (specifically Cys151) on the KEAP1 protein, the primary negative regulator of NRF2 (Brennan M.S. et al., 2015). This interaction prevents KEAP1 from targeting NRF2 for proteasomal degradation, thereby allowing the transcription factor to stabilize, accumulate in the cytoplasm, and translocate into the nucleus. Since cantharidin prevents NRF2 nuclear accumulation even in the presence of dimethyl fumarate (DMF). This observation indicates that the inhibition occurs at a subsequent stage to protein stabilization likely by either blocking the nuclear import machinery or by promoting massive nuclear export.

Subsequently, the investigation focused on determining whether NRF2 inhibition represented a conserved mechanism of action across other cellular models and whether norcantharidin, given its close structural and physiological similarity to its parent molecule, could exert a comparable effect. The investigation was expanded to include melanoma cells (MEL77-DM) and NHMS32 employing immunofluorescence assays and quantitative analysis via the ImageXpress system to accurately quantify the presence of the transcription factor within the nuclear compartment.

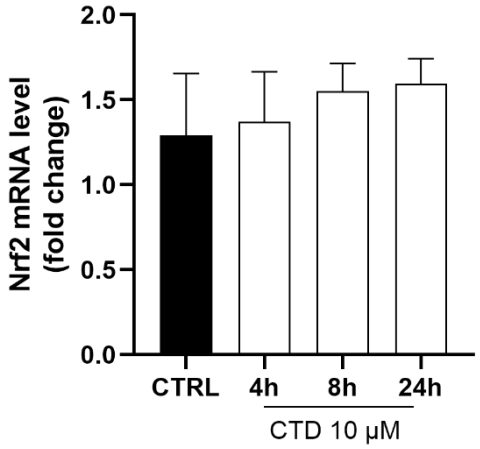

Fig. 28 Effect of CTD on the mRNA expression of antioxidant and stress-response activator Nrf2. Nrf2 mRNA fold change following treatment with 10 µM CTD for 4h, 8h, and 24h on U373 cells. Data are presented as mean ± SD with sample sizes of n = 3. Statistics was determined by One-way ANOVA followed by Tukey's post-hoc test.

The results confirm that both CTD and NCTD act as potent inhibitors of NRF2 nuclear translocation in the two cell lines that were examined (Fig. 29). Specifically, in Mel77-DM melanoma cells, treatment with CTD (7.5 µM) induced a 20% reduction in nuclear NRF2 levels, while NCTD (25 µM) showed drastically higher inhibitory efficacy, reaching 75%. An inhibitory profile was also observed in melanocytes, although the relative magnitudes between the two molecules were reversed: in this model, NCTD reduced nuclear NRF2 presence by 20%, whereas CTD treatment caused a much more pronounced decrease of 65%.

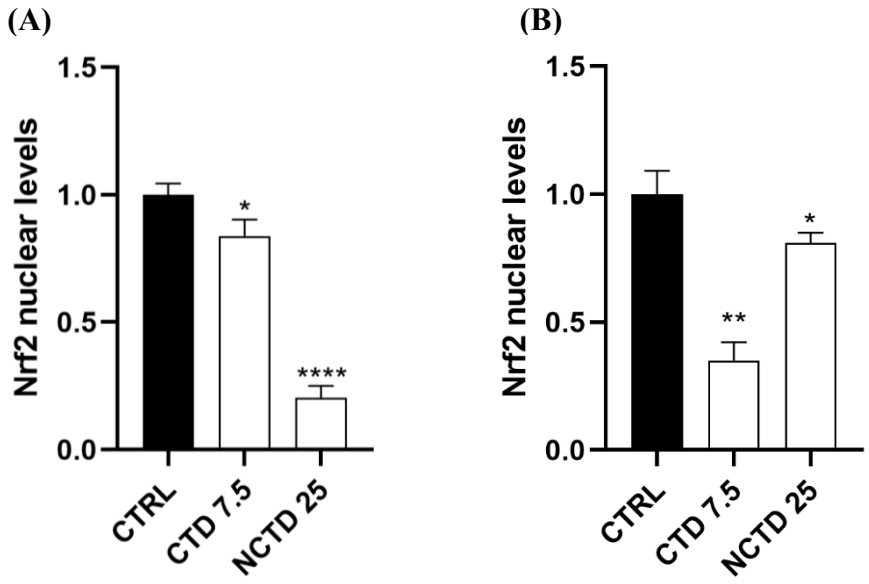

Fig. 29 Comparative analysis of Nrf2 nuclear levels in MEL77-DM and NHMS32 cell lines. The graphs illustrate the relative Nrf2 levels in (A) MEL77-DM and (B) NHMS32 cells following treatment with 7.5 µM Cantharidin (CTD) or 25 µM Norcantharidin (NCTD). Data are expressed as mean ± SD of n = 3. Statistical significance: * $p < 0.05$, ** $p < 0.01$, **** $p < 0.0001$ vs. CTRL.

These data consolidate the hypothesis that interference with the NRF2 pathway is a central and shared mechanism of action for this class of compounds, suggesting that their cytotoxicity is closely linked to their ability to preemptively "disarm" the cell's antioxidant defenses.

2.5 The ROS scavenger N-acetylcysteine reduces reactive oxygen species levels but does not restore cell viability

In light of the previously obtained results, which highlighted a massive production of reactive oxygen species and a concomitant inhibition of the transcription factor NRF2, it became essential to establish if exist a causal link between oxidative stress and cell death. To address this question, N-acetylcysteine (NAC) was employed. NAC is a well-known antioxidant agent that acts both as a direct free radical scavenger and as a precursor for reduced glutathione (GSH).

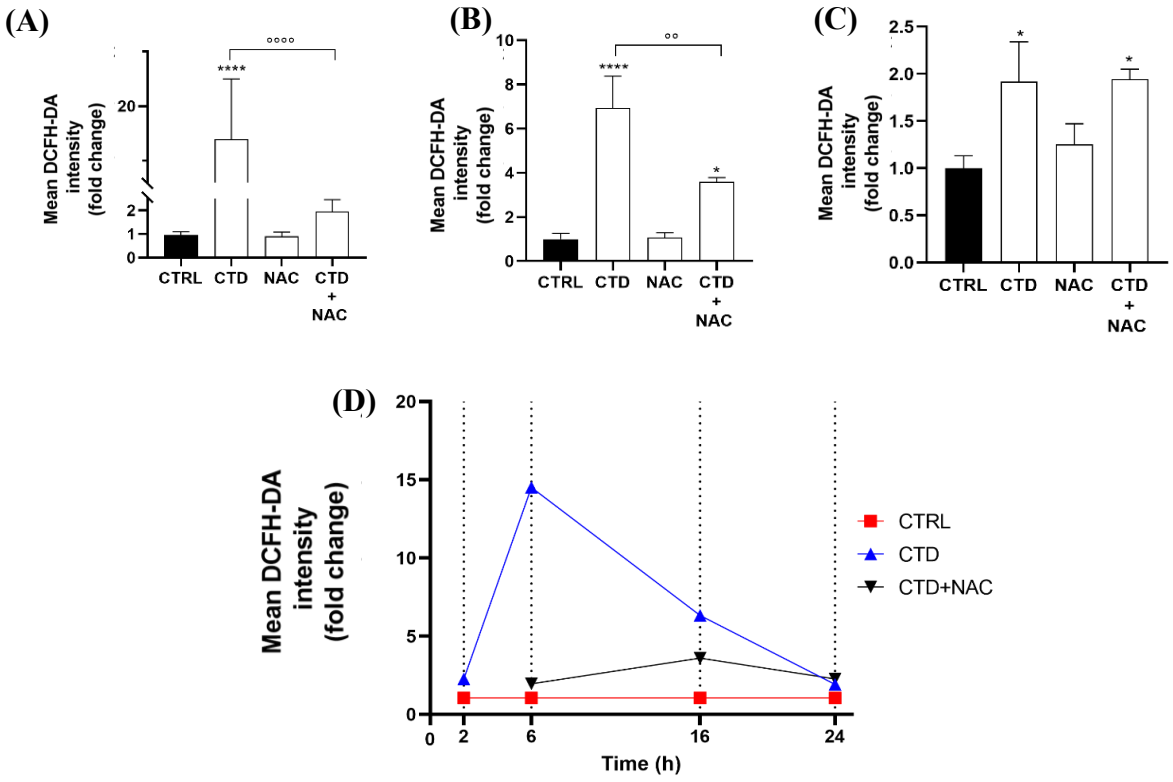

Fig. 30 Flow cytometric analysis of intracellular ROS production following treatment with Cantharidin (CTD) in presence or absence of the ROS scavenger, NAC on U373 cells. Representative histograms showing the mean fluorescence intensity (MFI) of DCFH-DA after 6h (A), 16h (B), and 24h (C). In panel D there is a sum of the ROS trend. Bars represent the mean ± standard deviation (SD) of *n=3*. Statistical significance was determined by One-way ANOVA followed by Tukey's post-hoc test. Significance levels: **** $p < 0.0001$ and * $p < 0.05$ vs. CTRL; °°°° $p <$

Firstly, the efficacy of NAC (2mM) as a scavenger was validated in U373 cells treated with 10µM CTD. Flow cytometric analysis using the DCFH-DA probe confirmed that the presence of NAC restores ROS levels to values comparable to the control at all analyzed time points (6, 16, and 24 hours), effectively neutralizing the treatment-induced ROS increase (Fig. 30).

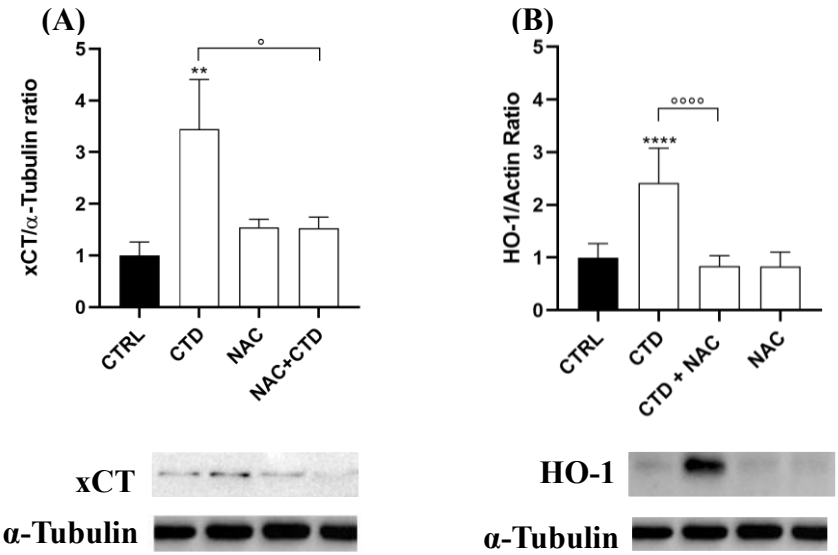

Fig. 31 Effect of CTD on the protein expression of antioxidant and stress-response genes in presence or absence of NAC. Relative ratio protein/housekeeping (Tubulin-α) of (A) System X_c- (xCT) and (B) Heme Oxygenase-1 (HO-1) following treatment with 10 µM CTD and 2mM of NAC for 24h on U373 cells. Data are presented as mean ± SD with varying sample sizes: $n = 3$ (4 h panel A and panel B), $n = 6$ (C), and $n = 12$ (24 h panel A). Statistical significance was determined by One-way ANOVA followed by Tukey's post-hoc test (A) and Student's t-test for pairwise comparisons between the treated groups and the control (CTRL). Significance levels: **** $p < 0.0001$ and ** $p < 0.01$ vs. CTRL; °°°° $p < 0.0001$, and ° $p < 0.05$.

Subsequently, we evaluated whether the induction of ARE-genes observed earlier, despite NRF2 inhibition, was directly linked to the increase of ROS. Western Blot analysis revealed that neutralizing ROS with NAC leads to a full restoration of baseline levels for both System Xc- and HO-1 (Fig. 31). This finding suggests that the up-regulation of these specific protective elements was a direct response to the oxidative stimulus, likely mediated by redox-sensitive pathways alternative to NRF2.

The subsequent pivotal stage was to assess whether the restoration of redox balance and protein levels would result in enhanced cell survival. To this aim, the MTT assay was performed on U373 cells treated with CTD, in the presence or absence of NAC (2 mM). The results demonstrate that in cells treated with CTD in the presence of NAC, there is a restoration of viability of approximately 10% compared to cells treated with cantharidin alone (Fig. 32).

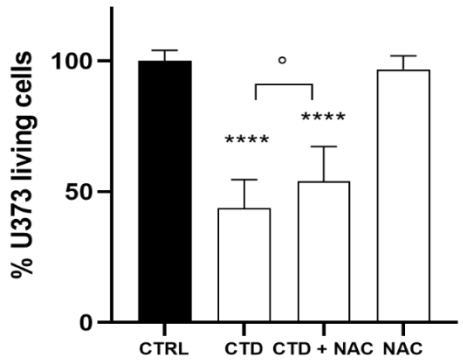

Fig. 32 Effect of a 24-hour treatment with CTD and the ROS scavenger NAC on the viability of U373 cells. Cell viability was assessed by MTT that was performed as specified in materials and methods. Data are expressed as a percentage of viable cells relative to the untreated control (CTRL). Bars represent the mean ± standard deviation (SD) of *n=15* independent experiments. Statistical significance was determined by One-way ANOVA followed by Tukey's post-hoc test. Significance levels: **** $p < 0.0001$ and ° $p < 0.05$.

This finding suggests that the enhancement of ROS levels plays a modest role in the cytotoxic action of cantharidin. Indeed, despite the decline in ROS, the presence of NAC has been shown to only offer partial protection against cell death. These results unequivocally indicate that, although CTD induce massive ROS production, oxidative stress is not the primary mechanism through which these molecules induce cell death, shifting the focus toward other molecular targets.

2.6 NCTD and CTD both increase cytosolic Ca^{2+} levels

It is well-established that ROS and cytosolic calcium are closely interconnected in a vicious cycle: oxidative stress can alter organelle membrane permeability or inhibit calcium extrusion pumps, leading to a cytosolic overload that, in turn, triggers programmed cell death. Based on this, we hypothesized that the disruption of calcium homeostasis might represent a critical and potentially independent mechanism through which CTD exerts its cytotoxic effects.

To monitor real-time changes in cytosolic calcium concentration, the Fluo-4 direct Calcium Assay was employed as described in methods, the probe binds cytosolic calcium increasing its fluorescence for a maximum of 6 hours. U373 cells were analyzed using the ImageXpress system under controlled temperature and CO_2 conditions. The study was structured across three-time windows in order to capture the full dynamics of calcium: 1-6h, 5-10h, and 20-25h. The results indicate that the rise in calcium levels is not immediate but becomes statistically significant starting from 170 minutes of CTD treatment (10µM). This increase is not transient; fluorescence continues to rise progressively across all analyzed time windows (Fig. 33).

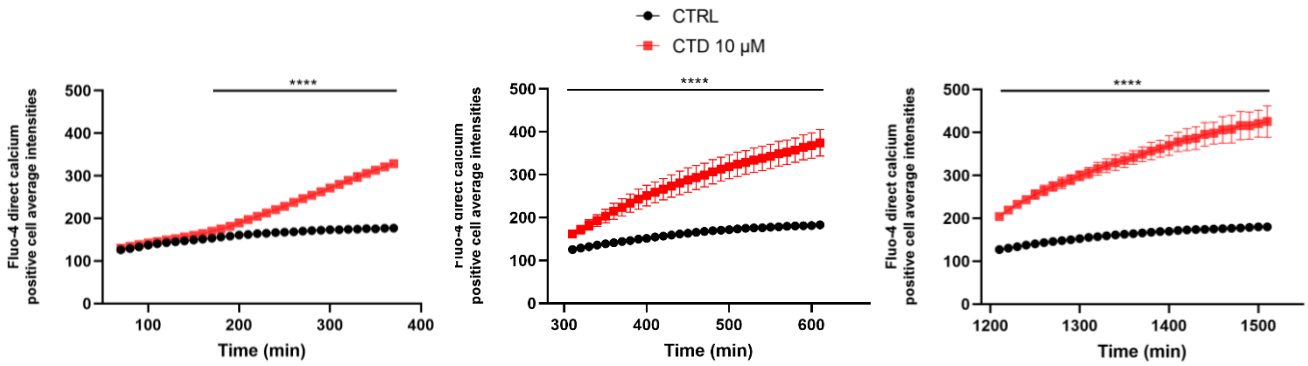

Fig. 33 Time-course analysis of intracellular calcium levels induced by Cantharidin on U373. The graphs illustrate the average intensities of Fluo-4 direct calcium-positive cells over three-time intervals: 1h–6h (left), 5h–10h (center), and 20h–25h (right). Cells were treated with 10 µM CTD (red squares) or kept as control (CTRL, black circles). Data are presented as mean ± SD (n = 6). Cytosolic calcium concentration was measured according to the manufacturer's instructions as presented in the Materials and methods' section Statistical analysis was performed using two-way ANOVA followed by Sidak's multiple comparisons test. Significant differences between CTD and CTRL groups ****p < 0.0001 were observed starting from 170 minutes post-treatment.

To further investigate the nature of this accumulation and assess its generation, the experiment was extended to include the melanoma cell lines (MEL77-DM and MEL66-CL) as well as NHMS32 cells. The action of CTD (10µM) was compared with that of norcantharidin (25µM). To identify the origin of the calcium, whether derived from extracellular space or from intracellular stores, EGTA (1 mM), an extracellular calcium chelator, and SKF96365 (20µM), a non-specific inhibitor of SOCE and TRP calcium channels, were used.

The data confirm that CTD induces a massive increase in cytosolic calcium in all tested lines. Strikingly, neither extracellular calcium chelation via EGTA nor membrane channel inhibition via SKF (with the exception of a slight reduction in MEL66-CL) was able to prevent or mitigate this increase (Fig. 34).

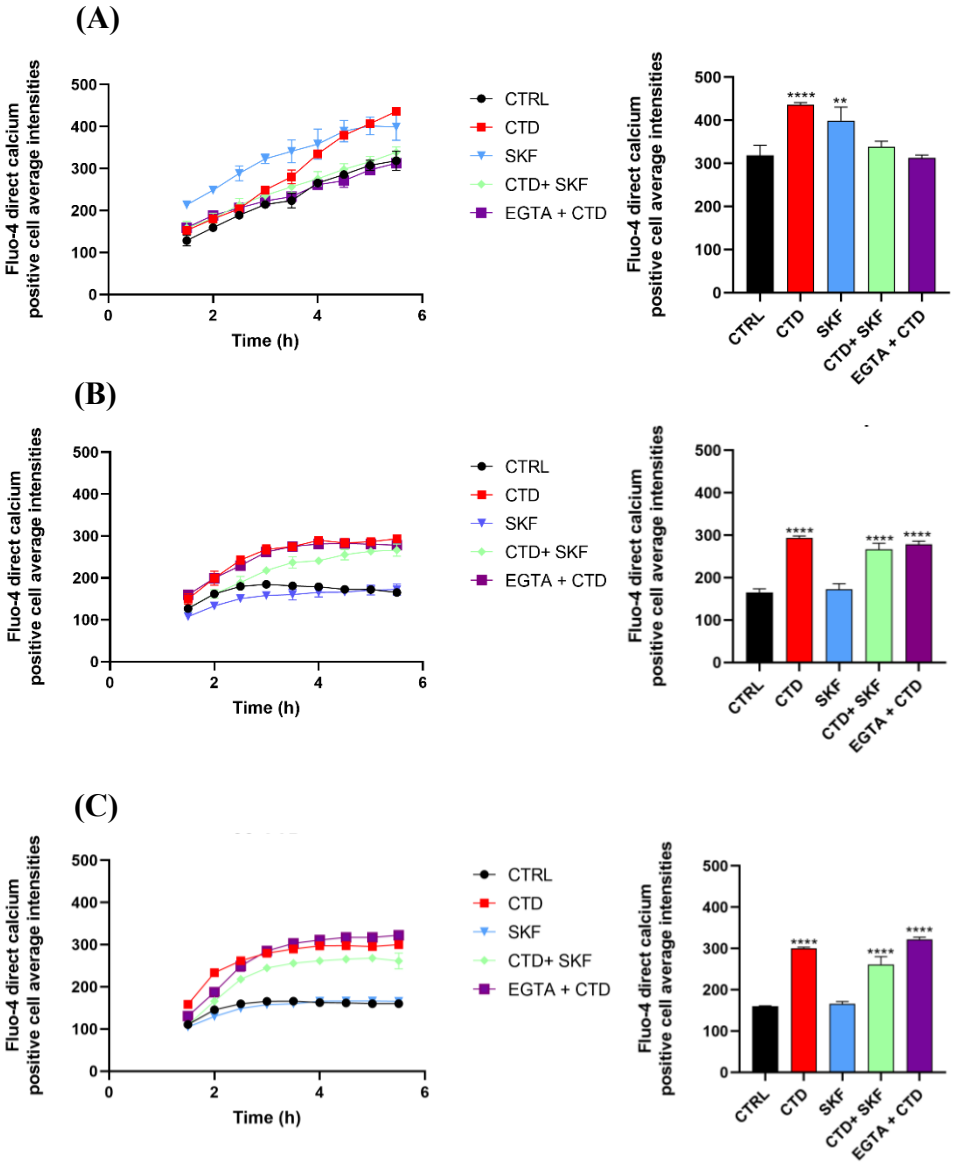

Fig. 34 Assessment of CTD-induced increase in cytosolic calcium. Real-time monitoring and endpoint analysis of intracellular calcium levels in NHM (A), MEL77-DM (B), and MEL66-CL (C) cell lines. Cells were treated with 10 µM Cantharidin (CTD), 20 µM of the non-specific calcium channel inhibitor SKF-96365 (SKF), and 1mM of the extracellular calcium chelator EGTA. Cytosolic calcium concentration was measured according to the manufacturer's instructions as presented in the Materials and methods' section. Data are expressed as mean ± SD (n = 3). Statistical analysis was performed using one-way ANOVA followed by Tukey's post-hoc test for the endpoint. Significance levels: ** $p < 0.01$, **** $p < 0.0001$ vs. CTRL; °° $p < 0.01$.

With regard to NCTD, a comparable effect to that of CTD was observed in melanoma cell lines, characterised by an increase in calcium that was not reversible with the two calcium blockers. However, in melanocytes, NCTD produced no significant changes, confirming the greater resistance of these cells toward the nor-derivative compared to the parent molecule (Fig. 35).

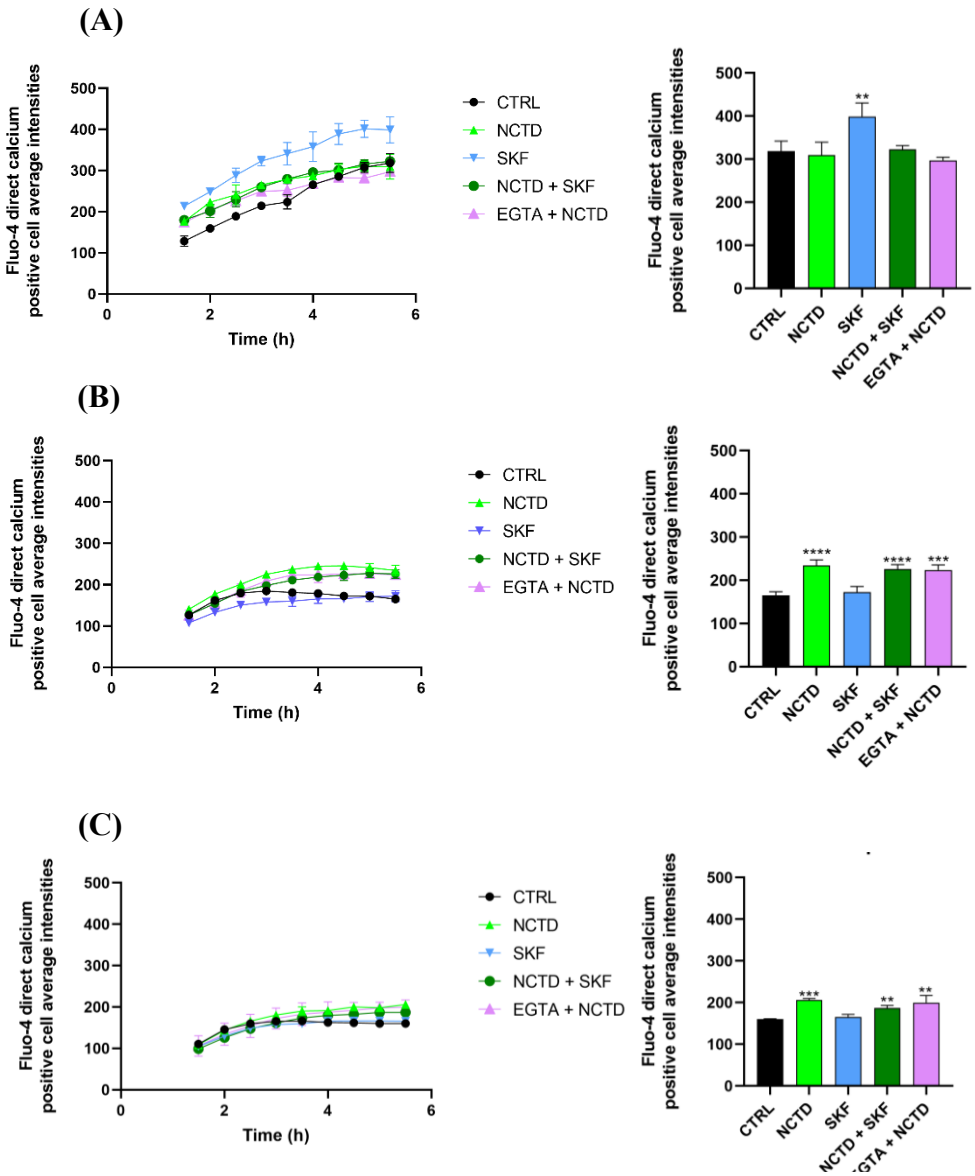

Fig. 35 Assessment of NCTD-induced increase in cytosolic calcium. Real-time monitoring and endpoint analysis of intracellular calcium levels in NHMS32 (A), MEL77-DM (B), and MEL66-CL (C) cell lines. Cells were treated with 50 µM Norantharidin (NCTD), 20 µM of the non-specific calcium channel inhibitor SKF-96365 (SKF), and 1 mM of the extracellular calcium chelator EGTA. Cytosolic calcium concentration was measured according to the manufacturer's instructions as presented in the Materials and methods' section Data are expressed as mean ± SD (n = 3). Statistical analysis was performed using one-way ANOVA followed by Tukey's post-hoc test for the endpoint. Significance levels: ** $p < 0.01$, **** $p < 0.0001$ vs. CTRL; °° $p < 0.01$.

In conclusion, the inability of EGTA to prevent the increase in fluorescence indicates that the calcium accumulating in the cytosol does not originate from the extracellular environment but rather from a massive release from intracellular stores (likely the endoplasmic reticulum). This phenomenon, which is common to both compounds in cancer cells but selective for CTD in healthy cells, suggests that the collapse of calcium homeostasis is a fundamental pillar of the cytotoxicity of these compounds, acting as a damage signal that persists independently of the cell's redox state. Further investigation is required to achieve a better understanding of the precise mechanisms that lead to cellular death and the accumulation of calcium within the cytosol

3. Evaluation of potential tumour targets for the design of antibody-drug conjugates

Given the significant effects on cell viability observed in previous experiments, it is of primary importance to target the cytotoxic action of CTD or NCTD towards tumour cells. In order to develop an antibody-drug conjugate, it is essential to identify a specific tumour target once the molecule to be delivered has been analysed. To ascertain the protein with the greatest specificity and to obtain a minimum of side effects, we evaluated the expressi on of the following markers as mentioned in the introduction: System Xc, CD44 and some of the proteins belonging to the EGFR family.

3.1 System X_c^- expression in astrocytes and glioma cells

We initially assessed the levels of System X_c^- on U373 and HA cells. The evaluation was performed on total RNA extracts using the Real Time qPCR technique. Subsequently the analysis was conducted on total protein extracts by Western Blotting (WB) . The results indicate that both cell types express

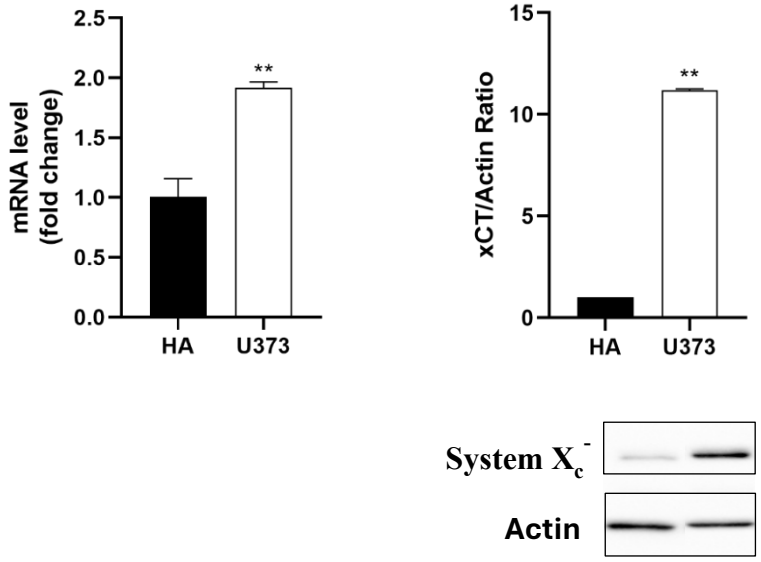

Fig. 36 Baseline expression of System X_c-(xCT) in U373 glioblastoma cells compared to Human Astrocytes (HA). The graphs illustrate (left) the relative mRNA fold change of xCT and (right) the xCT/Actin protein ratio as determined by Western Blotting. Data are expressed as mean ± SD (n = 3). Statistical significance was determined by Student's t-test for pairwise comparisons between the treated groups and the control (CTRL). Significance levels ** $p < 0.01$

the protein, but that there is greater expression in tumour cells, respectively 2 times in RNA extracts and 10 times in WB compared to normal cells. (Fig. 36)

3.2 CD44 expression in cells from brain and skin cancers

CD44 expression was analysed in cells from various tumour types and their healthy counterparts at both the RNA and protein levels by using Real Time qPCR and WB techniques, respectively.

With regard to the glioma, the results indicate protein expression in both cancerous and normal cells, with a higher abundance of the target protein observed in tumour cells. In particular, CD44 mRNA expression levels were found to be 2.7 times higher in U373 cells than in HA, while protein levels were observed to be 2 times higher. (Fig. 37)

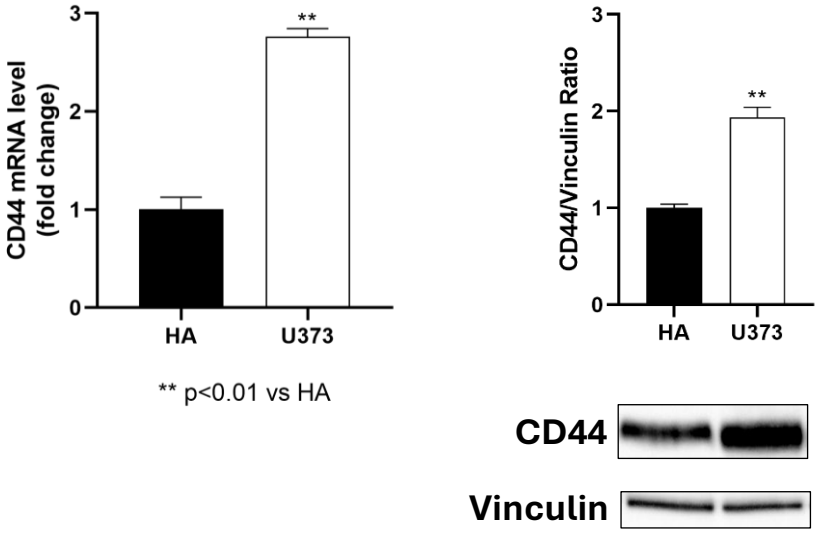

Fig. 37 Baseline expression of CD44 in U373 glioblastoma cells compared to Human Astrocytes (HA). The graphs illustrate (left) the relative mRNA fold change of CD44 and (right) the CD44/Actin protein ratio as determined by Western Blotting. Data are expressed as mean ± SD (n = 3). Statistical significance was determined by Student's t-test for pairwise comparisons between the treated groups and the control (CTRL). Significance levels ** $p < 0.01$

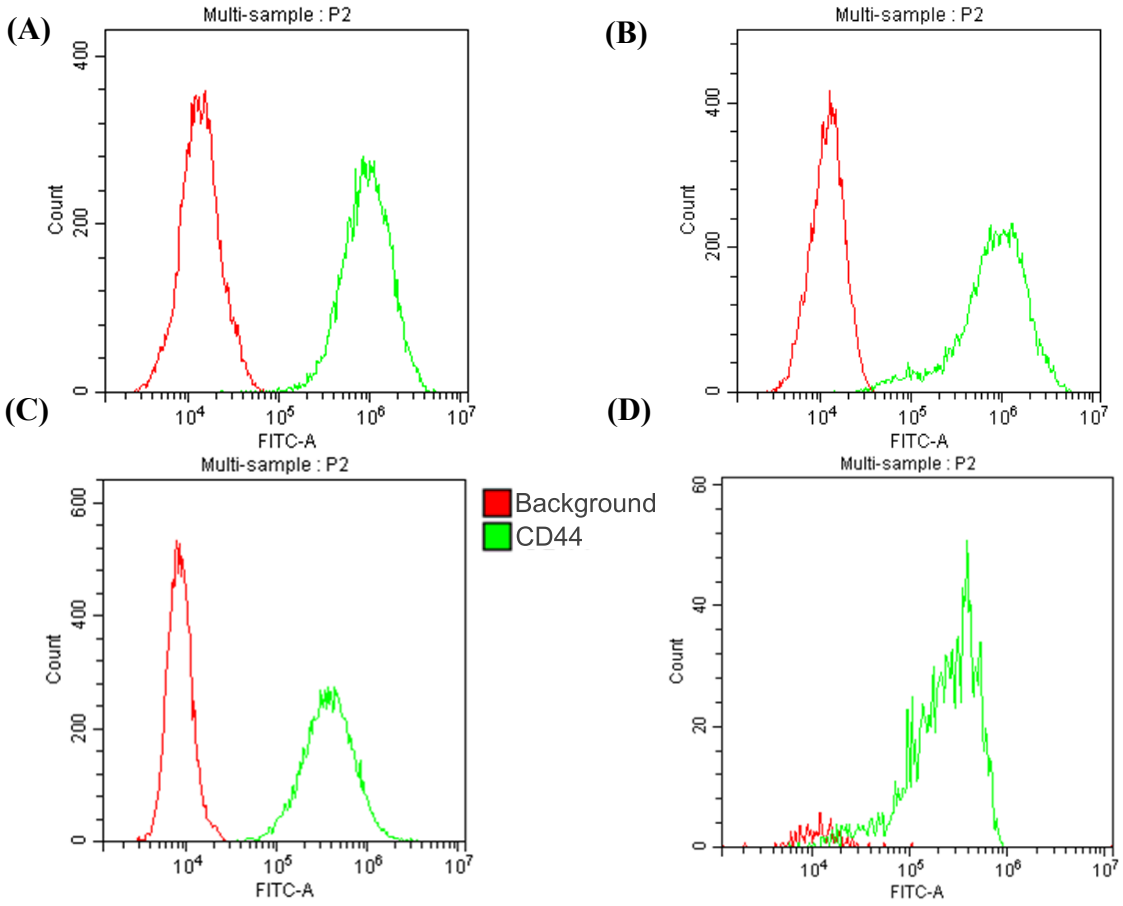

Fig. 38 Flow cytometric characterization of CD44 surface expression. Histograms illustrate the fluorescence intensity of CD44-stained cells (green and magenta lines) compared to the negative control (secondary antibody only, red line) in four different cell lines. The percentage of CD44-positive cells is 99**%** for MEL77-DM (A), 99**%** for MEL66-CL (B), 99**%** for SCC1300-UC (C) , and 94**%** for NHMS32 (D). Data are representative of n = 3 independent experiments.

With regard to the expression of this protein in skin tumour cells, the evaluation was performed using immunofluorescence technique and subsequent analysis by flow cytometry. This allowed us to understand the percentage of cells expressing the marker rather than the total quantity expressed. The results indicate that almost all melanoma cells (99%), as well as melanocytes (94%) and SCC1300-UC (99%) express CD44 (Fig. 38).

3.3 Analysis of the expression of different CD44 isoforms in glioma cells.

Furthermore, as previously discussed, CD44 is a protein that is subject to variation in a specific region, thereby determinig different roles in tumour progression. CD44 is comprised of two distinct regions: a conserved portion and a variable portion. The conserved portion is present in all isoforms,

while the variable portion exhibits variation in terms of the number and combination of exons present. The protein in its form without variable exons is referred to as CD44s, while all other variants are designated CD44v, followed by the number of the exons included in the variable portion (Misra S. et al., 2015).

We therefore evaluated the expression of CD44 variants in gliomas as well as the percentage of CD44s and CD44v they represented. To do this, a pair of primers was designed for each exon, another for the conserved region that includes all variant and non-variant proteins, and finally a pair of primers that could discriminate only CD44s.

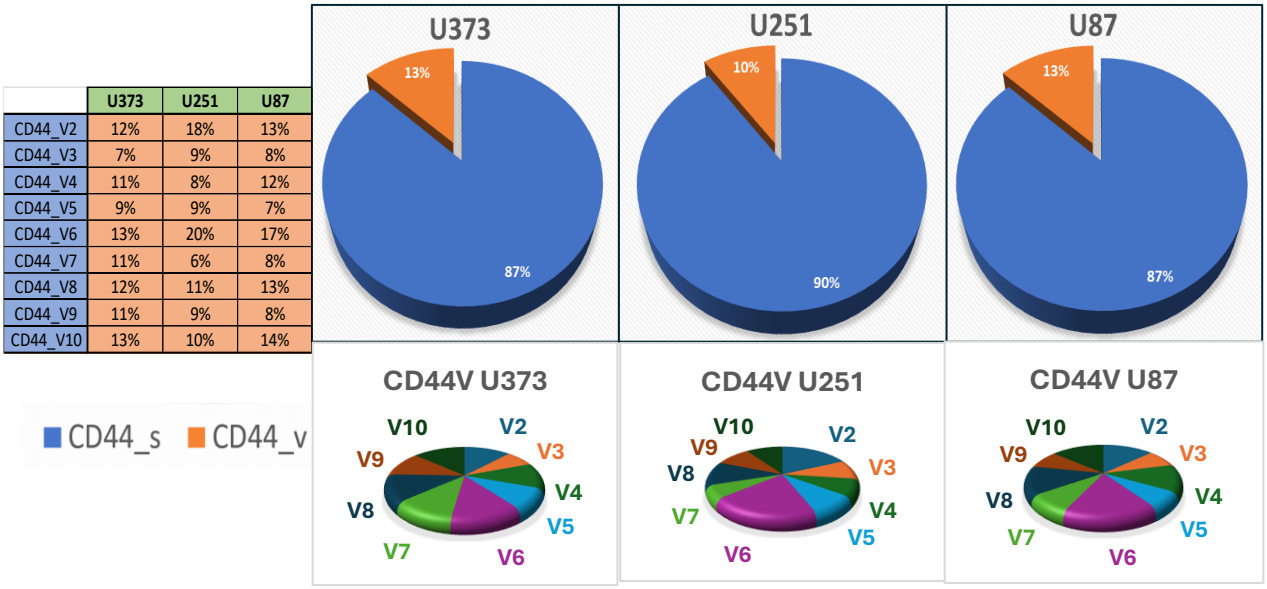

	U373	U251	U87
CD44_V2	12%	18%	13%
CD44_V3	7%	9%	8%
CD44_V4	11%	8%	12%
CD44_V5	9%	9%	7%
CD44_V6	13%	20%	17%
CD44_V7	11%	6%	8%
CD44_V8	12%	11%	13%
CD44_V9	11%	9%	8%
CD44_V10	13%	10%	14%

Fig. 39 Expression profile and distribution of CD44 isoforms in glioma cell lines. The top-left table and pie charts illustrate the relative abundance of the standard isoform (CD44s) versus variant isoforms (CD44v) in U373, U251, and U87 cells, with CD44s representing 87% to 90% of the total pool. The lower pie charts provide a detailed breakdown of the individual variable exons (V2–V10) within the CD44v population. Data obtained via RT-qPCR show that while all variable exons are present, v6 exhibits the highest prevalence among variants in U251 (20%) and U87 (17%).

The results indicate that CD44s represent most of the present isoforms, while the variants account for 13%, 10% and 13% in U373, U251 and U87, respectively (Fig. 39). All exons are expressed; however this test cannot discriminate between their combinations, meaning it is not possible to determine the precise variants expressed by these cell lines. Further studies are therefore needed to fully analyse this topic.

Given the high level of expression of CD44 in non-tumour cells, the possibility of side effects remains, and therefore the search for a variant that can be specific to tumours opens up the possibility of an even more specific target, also with a view to ADC research into cancer stem cells, which are the main cause of recurrence.

3.4 The expression of the EGFR family of proteins in glioma and melanoma cells shows promise as a tumour marker.

Finally, the expression levels of three proteins belonging to the EGFR family were analysed: HER1 (ERBB1), HER2 (ERBB2) and HER3 (ERBB3). These proteins have already been shown to play an important role in tumour growth, and several studies have already identified them as possible targets for ADCs.

Initial evaluation of the expression levels of EGFR (HER1) in gliomas and normal cells was performed using total protein extraction and Western Blot analysis. The results show that, as with

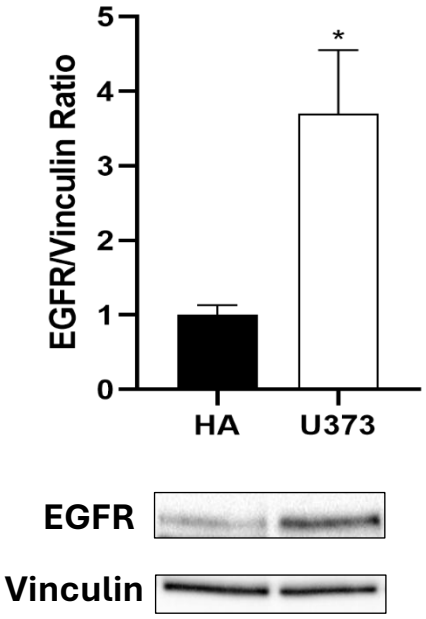

Fig. 40 Baseline expression of CD44 in U373 glioblastoma cells compared to Human Astrocytes (HA). The graphs illustrate the EGFR(HER1)/Vinculin protein ratio as determined by Western Blotting. Data are expressed as mean ± SD (n = 3). Statistical significance was determined by Student's t-test for pairwise comparisons between the treated groups and the control (CTRL). Significance levels * $p < 0.05$ vs CTRL

previous markers, EGFR is expressed in both cell lines, but its expression increases significantly in tumour cells (Fig. 40).

Subsequently, the expression of the three proteins of the EGFR family was analysed in all tumour lines using a screening process. The evaluation was performed by immunofluorescence followed by analysis via flow cytometry. The aim was to analyse which of these proteins exhibited the highest levels of expression in the various cell lines.

The study was performed on both glioma and melanoma cells, and the results show considerable variation between the two types of tumour. In the context of gliomas, the majority of cells express the HER1 receptor, with HER2 expression occurring subsequently and HER3 expression occurring finally (Fig. 41).

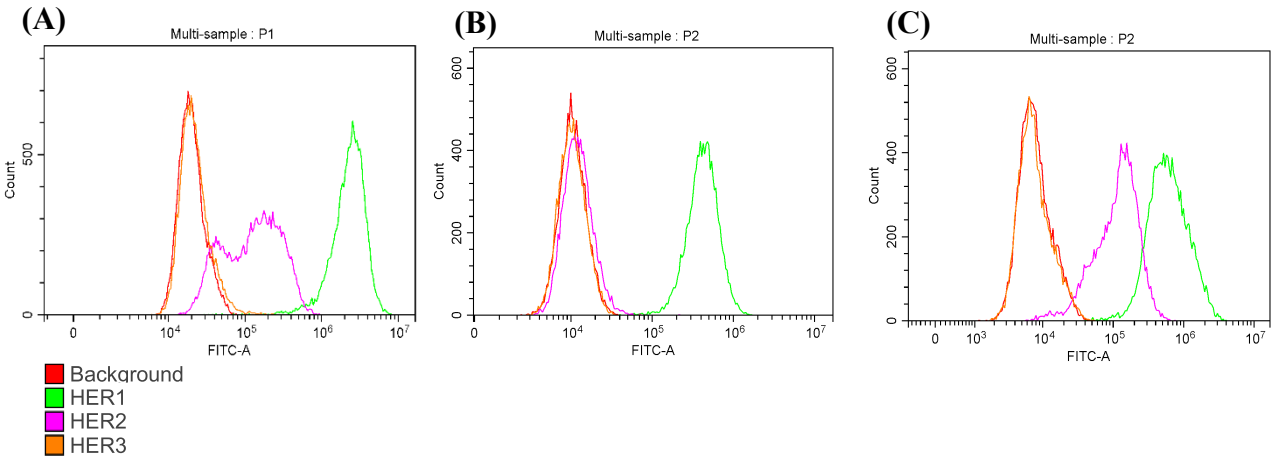

Figure 41. Flow cytometric characterization of EGFR family protein surface expression. Histograms illustrate the fluorescence intensity of HER1-stained cells (green), HER2 (magenta), and HER3 (orange) compared to the negative control (secondary antibody only, red line) in three glioblastoma cell lines: U373 (A), U87 (B), and U251 (C). The percentage of positive cells for each marker is as follows: U251 (99% HER1, 96% HER2, and 1.8% HER3); U87 (99% HER1, 4.5% HER2, and 1.1% HER3); and U373 (99% HER1, 88% HER2, and 8% HER3). Data are representative of n = 3 independent experiments.

In melanomas, the expression levels of these proteins differ considerably. Indeed, the expression of HER1 is almost undetectable, while the other two receptors, HER2 and HER3, show a high percentage of expression in all lines (Fig. 42).

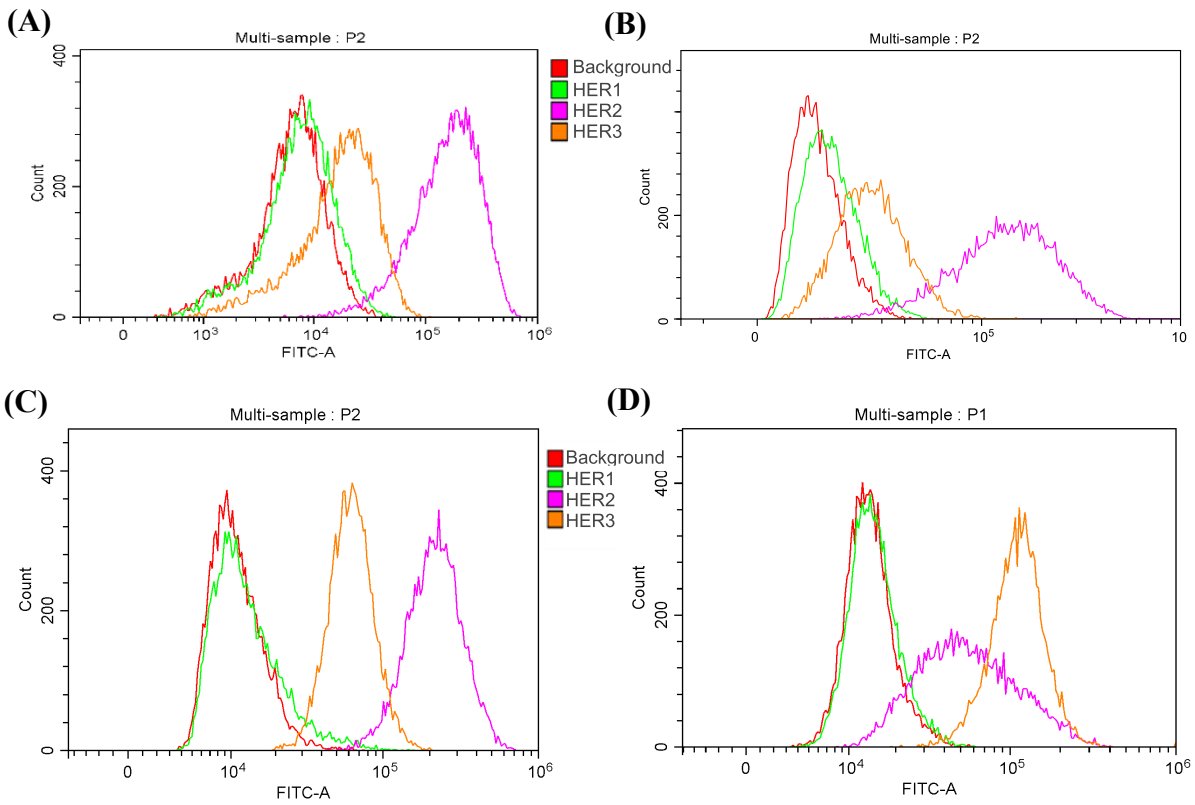

Fig. 42. Flow cytometric characterization of EGFR family protein surface expression. Histograms illustrate the fluorescence intensity of HER1-stained cells (green), HER2 (magenta), and HER3 (orange) compared to the negative control (secondary antibody only, red line) in four melanoma cell lines: MEL16-AR-P (A), MEL16-AR-LDX (B), MEL66-CL (C) and MEL77-DM(D). The percentage of positive cells for each marker is as follows: MEL16-AR-P (4% HER1, 99% HER2, and 43% HER3); MEL16-AR-LDX (3% HER1, 85% HER2, and 36% HER3); MEL66-CL (9% HER1, 99% HER2, and 99% HER3); and MEL77-DM (1% HER1, 90% HER2, and 97% HER3). Data are representative of n = 3 independent experiments.

Subsequently, it was also important to evaluate the expression levels of these proteins on melanocyte and keratinocyte cells in order to assess possible side effects. In this evaluation, two primary lines of normal melanocytes were utilised, with the analysis focused exclusively on only one of the three proteins that had previously been examined, namely HER3. This data was assessed using immunofluorescence and flow cytometry.

The results obtained demonstrate that the expression level of this receptor is notably elevated in both lines of normal melanocytes (NHMS32 and NHMA29) (Fig. 43 A and B). This suggests the possibility of adverse effects resulting from drug delivery to this protein.

Given the close proximity and functional interdependence of melanocytes and keratinocytes, the side effects could also affect this latter cell type. We therefore evaluated HER3 receptor on normal keratinocytes. The results obtained revealed that the percentage of cells expressing the protein was found to be almost negligible (4.5%), thereby suggesting a low probability of binding with the ADC (Fig. 43 C).

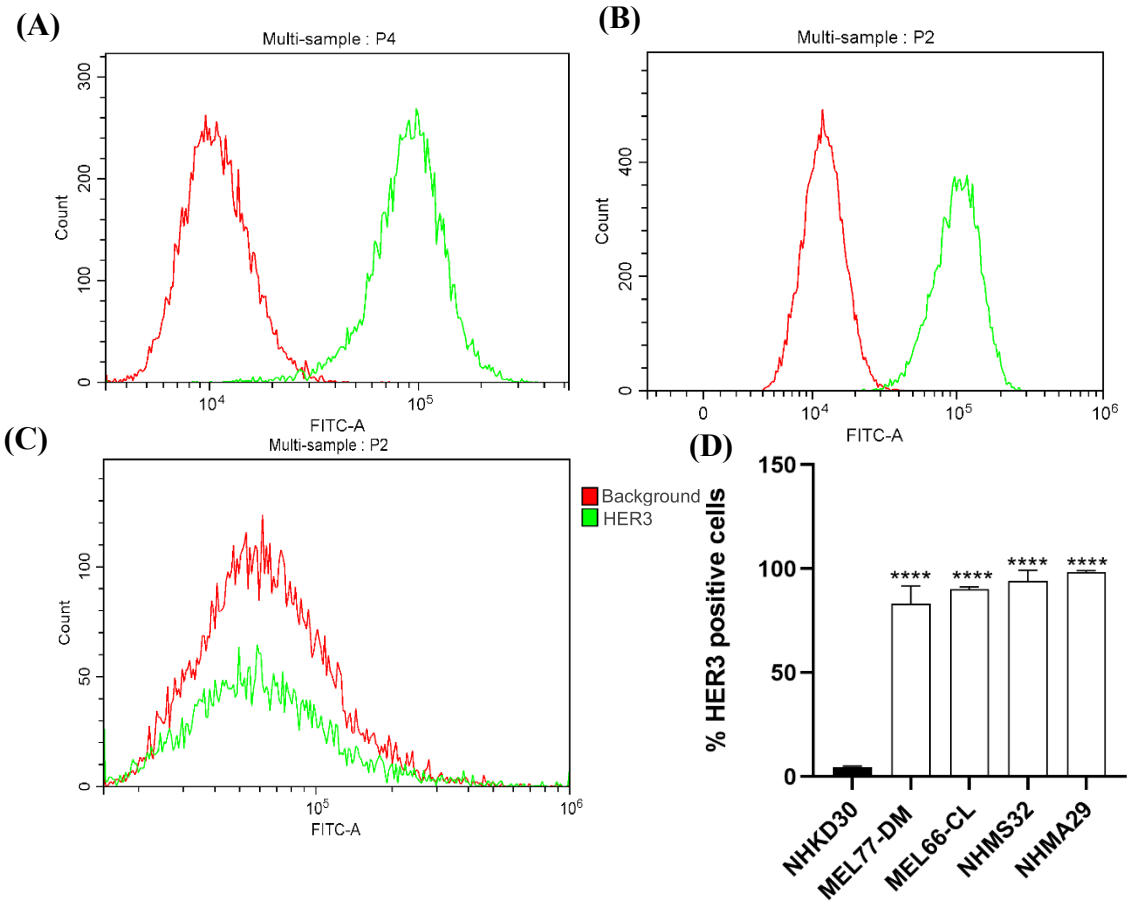

Fig. 43 Flow cytometric analysis of HER3 surface expression across multiple cell lines. Histograms illustrate the fluorescence intensity of HER3-stained cells (green) compared to the negative control (secondary antibody only, red line) in (A) NHMA29, (B) NHMS32, and (C) NHKD30 cell lines. The bar graph (D) summarizes the percentage of HER3-positive cells in NHKD30, MEL77-DM, MEL66-CL, NHMS32, and NHMA29 lines. Data are expressed as mean ± SD (n = 3). Statistical significance: **** $p < 0.0001$ vs. NHKD30.

4. Development of the antibody-drug conjugate and analysis of its effects on melanoma cells

Following a thorough analysis of the effects of CTD and NCTD on cell viability and an evaluation of the expression levels of potential tumour markers, a series of feasibility tests were conducted in order to ascertain the potential for conjugation of the two toxic molecules to the antibody. This assessment was performed by the company ProteoGenix SAS (19 rue de la Haye 67300 Schiltigheim, France), which assisted in the evaluation phase and the actual conjugation of the antibody to the cytotoxic molecule.

The analysis of the data set revealed that both CTD and NCTD caused significant cell death in the majority of the lines examined at equivalent concentrations. While there is almost total homogeneity of toxicity for the effects of CTD, except for greater resistance in skin carcinoma and melanocyte cells, for NCTD there are three lines that proved to be less sensitive: normal melanocytes, skin carcinomas and U373 astrocytoma. In particular, the NHMS32 line exhibited a high degree of resistance to the effects of NCTD, suggesting that the observed side effects may be minimal.

With regard to the expression of markers, none of the proteins showed total exclusivity of expression on tumour lines; however, all provided encouraging results in terms of their higher expression in cancer cells. Moreover, the expression levels of EGFR family receptors exhibited significant heterogeneity between the two tumour classes of glioma and melanoma.

In addition, further analysis of CD44 variants may enable the identification of specific markers of tumour progression and pathological expression exclusivity.

In conclusion, the response provided by the company responsible for evaluating the feasibility of conjugating CTD or NCTD to the antibody indicated that the latter provided superior safety and efficiency in the process.

Considering the aforementioned results, it was determined that NCTD molecule should be conjugated to the antibody directed against HER3. This approach facilitates the correlation of the reduced sensitivity of normal cells to NCTD with the negligible expression of the marker in keratinocyte cells. This finding suggests that the effects of the antibody-NCTD conjugate may be specific to the tumour condition of melanomas, without affecting surrounding cells. This choice is regrettable insofar as it restricts the utilization of ADC to a single tumour category among those analysed. Nevertheless, efforts are underway to expand this approach to gliomas by means of conjugating an additional ADC specifically designed for the treatment of that condition.

4.1 The antibody chosen for the ADC internalize efficiently before and after the conjugation

As described above, in order to release its cargo, the ADC needs to be internalised. This means that the antibody carrying the cargo reaches the lysosomes, where it can release the molecule. Consequently, before proceeding with the conjugation, a final test was conducted to verify the effective internalisation of the antibody within the cells under investigation. To achieve this, immunofluorescence was performed, whereby a cell suspension was labelled with an anti-HER3 antibody keeping it in an incubator at a standard temperature of 37°C. Another cell suspension was kept in the same incubator for the same amount of time but at a temperature of 4°C, to block internalisation.

The results obtained show that, during the incubation period, the majority of the antibody was endocytosed, confirming its suitability as a candidate for the development of the ADC (Fig. 44).

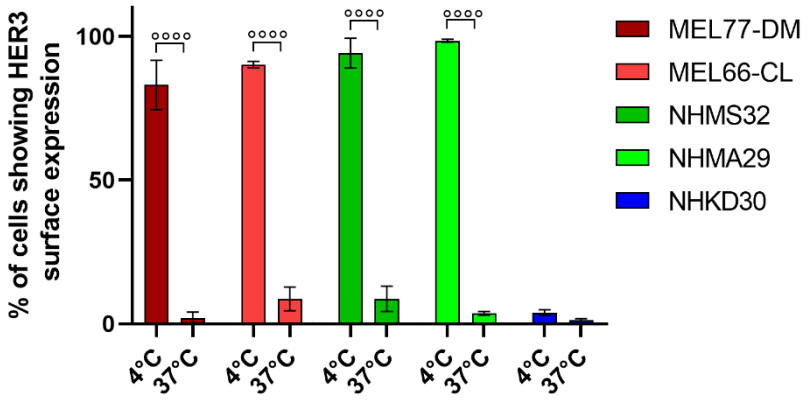

Fig. 44 Analysis of HER3 antibody internalization by temperature-dependent surface depletion. Surface binding was measured at 4°C (blocking endocytosis) and compared to expression at 37°C (standard incubator conditions). The bar graph shows the percentage of cells that express HER3 on their surfaces. The signal decreases at 37°C by 81% in MEL77-DM, 81% in MEL66-CL, 86% in NHMS32, 95% in NHMA29, and 1% in NHKD30. Data are presented as mean ± SD. Statistical significance: °°°° $p < 0.0001$ between 4°C and 37°C for each respective cell line.

After evaluating the internalisation capacity of the tumour marker and the antibody, the conjugation process was initiated.

The final product is a DAR4-conjugated antibody-NCTD (*i.e.*, an anti-HER3 antibody that binds four NCTD molecules via a linker). Once the antibody reaches the lysosomes, it breaks down and releases the NCTD.

Subsequent to the acquisition of the conjugate, an investigation was conducted into whether the ADC exhibited equivalent binding and internalisation capacity to the parent antibody (αHER3).

The internalisation experiment displayed above was then repeated, with immunofluorescence added with the ADC. The result suggests that the efficacy of the unconjugated antibody was equivalent to that of the ADC (Fig. 45) across all cell lines examined.

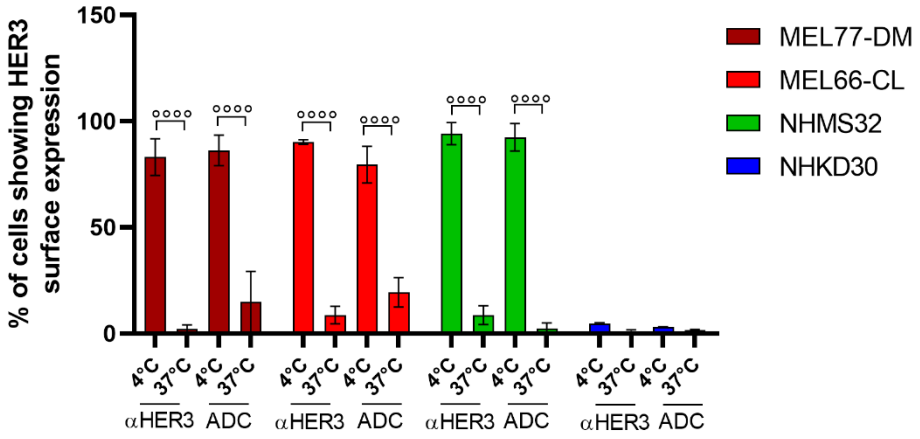

Fig. 45 Comparison between parent HER3 antibody internalization and novel ADC by temperature-dependent surface depletion in different cell lines. The experiment was conducted with the same protocol used for Fig. 43. Data are presented as mean ± SD. Statistical significance: °°°° $p < 0.0001$ with $n=3$.

4.2 The validation assays for ADC demonstrate its effectiveness in reducing tumour vitality without causing side effects.

At this stage, an MTT assay was employed to assess the toxicity of the conjugate at varying concentrations. The cells were treated with both the ADC and the amount of NCTD corresponding to that carried by the ADC molecules, *i.e.* approximately 4 times more concentrated.

In the initial experiment, a low concentration of ADC (1 µM) was utilised as a sub-lethal dose on cells that expressed the marker. The treatment was maintained for five days, and the results showed that there were no alterations in cell viability (Fig. 46).

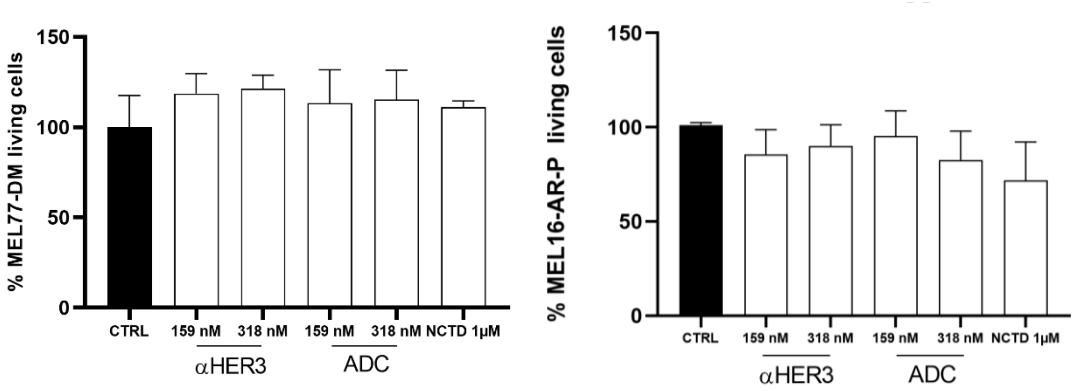

Fig. 46 Effect of a 5-days treatment with ADC, αHER3 with two doses 159 µM and 318 µM and 1 µM NCTD on MEL77-DM and MEL16-AR-P cell viability. Results were assessed by MTT that was performed as specified in materials and methods. Data are expressed as a percentage of viable cells relative to the untreated control (CTRL). Bars represent the mean ± standard deviation (SD) of *n=3* independent experiments. Statistical significance was determined by One-way ANOVA followed by Tukey's post-hoc test.

The experiment was then repeated using higher concentrations of ADC, and the following three distinct cell lines to assess the occurrence of side effects.

Mel77-DM cells that have already been shown to be sensitive to 50 µM NCTD and should therefore respond to the treatment at these higher concentrations; NHMS32 cells that have been observed to have a higher tolerance to NCTD and should maintain high levels of viability; and finally, U373 cells that have not only a lower sensitivity to NCTD but also an almost absent expression of the HER3 protein.

The treatment was maintained for 72 hours, and the results of this experiment indicate that the effects of ADC are not evident in either NHM or U373 cells. NHMS32 cells exhibit a significant degree of tolerance to NCTD. Moreover, even in sensitive cells, such as MEL77-DM, that are expected to be susceptible to the effects of the antibody, no detrimental impact on viability has been observed. This finding suggests that higher doses of ADC may be required to elicit the desidered effect of NCTD (Fig. 47).

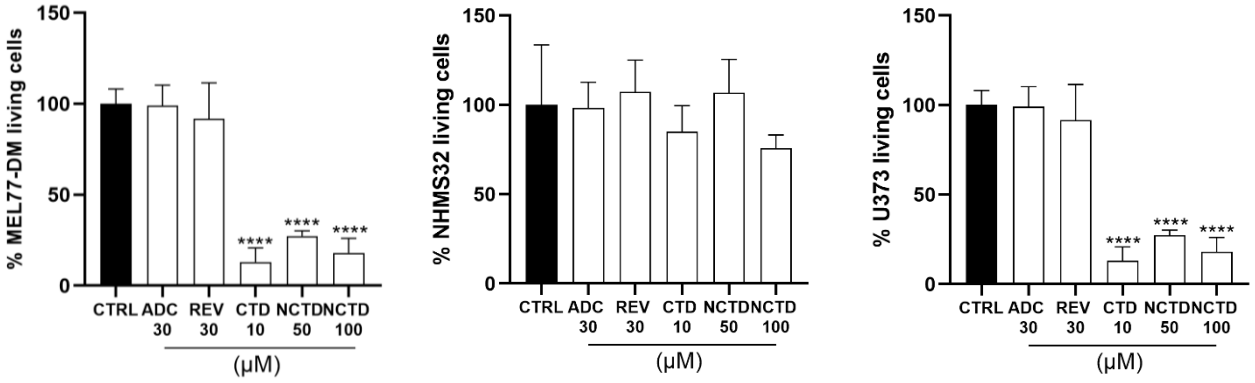

Fig. 47 Effect of a 72 h treatment with ADC and αHER3 (30 μM), 50 μM NCTD and 10 μM CTD on MEL77-DM, NHMS32 and U373 cell viability. Results were assessed by MTT that was performed as specified in materials and methods. Data are expressed as a percentage of viable cells relative to the untreated control (CTRL). Bars represent the mean ± standard deviation (SD) of *n=3* independent experiments. Statistical significance was determined by One-way ANOVA followed by Tukey's post-hoc test. Significance levels: **** $p < 0.0001$ vs. CTRL.

The experiment was thus repeated, with the ADC concentration being doubled. In this third experiment, a sensitive cell line, MEL77-DM, and a cell line that does not carry the marker on its

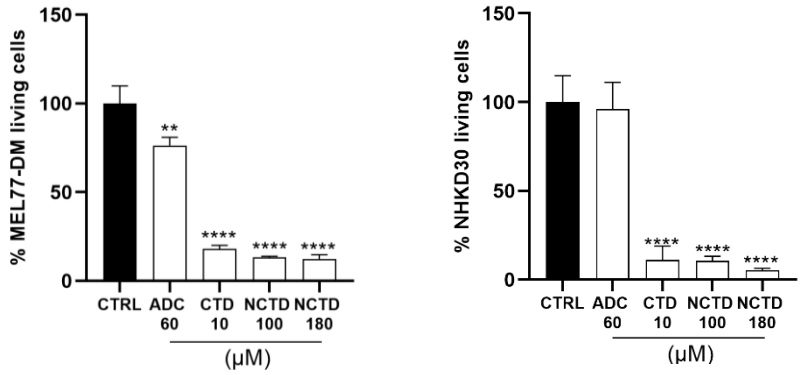

Fig. 48 Effect of a 72 h treatment with ADC 60 μM, 100 μM and 180 μM NCTD, and 10μM CTD on MEL77-DM and NHKD30 cell viability. Results were assessed by MTT that was performed as specified in materials and methods. Data are expressed as a percentage of viable cells relative to the untreated control (CTRL). Bars represent the mean ± standard deviation (SD) of *n=3* independent experiments. Statistical significance was determined by One-way ANOVA followed by Tukey's post-hoc test. Significance levels: **** $p < 0.0001$ and ** $p < 0.01$ vs. CTRL.

membrane, normal human keratinocytes (NHKD30), were utilised.

As shown in Fig. 48, there was a 24% decrease in cell viability in those treated with ADC after 72 hours, while cell viability remained unchanged in those not expressing the membrane protein.

The results obtained provide significant information regarding the efficacy of the ADC under investigation. They serve also to confirm the suitability of the HER3 antigen as a tumour marker for cutaneous melanoma. Nevertheless, further studies are required in order to evaluate the efficiency of payload release, as well as its concentration inside the targeted cells.

DISCUSSION

The present study systematically investigated the cytotoxic mechanisms of cantharidin and its demethylated analogue norcantharidin across glioma and melanoma cell lines alongside their normal counterparts. The results reveal a complex and heterogeneous mechanism of action of CTD and NCTD, with a focus on ROS increase, calcium dysregulation, and impairment of Nrf2. With regard to the drug efficiency, the data demonstrate that NCTD exhibits a focused therapeutic window in comparison to CTD, particularly in melanocytes. Furthermore, the combination with a HER3-targeted antibody represents a promising strategy for tumour-selective delivery.

The PAMPA results demonstrate that both CTD and NCTD exhibit robust passive membrane permeability, with NCTD showing particularly high permeability (P_e = 11.10 × 10^{-6} cm/s) comparable to caffeine (P_e = 12.10 × 10^{-6} cm/s), while CTD displayed slightly lower but still substantial permeability (P_e = 7.38 × 10^{-6} cm/s). Both compounds significantly exceeded the P_e of the low-permeability marker Trypan Blue, thus confirming their ability to readily access the intracellular compartment via passive diffusion.

These findings are consistent with the physicochemical properties of these molecules—low molecular weight (CTD: 196.20 g/mol; NCTD: 168.15 g/mol) and favourable lipophilicity. Although direct PAMPA data for CTD and NCTD is scarce in the published literature, formulation studies have validated their bioavailability. A comprehensive review of NCTD pharmacology has highlighted its favourable ADME characteristics in comparison to CTD (Pan M.S. et al., 2020).

The elevated passive permeability provides a robust foundation for the swift onset of the biological effects observed in our viability and cellular signalling experiments. This rapid cellular entry eliminates the need for active transport mechanisms and suggests that intracellular target affliction is the rate-limiting step.

CTD and NCTD are well-established inhibitors of the serine/threonine protein phosphatase PP2A (Liu X.H. et al., 1995) (Li W. et al., 2010). PP2A is an important enzyme that regulates critical cellular processes, including cell cycle control, apoptosis and cell fate determination (Li W. et al., 2010). Inhibiting this enzyme significantly alters the cellular phosphorylation balance. This alteration affects multiple downstream signalling pathways involved in cell cycle regulation, stress responses and the initiation of apoptotic mechanisms (Su CC. et al., 2015). Therefore, the inhibition of PP2A by CTD/NCTD could lead to profound dysregulation of the kinase-phosphatase balance and hyperphosphorylation of multiple signalling nodes.

Several studies have shown that CTD inhibits PP2A, thereby activating or dysregulating key kinase pathways, including ERK, JNK, PKC and NF-κB (Shen M. et al., 2021). This kinase dysregulation could have direct consequences for calcium homeostasis and ER stress. In human bladder cancer cells, it has been demonstrated that cantharidin increases intracellular Ca^{2+}, activates PKC, induces ER stress markers (phospho-eIF2α, GRP78), and increased calpain activity and caspase cleavage (Su CC. et al., 2015). The findings of my thesis find confirmation in this above-mentioned studies, in particular with a hypothesized model:

PP inhibition → PKC activation → Ca^{2+} dysregulation → ER stress → apoptosis.

We observed that CTD and NCTD induced a progressive increase in cytosolic Ca^{2+} levels starting from 170 minutes after treatment in U373 cells, with sustained elevation across all examined time windows (1–6 h, 5–10, and 20–25 hours). Note that neither extracellular calcium chelation (EGTA) nor inhibition of store-operated calcium entry channels (SKF96365) prevented this calcium accumulation This suggests that the calcium may originate from intracellular stores, most likely the endoplasmic reticulum. This finding is consistent with Su et al. that BAPTA-AM (an intracellular chelator) but not the removal of extracellular calcium blocks CTD-induced apoptosis (Su CC. et al., 2015).

While the mechanism linking CTD/NCTD activity to PP2A inhibition and ultimately ER calcium release was not fully explored in this thesis, it is likely to involve altered phosphorylation of calcium-handling proteins. Although direct phosphorylation mapping of IP3 receptors, ryanodine receptors, or SERCA pumps was not performed in the present study, the literature supports the concept that the balance between kinases and phosphatases regulates ER calcium channel activity. For instance, PKC and other kinases modulate IP3 receptor sensitivity, and JNK signalling has been demonstrated to influence ER stress sensors (Su CC. et al., 2016). Further studies are therefore necessary to fully understand the mechanism that correlates the direct relationship between CTD/NCTD and calcium accumulation in the cell.

A salient finding of this study pertained to the vigorous production of ROS and the subsequent inhibition of Nrf2. The flow cytometry analysis, using DCFH-DA, demonstrated that CTD (10 μM) induced an increase in ROS in U373 cells, peaking at 6 hours and subsequently declining by 16–24 hours. In melanoma cells (MEL66-CL and MEL77-DM), levels of ROS began to increase after 6 hours and remained elevated up to 24 hours, reaching 4- to 6-fold compared to the control group. Normal human melanocytes exhibited a transient increase in ROS levels of 2.7-fold at 6 hours, which return to normal levels by 24 hours.

NCTD (25 μM) induced similar progressive increases in ROS in melanoma cells, peaking at 24 hours, while in NHM, even at 100 μM NCTD, ROS peaked transiently at 6 hours and returned to baseline by 24 hours.

To assess whether oxidative stress was the primary lethal mechanism, a ROS scavenging procedure was performed in order to prevent cell death. However, MTT assay demonstrated that co-treatment with N-acetylcysteine (2 mM)—which fully restored ROS levels to control values at all time points examined (6, 16, and 24 hours)—provided only a modest 10% improvement in viability in CTD-treated U373 cells. This minimal rescue suggests that ROS contribute to the process, but do not act as the primary drives of the cytotoxic process.

A salient finding of this study is the inhibition of Nrf2 nuclear translocation by both CTD and NCTD. Nrf2 is the principal regulator of the cellular antioxidant response, governing the expression of genes containing antioxidant response elements. These include HO-1, xCT, GPX4, SOD1 and catalase.

Under basal conditions, Nrf2 is sequestered in the cytoplasm by KEAP1, which targets it for proteasomal degradation. Upon oxidative or electrophilic stress, Nrf2 stabilizes, accumulates, and translocates to the nucleus to activate cytoprotective gene pathways (D'Ezio et al., 2021).

Western blot analysis of nuclear extracts from U373 cells has revealed a significant reduction in nuclear Nrf2 levels in response to CTD treatment: 50% after 2 hours, 40% after 4 hours and a further decrease to 0.45- and 0.37-fold at 16 and 24 hours, respectively. This inhibition was not due to reduced Nrf2 mRNA expression, as RT-qPCR demonstrated unchanged transcript levels at all examined time points (4, 8, and 24 hours). This finding suggests that CTD acts at a post-translational level, impacting the stability, subcellular localization, or the machinery responsible for nuclear import of the Nrf2 protein, rather than affecting gene transcription.

Most remarkably, CTD prevented Nrf2 nuclear accumulation even in the presence of dimethyl fumarate , a well-characterized Nrf2 activator which works by covalently modifying Cys151 on KEAP1, thereby releasing Nrf2 from KEAP1-mediated degradation (Brennan M.S. et al., 2015). In the present experiments, while DMF alone increased nuclear Nrf2 by 60%, co-treatment with CTD and DMF resulted in Nrf2 levels equivalent to the control group. This finding indicates that CTD blocks a step downstream of KEAP1-Nrf2 dissociation most likely nuclear import or promoting rapid nuclear export.

Immunofluorescence studies in melanoma cells (MEL77-DM) and melanocytes (NHMS32) confirmed that Nrf2 inhibition is a conserved mechanism across cell types. Interestingly, CTD (7.5 μM) reduced nuclear Nrf2 by 20% in MEL77-DM cells, whereas NCTD (25 μM) produced a much

stronger reduction of 75%. In melanocytes, however, the pattern was reversed with NCTD causing a 20% reduction and CTD inducing a 65% decrease. These cell-type-specific differences may reflect variations in the expression of nuclear transport machinery, phosphatase isoforms, or compensatory pathways, and further investigation is warranted.

The functional consequences of Nrf2 inhibition were evident in the antioxidant gene expression profiling. The data obtained from U373 cells revealed a more complex picture. While catalase mRNA decreased consistently across all time points and GPX4 protein levels dropped to 0.65-fold, xCT and HO-1 showed paradoxical induction at both the mRNA and protein levels. xCT mRNA increased 3.8-fold at 4 hours and peaked at 5-fold, while HO-1 exhibited a 2.2-fold increase from 8 hours onward. At the protein level, xCT showed a modest 1.5-fold increase at 24 hours, while HO-1 protein exhibited a 3.9-fold increase.

This seemingly paradoxal antioxidant response, involving the simultaneous suppression of some defences (Catalase and GPX4) and induction of others (xCT and HO-1), suggests that multiple, potentially competing regulatory mechanisms are in operation. The induction of xCT and HO-1 may represent a direct response to elevated ROS via redox-sensitive transcription factors other than Nrf2, such as AP-1 (Medina M.V. et al., 2020) or ATF4 (Li J.K.M. et al., 2019), which can also regulate ARE-containing genes. Western blot data, which show that NAC fully restores basal xCT and HO-1 protein levels, support the interpretation that their induction is a direct response to ROS rather than an Nrf2-driven program.

A critical consideration for any anticancer agent is its cytotoxic effect in terms of cellular the viability of healthy cells. We studied by MTT assay the lethal concentration of both molecules, in the two types of tumour, and then we evaluated possible side effects on their normal counterparts. Our results demonstrate that NCTD exhibits a superior therapeutic window compared to CTD, particularly in

melanocytes. While melanoma cells (MEL66-CL, MEL77-DM, MEL16-AR-P) showed significant toxicity at 5–7.5 μM CTD and 12.5–25 μM NCTD, normal human melanocytes (NHMS32) required 10-fold higher NCTD concentrations to achieve comparable toxicity. In contrast, CTD exhibited more similar toxicity profiles between melanoma and melanocytes, and both agents showed comparable toxicity in glioma cells and astrocytes when normalized for proliferation rate. The effect observed in glioma cells is analogous to that seen in melanoma cells following CTD treatments, with a marginal increase in CTD toxicity in the second cell type. Conversely, NCTD exhibited a substantially less pronounced effect on astrocytoma cells compared to melanomas.

The structural difference between CTD and NCTD (demethylation at the bridge position) has given some interesting consequences for their pharmacological profile. As is evident in reviews and comparative studies, NCTD generally exhibits reduced systemic toxicity while retaining anticancer activity (Zhai BT et al., 2022). The mechanisms underlying this differential toxicity may include the following factors: altered PP1/PP2A inhibition potency(Wang G. et al., 2018); differential pharmacokinetics and tissue distribution; variations in cellular uptake or efflux; and cell-type-specific differences in compensatory pathways or stress tolerance.

Importantly, these data suggest that the therapeutic window is context-dependent. This underscores the need for tumour-selective delivery strategies, such as the design and development of antibody-drug conjugates, to maximize the therapeutic benefit while minimizing systemic toxicity.

Given the strong reduction in cell viability observed in preceding experiments, a major objective of this study was to selectively direct the cytotoxic activity of cantharidin and norcantharidin toward tumour cells in order to limit the important side effects of these molecules. Norcaritidin has already been shown to be quite effective in treating skin cancer, further confirming the importance of CTD and its derivatives as potential anti-cancer drugs (Martínez-Razo G. et al., 2025). To achieve this goal and enable the development of an antibody–drug conjugate, a screening of potential tumour associated surface markers has been performed. The expression of System Xc^-, CD44 and selected

members of the EGFR family was analysed in tumour cell lines and compared with their normal counterparts.

System Xc^- expression was first evaluated in glioma cells (U373) and normal human astrocytes (HA). The expression of the transporter was observed at the mRNA and protein levels in both cell types; however, a heightened expression was exhibited by tumour cells, with a two-fold upregulation at the RNA level and an approximately ten-fold increase at the protein level. Despite this difference, the presence of lower levels of System Xc^- in normal cells renders it a suitable candidate as an ADC target.

A similar pattern was observed for CD44. In glioma cells, CD44 expression was detected in both tumour and normal astrocytes, with higher levels in cancer cells (2.7-fold at the mRNA level and two-fold at the protein level). In skin-derived cells, CD44 expression was detected not only in melanoma cells but also in melanocytes, indicating widespread expression in both pathological and physiological conditions. Analysis of CD44 isoforms in glioma cell lines revealed a strong predominance of the standard isoform (CD44s), while variant isoforms accounted for only a minor fraction of total CD44 expression. Given the abundance of CD44 and its major isoform expression in non-tumour cells, the risk of adverse effects remains significant due to the high general levels of expression. However, the potential for future opportunities exists with the identification of tumour-specific variants. To achieve this, further specialized investigations are required to characterize these variants with high precision, such as RNA-sequencing (RNAseq) and long-read sequencing technologies (such as Oxford Nanopore or PacBio). These advanced transcriptomic approaches will allow us to accurately map the complex alternative splicing patterns and identify specific combinations of variable exons that may be exclusively associated with tumor progression and cancer stemnessIn contrast, members of the EGFR family displayed more promising and heterogeneous expression profiles. HER1, HER2 and HER3 were analysed by Western blotting, immunofluorescence and flow cytometry. In glioma cells, HER1 was the most highly expressed receptor, followed by HER2 and HER3, whereas melanoma

cells showed an almost complete absence of HER1 but high expression of HER2 and HER3. Importantly, HER3 expression was further evaluated in normal skin cells to assess potential side effects. While HER3 was expressed at high levels in normal melanocytes, its expression in keratinocytes was negligible, suggesting a low probability of off-target binding in surrounding epithelial tissue.

Parallel viability assays demonstrated that NCTD induced strong cytotoxic effects in most tumour cell lines, while normal melanocytes cells exhibited an important resistance, supporting the hypothesis of limited side effects. Based on the combined analysis of cytotoxicity, marker expression and conjugation feasibility, NCTD was selected as the payload and HER3 as the targeting antigen.

The internalization studies confirmed that the anti-HER3 antibody (and successively the resulting ADC with DAR4 configuration) efficiently internalized in melanoma cells expressing HER3.

Cytotoxicity assays demonstrated tumor-selective killing: at high ADC concentrations (60 μM), MEL77-DM melanoma cells showed a 24% reduction in viability after 72 hours, while HER3-negative keratinocytes (NHKD30) maintained viability. Normal melanocytes (NHMS32), despite expressing HER3, showed considerable tolerance to NCTD, indicating a potential reduction in adverse effects.

These results provide proof-of-concept that targeted delivery of NCTD to HER3-positive tumours can result in selective toxicity. However, the relatively modest 24% viability reduction at high ADC doses suggests that further optimization is required. Moreover, it is essential to assess the efficacy of payload release and its distribution within the targeted cells.

Although the findings of this research provide a solid foundation for the development of novel therapeutic strategies, several intrinsic limitations must be considered to define the scope of future investigations. The use of *in vitro* models based on two-dimensional (2D) cell cultures allowed for a detailed characterization of the mechanisms of action, yet they do not fully reflect the architectural

complexity and dynamic interactions typical of the solid tumor microenvironment. Consequently, the integration of future studies based on 3D models and organoids would represent a fundamental step toward more accurately assessing tissue penetration and drug efficacy in a more physiologically relevant context.

Another area for future inquiry involves the evaluation of the "bystander effect," which is essential for determining whether the released cytotoxic payload can eliminate neighboring tumor cells lacking the HER3 marker, thereby optimizing tumor eradication.

Furthermore, there is a clear need for *in vivo* validation before clinical translation can be considered, which is an indispensable step for defining pharmacokinetic parameters and the systemic safety profile. Finally, the collected data pave the way for evaluating new ADCs specifically targeted at gliomas, extending the precision therapeutic approach beyond the melanoma model.

CONCLUSIONS

This thesis establishes cantharidin (CTD) and norcantharidin (NCTD) as promising multi-mechanistic anticancer agents with significant potential for clinical translation, particularly in melanoma therapy. The present study constitutes a comprehensive investigation which demonstrates that both compounds exhibit potent cytotoxic activity across glioblastoma and melanoma cell lines, with IC_{50} values of 5–10 μM for CTD and 25–100 μM for NCTD. Crucially, a superior therapeutic window for NCTD was identified in normal melanocytes, which require approximately 10-fold higher concentrations to achieve comparable toxicity, thus positioning NCTD as the preferred candidate for melanoma therapy.

The PAMPA permeability studies confirm that both CTD and NCTD cross biological membranes via passive diffusion.

The finding that Nrf2 inhibition, triggered by CTD and NCTD, occurs at the post-translational level, represents a novel mechanism with significant implications for overcoming chemoresistance in tumours with elevated Nrf2 levels. Furthermore, the findings suggest that, while ROS levels are elevated, they do not act as the primary catalysts for cell death. Conversely, the present study places greater emphasis on the potential involvement of endoplasmic reticulum stress and calcium dysregulation.

The successful development of a HER3-targeted antibody-NCTD conjugate provides proof of concept for tumour-selective delivery in melanoma. Negligible HER3 expression in keratinocytes (4.5% positive cells), in combination with NCTD's intrinsic selectivity for tumour cells over melanocytes, creates a dual-selectivity mechanism that minimizes off-target toxicity.

In conclusion, this work establishes a foundation for the clinical development of NCTD-based therapies, particularly HER3-targeted ADCs for melanomas. Their multi-mechanistic action, ability

to bypass Nrf2-mediated resistance and demonstrated tumour selectivity position these compounds as innovative therapeutic agents warranting further preclinical validation and clinical investigation.

ABBREVIATIONS

ADC	Antibody drug Conjugate
AP-1	Activator protein 1
ARE	Antioxidant Response Element
BBB	Blood-brain barrier
CAT	Catalase
CSC	Cancer stem cell
CTD	Cantharidin
DCFH-DA	Dichlorofluorescein diacetate
DISC	Death-Inducing Signaling Complex
DMF	Dimethyl fumarate
ER	Endomplasmic reticulum
EGFR	Epidermal growth factor receptor
EGTA	Extracellular calcium chelation
ERK	Extracellular signal-regulated kinases
GBM	Glioblastoma multiforme
GSC	Glioblastoma stem cells
GCL	Glutamylcysteine ligase
GPX	Glutathione Peroxidase
GSH	Reduced glutathione
IDH	Isocitrate dehydrogenase
JNK	c-Jun N-terminal kinases
HA	Human astrocytes
HFF2	Human Foreskin Fibroblast-2
HO-1	Heme Oxygenase 1
Keap1	Kelch-like ECH-associated protein 1
MMP	Matrix metalloproteinases
NAC	N-acetylcysteine
NCTD	Norcantharidin
NF-kB	Nuclear factor kappa-light-chain-enhancer of activated B cells
NHK	Normal human keratinocytes
NHM	Normal human melanocytes
Nrf2	Nuclear factor erythroid 2-related factor 2
NMSC	Non-melanoma skin cancer
NSCLC	Non-Small Cell Lung Cancer
Pe	Permeability coefficients
PAMPA	Parallel Artificial Membrane Permeability Assay
PP1	Protein Phosphatase 1
PP2	Protein Phosphatase 2
ROS	Reactive Oxygen Species
SCC	Squamous cell carcinoma
SHSY5Y	Human neuroblastoma cells

SMs	Small molecules
SOD	SuperOxide Dismutase
TAM	Tumor-associated macrophages
TME	Tumor microenvironment
TGF	Transforming growth factor beta
TNF-α	Tumor Necrosis Factor alpha
VEGF	Vascular endothelial growth factor
WB	Western Blotting
WHO	World Health Organization
xCT	System Xc-

ACKNOWLEDGMENTS

This research was supported by European Union – Next Generation EU funding, Mission 4 Component 2 Investment 1.5, within the "Rome Technopole" project (code ECS 00000024).

Sincere gratitude is extended to the Laboratorio di Fisiopatologia Cutanea dell'Istituto San Gallicano, particularly to Dr. Barbara Bellei and Dr. Daniela Kovacs, for their constant support and for providing the Melanoma, Carcinoma, Keratinocytes and Melanocytes cell lines.

Gratitude is also expressed to Takis Biotech for their valuable collaboration and for providing antibodies from the EGFR family.

Professor Marco Alberto Bologna of Roma Tre University for his significant scientific contribution and intellectual guidance provided throughout the development of this project

REFERENCES

AA.VV., 2023. I numeri del cancro in Italia [WWW Document]. AIOM. URL https://www.aiom.it/i-numeri-del-cancro-in-italia/ (accessed 7.17.24).

Bellei B, Caputo S, Migliano E, Lopez G, Marcaccini V, Cota C, Picardo M. Simultaneous Targeting Tumor Cells and Cancer-Associated Fibroblasts with a Paclitaxel-Hyaluronan Bioconjugate: In Vitro Evaluation in Non-Melanoma Skin Cancer. Biomedicines. 2021 May 24;9(6):597. doi: 10.3390/biomedicines9060597. PMID: 34073987; PMCID: PMC8225214.

Bischoff K. Cantharidin. Vet Clin North Am Equine Pract. 2024 Apr;40(1):113-119. doi: 10.1016/j.cveq.2023.08.002. Epub 2023 Sep 15. PMID: 37716858.

Bologna MA, Oliverio M, Pitzalis M, Mariottini P (2008) Phylogeny and evolutionary history of the blister beetles (Coleoptera, Meloidae). Molecular Phylogenetics & Evolution 48, 679–693

Brennan MS, Matos MF, Li B, Hronowski X, Gao B, Juhasz P, Rhodes KJ, Scannevin RH. Dimethyl fumarate and monoethyl fumarate exhibit differential effects on KEAP1, NRF2 activation, and glutathione depletion in vitro. PLoS One. 2015 Mar 20;10(3):e0120254. doi: 10.1371/journal.pone.0120254. PMID: 25793262; PMCID: PMC4368598.

Chen RT, Hua Z, Yang JL, Han JX, Zhang SY, Lü FL, Xü B. Studies on antitumor actions of cantharidin. Chin Med J (Engl). 1980 Mar;93(3):183-7. PMID: 6766849.

Cozma EC, Banciu LM, Soare C, Cretoiu SM. Update on the Molecular Pathology of Cutaneous Squamous Cell Carcinoma. Int J Mol Sci. 2023 Apr 2;24(7):6646. doi: 10.3390/ijms24076646. PMID: 37047618; PMCID: PMC10095059.

De tuto cantharidum in medicina usu interno / [Joannes Groeneveld]. Londini : Typis J. H. prostant venales apud Johannem Taylor, 1698 Public Domain Mark. Source: Wellcome Collection. https://wellcomecollection.org/works/bxqfkqnq

D'Ezio V, Colasanti M, Persichini T. Amyloid-β 25-35 Induces Neurotoxicity through the Up-Regulation of Astrocytic System X_c. Antioxidants (Basel). 2021 Oct 26;10(11):1685. doi: 10.3390/antiox10111685. PMID: 34829555; PMCID: PMC8615014.

Edupuganti VVSR, Tyndall JDATDA, Gamble AB. Self-immolative Linkers in Prodrugs and Antibody Drug Conjugates in Cancer Treatment. Recent Pat Anticancer Drug Discov. 2021;16(4):479-497. doi: 10.2174/1574892816666210509001139. PMID: 33966624.

Fantone S, Piani F, Olivieri F, Rippo MR, Sirico A, Di Simone N, Marzioni D, Tossetta G. Role of SLC7A11/xCT in Ovarian Cancer. Int J Mol Sci. 2024 Jan 2;25(1):587. doi: 10.3390/ijms25010587. PMID: 38203758; PMCID: PMC10779187.

Fu Z, Li S, Han S, Shi C, Zhang Y. Antibody drug conjugate: the "biological missile" for targeted cancer therapy. Signal Transduct Target Ther. 2022 Mar 22;7(1):93. doi: 10.1038/s41392-022-00947-7. PMID: 35318309; PMCID: PMC8941077.

Giraud J, Seeneevassen L, Rousseau B, Bouriez D, Sifré E, Giese A, Nguyen TL, Tiffon C, Lippi Y, Azzi-Martin L, Pannequin J, Ménard A, Bessède E, Staedel C, Mégraud F, Belleannée G, Lehours P, Gronnier C, Dubus P, Varon C. CD44v3 is a marker of invasive cancer stem cells driving metastasis in gastric carcinoma. Gastric Cancer. 2023 Mar;26(2):234-249. doi: 10.1007/s10120-022-01357-y. Epub 2022 Dec 18. PMID: 36528833; PMCID: PMC9950191.

Gomari MM, Farsimadan M, Rostami N, Mahmoudi Z, Fadaie M, Farhani I, Tarighi P. CD44 polymorphisms and its variants, as an inconsistent marker in cancer investigations. Mutat Res Rev Mutat Res. 2021 Jan-Jun; 787:108374. doi: 10.1016/j.mrrev.2021.108374. Epub 2021 Mar 26. PMID: 34083044.

Gritsch S, Batchelor TT, Gonzalez Castro LN. Diagnostic, therapeutic, and prognostic implications of the 2021 World Health Organization classification of tumors of the central nervous system. Cancer. 2022 Jan 1;128(1):47-58. doi: 10.1002/cncr.33918. Epub 2021 Oct 11. PMID: 34633681.

Guo Y, Chen X, Hu J, Su Y, Yin F, Liu X. The dual role of SLC7A11 in tumor drug resistance: mechanisms, challenges, and therapeutic potential. Am J Cancer Res. 2025 Oct 25;15(10):4516-4532. doi: 10.62347/GSBB1090. PMID: 41244134; PMCID: PMC12616170.

Han W, Wang S, Liang R, Wang L, Chen M, Li H, Wang Y. Non-ionic surfactant vesicles simultaneously enhance antitumor activity and reduce the toxicity of cantharidin. Int J Nanomedicine. 2013; 8:2187-96. doi: 10.2147/IJN.S43568. Epub 2013 Jun 14. PMID: 23807847; PMCID: PMC3686241.

Hong CY, Huang SC, Lin SK, Lee JJ, Chueh LL, Lee CH, Lin JH, Hsiao M. Norcantharidin-induced post-G(2)/M apoptosis is dependent on wild-type p53 gene. Biochem Biophys Res Commun. 2000 Sep 16;276(1):278-85. doi: 10.1006/bbrc.2000.3341. PMID: 11006118.

Hsiao YP, Tsai CH, Wu PP, Hsu SC, Liu HC, Huang YP, Yang JH, Chung JG. Cantharidin induces G2/M phase arrest by inhibition of Cdc25c and Cyclin A and triggers apoptosis through reactive oxygen species and the mitochondria-dependent pathways of A375.S2 human melanoma cells. Int J Oncol. 2014 Dec;45(6):2393-402. doi: 10.3892/ijo.2014.2689. Epub 2014 Sep 30. PMID: 25340978.

Jain KK. An Overview of Drug Delivery Systems. Methods Mol Biol. 2020; 2059:1-54. doi: 10.1007/978-1-4939-9798-5_1. PMID: 31435914.

Jyotsana N, Ta KT, DelGiorno KE. The Role of Cystine/Glutamate Antiporter SLC7A11/xCT in the Pathophysiology of Cancer. Front Oncol. 2022 Feb 23; 12:858462. doi: 10.3389/fonc.2022.858462. PMID: 35280777; PMCID: PMC8904967.

Kansy M, Senner F, Gubernator K. Physicochemical high throughput screening: parallel artificial membrane permeation assay in the description of passive absorption processes. J Med Chem. 1998 Mar 26;41(7):1007-10. doi: 10.1021/jm970530e. PMID: 9544199

Kim JA, Kim Y, Kwon BM, Han DC. The natural compound cantharidin induces cancer cell death through inhibition of heat shock protein 70 (HSP70) and Bcl-2-associated athanogene domain 3 (BAG3) expression by blocking heat shock factor 1 (HSF1) binding to promoters. J Biol Chem. 2013 Oct 4;288(40):28713-26. doi: 10.1074/jbc.M113.488346. Epub 2013 Aug 27. PMID: 23983126; PMCID: PMC3789968.

Koss DJ, Hindley KP, Riedel G, Platt B. Modulation of hippocampal calcium signalling and plasticity by serine/threonine protein phosphatases. J Neurochem. 2007 Aug;102(4):1009-23. doi: 10.1111/j.1471-4159.2007.04579. x. Epub 2007 Apr 17. PMID: 17442047.

Kovacs D, Migliano E, Muscardin L, Silipo V, Catricalà C, Picardo M, Bellei B. The role of Wnt/β-catenin signaling pathway in melanoma epithelial-to-mesenchymal-like switching: evidences from patients-derived cell lines. Oncotarget. 2016 Jul 12;7(28):43295-43314. doi: 10.18632/oncotarget.9232. PMID: 27175588; PMCID: PMC5190024.

Lara-Vega I, Nájera-Martínez M, Vega-López A. Pentoxifylline and Norcantharidin Synergistically Suppress Melanoma Growth in Mice: A Multi-Modal In Vivo and In Silico Study. Int J Mol Sci. 2025 Aug 4;26(15):7522. doi: 10.3390/ijms26157522. PMID: 40806647; PMCID: PMC12347239.

Li F, Li Z, Wei C, Xu L, Liang Y, Yan J, Li Y, He B, Sun C. Application of hydrogels for targeting cancer stem cells in cancer treatment. Biomed Pharmacother. 2024 Nov; 180:117486. doi: 10.1016/j.biopha.2024.117486. Epub 2024 Sep 24. PMID: 39321506.

Li W, Xie L, Chen Z, Zhu Y, Sun Y, Miao Y, Xu Z, Han X. Cantharidin, a potent and selective PP2A inhibitor, induces an oxidative stress-independent growth inhibition of pancreatic cancer cells through G2/M cell-cycle arrest and apoptosis. Cancer Sci. 2010 May;101(5):1226-33. doi: 10.1111/j.1349-7006.2010.01523. x. Epub 2010 Feb 5. PMID: 20331621; PMCID: PMC11158714.

Li Y, Ge Y, Liu FY, Peng YM, Sun L, Li J, Chen Q, Sun Y, Ye K. Norcantharidin, a protective therapeutic agent in renal tubulointerstitial fibrosis. Mol Cell Biochem. 2012 Feb;361(1-2):79-83. doi: 10.1007/s11010-011-1091-z. Epub 2011 Sep 29. PMID: 21956672.

Lim JKM, Delaidelli A, Minaker SW, Zhang HF, Colovic M, Yang H, Negri GL, von Karstedt S, Lockwood WW, Schaffer P, Leprivier G, Sorensen PH. Cystine/glutamate antiporter xCT (SLC7A11) facilitates oncogenic RAS transformation by preserving intracellular redox balance. Proc Natl Acad Sci U S A. 2019 May 7;116(19):9433-9442. doi: 10.1073/pnas.1821323116. Epub 2019 Apr 18. PMID: 31000598; PMCID: PMC6511045.

Liu N, Zhang J, Yin M, Liu H, Zhang X, Li J, Yan B, Guo Y, Zhou J, Tao J, Hu S, Chen X, Peng C. Inhibition of xCT suppresses the efficacy of anti-PD-1/L1 melanoma treatment through exosomal PD-L1-induced macrophage M2 polarization. Mol Ther. 2021 Jul 7;29(7):2321-2334. doi: 10.1016/j.ymthe.2021.03.013. Epub 2021 Mar 17. PMID: 33744468; PMCID: PMC8261162.

Liu XH, Blazsek I, Comisso M, Legras S, Marion S, Quittet P, Anjo A, Wang GS, Misset JL. Effects of norcantharidin, a protein phosphatase type-2A inhibitor, on the growth of normal and

malignant haemopoietic cells. Eur J Cancer. 1995 Jun;31A(6):953-63. doi: 10.1016/0959-8049(95)00050-x. PMID: 7646929.

Liu YP, Li L, Xu L, Dai EN, Chen WD. Cantharidin suppresses cell growth and migration, and activates autophagy in human non-small cell lung cancer cells. Oncol Lett. 2018 May;15(5):6527-6532. doi: 10.3892/ol.2018.8141. Epub 2018 Mar 1. PMID: 29731854; PMCID: PMC5920915.

Louis, D.N., Perry, A., Reifenberger, G., et al. (2016). "The 2016 World Health Organization Classification of Tumors of the Central Nervous System: a summary." Acta Neuropathologica, 131(6), 803–820.

Louis DN, Perry A, Wesseling P, Brat DJ, Cree IA, Figarella-Branger D, Hawkins C, Ng HK, Pfister SM, Reifenberger G, Soffietti R, von Deimling A, Ellison DW. The 2021 WHO Classification of Tumors of the Central Nervous System: a summary. Neuro Oncol. 2021 Aug 2;23(8):1231-1251. doi: 10.1093/neuonc/noab106. PMID: 34185076; PMCID: PMC8328013.

Martínez-Razo G, Pires PC, Avilez-Colin A, Domínguez-López ML, Veiga F, Conde-Vázquez E, Paiva-Santos AC, Vega-López A. Evaluation of a Norcantharidin Nanoemulsion Efficacy for Treating B16F1-Induced Melanoma in a Syngeneic Murine Model. Int J Mol Sci. 2025 Jan 30;26(3):1215. doi: 10.3390/ijms26031215. PMID: 39940982; PMCID: PMC11818190.

Medina MV, Sapochnik D, Garcia Solá M, Coso O. Regulation of the Expression of Heme Oxygenase-1: Signal Transduction, Gene Promoter Activation, and Beyond. Antioxid Redox Signal. 2020 May 10;32(14):1033-1044. doi: 10.1089/ars.2019.7991. Epub 2020 Mar 12. PMID: 31861960; PMCID: PMC7153632.

Misra S, Hascall VC, Markwald RR, Ghatak S. Interactions between Hyaluronan and Its Receptors (CD44, RHAMM) Regulate the Activities of Inflammation and Cancer. Front Immunol. 2015 May 6; 6:201. doi: 10.3389/fimmu.2015.00201. PMID: 25999946; PMCID: PMC4422082.

Naz F, Wu Y, Zhang N, Yang Z, Yu C. Anticancer Attributes of Cantharidin: Involved Molecular Mechanisms and Pathways. Molecules. 2020 Jul 19;25(14):3279. doi: 10.3390/molecules25143279. PMID: 32707651; PMCID: PMC7397086.

Noorani I, de la Rosa J, Choi YH, Strong A, Ponstingl H, Vijayabaskar MS, Lee J, Lee E, Richard-Londt A, Friedrich M, Furlanetto F, Fuente R, Banerjee R, Yang F, Law F, Watts C, Rad R, Vassiliou G, Kim JK, Santarius T, Brandner S, Bradley A. PiggyBac mutagenesis and exome sequencing identify genetic driver landscapes and potential therapeutic targets of EGFR-mutant gliomas. Genome Biol. 2020 Jul 30;21(1):181. doi: 10.1186/s13059-020-02092-2. Erratum in: Genome Biol. 2020 Aug 17;21(1):206. doi: 10.1186/s13059-020-02127-8. PMID: 32727536; PMCID: PMC7392733.

OAKS WW, DITUNNO JF, MAGNANI T, LEVY HA, MILLS LC. Cantharidin poisoning. Arch Intern Med. 1960 Apr; 105:574-82. doi: 10.1001/archinte.1960.00270160072009. PMID: 14428136.

Pan MS, Cao J, Fan YZ. Insight into norcantharidin, a small-molecule synthetic compound with potential multi-target anticancer activities. Chin Med. 2020 May 29; 15:55. doi: 10.1186/s13020-020-00338-6. PMID: 32514288; PMCID: PMC7260769.

Piipponen M, Riihilä P, Nissinen L, Kähäri VM. The Role of p53 in Progression of Cutaneous Squamous Cell Carcinoma. Cancers (Basel). 2021 Sep 7;13(18):4507. doi: 10.3390/cancers13184507. PMID: 34572732; PMCID: PMC8466956.

Pistritto G, Trisciuoglio D, Ceci C, Garufi A, D'Orazi G. Apoptosis as anticancer mechanism: function and dysfunction of its modulators and targeted therapeutic strategies. Aging (Albany NY). 2016 Apr;8(4):603-19. doi: 10.18632/aging.100934. PMID: 27019364; PMCID: PMC4925817.

Prager BC, Bhargava S, Mahadev V, Hubert CG, Rich JN. Glioblastoma Stem Cells: Driving Resilience through Chaos. Trends Cancer. 2020 Mar;6(3):223-235. doi: 10.1016/j.trecan.2020.01.009. Epub 2020 Feb 3. PMID: 32101725; PMCID: PMC8779821.

Puerto Galvis CE, Vargas Méndez LY, Kouznetsov VV. Cantharidin-based small molecules as potential therapeutic agents. Chem Biol Drug Des. 2013 Nov;82(5):477-99. doi: 10.1111/cbdd.12180. Epub 2013 Aug 9. PMID: 23809227.

Rauh, R., Kahl, S., Boechzelt, H., Bauer, R., Kaina, B., & Efferth, T. (2007). Molecular biology of cantharidin in cancer cells. *Chinese Medicine*, *2*, 8. https://doi.org/10.1186/1749-8546-2-8

Safenraiter ME, Soldini MPC, Del Río MG. Cantharidin: A Multiporpuse Beetlejuice. Neotrop Entomol. 2024 Aug;53(4):964-971. doi: 10.1007/s13744-024-01164-3. Epub 2024 May 15. PMID: 38750300.

Schadendorf D, van Akkooi ACJ, Berking C, Griewank KG, Gutzmer R, Hauschild A, Stang A, Roesch A, Ugurel S. Melanoma. Lancet. 2018 Sep 15;392(10151):971-984. doi: 10.1016/S0140-6736(18)31559-9. Erratum in: Lancet. 2019 Feb 23;393(10173):746. doi: 10.1016/S0140-6736(19)30361-7. PMID: 30238891.

Shen B, He PJ, Shao CL. Norcantharidin induced DU145 cell apoptosis through ROS-mediated mitochondrial dysfunction and energy depletion. PLoS One. 2013 Dec 19;8(12): e84610. doi: 10.1371/journal.pone.0084610. PMID: 24367681; PMCID: PMC3868658.

Shen M, Wu MY, Chen LP, Zhi Q, Gong FR, Chen K, Li DM, Wu Y, Tao M, Li W. Cantharidin represses invasion of pancreatic cancer cells through accelerated degradation of MMP2 mRNA. Sci Rep. 2015 Jul 2; 5:11836. doi: 10.1038/srep11836. Erratum in: Sci Rep. 2021 Feb 25;11(1):5063. doi: 10.1038/s41598-021-84394-4. PMID: 26135631; PMCID: PMC4488834.

Sies, H., & Jones, D. P. (2020). Reactive oxygen species (ROS) as pleiotropic physiological signalling agents. *Nature Reviews Molecular Cell Biology*, *21*(7), 363–383. https://doi.org/10.1038/s41580-020-0230-3

Slominski RM, Kim TK, Janjetovic Z, Brożyna AA, Podgorska E, Dixon KM, Mason RS, Tuckey RC, Sharma R, Crossman DK, Elmets C, Raman C, Jetten AM, Indra AK, Slominski AT. Malignant Melanoma: An Overview, New Perspectives, and Vitamin D Signaling. Cancers (Basel). 2024 Jun 18;16(12):2262. doi: 10.3390/cancers16122262. PMID: 38927967; PMCID: PMC11201527.

Su CC, Lee KI, Chen MK, Kuo CY, Tang CH, Liu SH. Cantharidin Induced Oral Squamous Cell Carcinoma Cell Apoptosis via the JNK-Regulated Mitochondria and Endoplasmic Reticulum Stress-Related Signaling Pathways. PLoS One. 2016 Dec 8;11(12): e0168095. doi: 10.1371/journal.pone.0168095. PMID: 27930712; PMCID: PMC5145211.

Su CC, Liu SH, Lee KI, Huang KT, Lu TH, Fang KM, Wu CC, Yen CC, Lai CH, Su YC, Huang CF. Cantharidin Induces Apoptosis Through the Calcium/PKC-Regulated Endoplasmic Reticulum Stress Pathway in Human Bladder Cancer Cells. Am J Chin Med. 2015;43(3):581-600. doi: 10.1142/S0192415X15500366. PMID: 25967669.

Sun W, Liu Z, Zhang Y. Cantharidin and Its Anhydride-Modified Derivatives: Relation of Structure to Insecticidal Activity. International Journal of Molecular Sciences. 2013; 14(1):1-16. https://doi.org/10.3390/ijms14010001

Tang X, Zuo C, Fang P, Liu G, Qiu Y, Huang Y, Tang R. Targeting Glioblastoma Stem Cells: A Review on Biomarkers, Signal Pathways and Targeted Therapy. Front Oncol. 2021 Jul 8;11:701291. doi: 10.3389/fonc.2021.701291. PMID: 34307170; PMCID: PMC8297686.

Tarleton M, Gilbert J, Sakoff JA, McCluskey A. Synthesis and anticancer activity of a series of norcantharidin analogues. Eur J Med Chem. 2012 Aug; 54:573-81. doi: 10.1016/j.ejmech.2012.06.010. Epub 2012 Jun 15. PMID: 22796041.

Trinconi Cunha M, Wallace N, Porceddu S, Ferrarotto R. Top advances of the year: Developments of immunotherapy in cutaneous squamous cell carcinoma, 2023-2024. Cancer. 2025 Jun 1;131(11): e35920. doi: 10.1002/cncr.35920. PMID: 40445861; PMCID: PMC12124471.

Wang G, Dong J, Deng L. Overview of Cantharidin and its Analogues. Curr Med Chem. 2018;25(17):2034-2044. doi: 10.2174/0929867324666170414165253. PMID: 28413963.

Xiong G, Schätzlein AG, Uchegbu IF. Acetyl-lysine human serum albumin nanoparticles activate CD44 receptors, with preferential uptake by cancer stem cells, leading to tumor eradication. J Control Release. 2025 Jun 10; 382:113632. doi: 10.1016/j.jconrel.2025.113632. Epub 2025 Mar 24. PMID: 40139395.

Xu Y, Stamenkovic I, Yu Q. CD44 attenuates activation of the hippo signaling pathway and is a prime therapeutic target for glioblastoma. Cancer Res. 2010 Mar 15;70(6):2455-64. doi: 10.1158/0008-5472.CAN-09-2505. Epub 2010 Mar 2. PMID: 20197461; PMCID: PMC2840073.

Yu J, Fang T, Yun C, Liu X, Cai X. Antibody-Drug Conjugates Targeting the Human Epidermal Growth Factor Receptor Family in Cancers. Front Mol Biosci. 2022 Feb 28; 9:847835. doi: 10.3389/fmolb.2022.847835. PMID: 35295841; PMCID: PMC8919033.

Yu J, Li M, Liu X, Wu S, Li R, Jiang Y, Zheng J, Li Z, Xin K, Xu Z, Li S, Chen X. Implementation of antibody-drug conjugates in HER2-positive solid cancers: Recent advances and future directions. Biomed Pharmacother. 2024 May; 174:116522. doi: 10.1016/j.biopha.2024.116522. Epub 2024 Apr 1. PMID: 38565055.

Zeng W, Wen Z, Chen H, Duan Y. Exosomes as Carriers for Drug Delivery in Cancer Therapy. Pharm Res. 2023 Apr;40(4):873-887. doi: 10.1007/s11095-022-03224-y. Epub 2022 Mar 29. PMID: 35352281.

Zhai BT, Sun J, Shi YJ, Zhang XF, Zou JB, Cheng JX, Fan Y, Guo DY, Tian H. Review targeted drug delivery systems for norcantharidin in cancer therapy. J Nanobiotechnology. 2022 Dec 3;20(1):509. doi: 10.1186/s12951-022-01703-3. PMID: 36463199; PMCID: PMC9719664.

Zheng LC, Yang MD, Kuo CL, Lin CH, Fan MJ, Chou YC, Lu HF, Huang WW, Peng SF, Chung JG. Norcantharidin-induced Apoptosis of AGS Human Gastric Cancer Cells Through Reactive Oxygen Species Production, and Caspase- and Mitochondria-dependent Signaling Pathways. Anticancer Res. 2016 Nov;36(11):6031-6042. doi: 10.21873/anticanres.11192. PMID: 27793930.

Zhou, H., Xu, J., Wang, S., & Peng, J. (2018). Role of cantharidin in the activation of IKKα/IκBα/NF-κB pathway by inhibiting PP2A activity in cholangiocarcinoma cell lines. *Molecular Medicine Reports*, *17*(6), 8600–8608. https://doi.org/10.3892/MMR.2018.8860